ENERGY ANALYSIS AND ENTROPY PRODUCTION OF BINARY NANOFLUID FLOWING IN ELLIPTICAL DIMPLED TUBE MOUNTED IN PARABOLIC SOLAR COLLECTOR

2022
MASTER THESIS
MECHANICAL ENGINEERING

Noor Adil MOHAMMED

Thesis Advisor
Prof. Dr. Kamil ARSLAN

ENERGY ANALYSIS AND ENTROPY PRODUCTION OF BINARY NANOFLUID FLOWING IN ELLIPTICAL DIMPLED TUBE MOUNTED IN PARABOLIC SOLAR COLLECTOR

Noor Adil MOHAMMED

T.C.
Karabük University
Institute of Graduate Programs
The Department of Mechanical Engineering
Prepared as
Master Thesis

Thesis Advisor
Prof. Dr. Kamil ARSLAN

KARABUK
September 2022

I certify that in my opinion the thesis submitted by Noor Adil MOHAMMED titled "ENERGY ANALYSIS AND ENTROPY PRODUCTION OF BINARY NANOFLUID FLOWING IN ELLIPTICAL DIMPLED TUBE MOUNTED IN PARABOLIC SOLAR COLLECTOR" is fully adequate in scope and in quality as a thesis for the degree of Master of Science.

Prof. Dr. Kamil ARSLAN .....
Thesis Advisor, Department of Mechanical Engineering

This thesis is accepted by the examining committee with a unanimous vote in the Department of Mechanical Engineering as a Master of Science thesis. September 19. 2022.

Examining Committee Members (Institutions)	Signature
Chairman : Prof. Dr. Oğuz TURGUT (GU)	.....
Member : Prof. Dr. Kamil ARSLAN (KBU)	.....
Member : Assist. Prof. Dr. M. Kazım YETİK (KBU)	.....

The degree of Master of Science by the thesis submitted is approved by the Administrative Board of the Institute of Graduate Programs, Karabük University.

Prof. Dr. Hasan SOLMAZ .....
Director of the Institute of Graduate Programs

"I declare that all the information within this thesis has been gathered and presented in accordance with academic regulations and ethical principles and I have according to the requirements of these regulations and principles cited all those which do not originate in this work as well."

Noor Adil Mohammed

ABSTRACT

M.Sc. Thesis

ENERGY ANALYSIS AND ENTROPY PRODUCTION OF BINARY NANOFLUID FLOWING IN ELLIPTICAL DIMPLED TUBE MOUNTED IN PARABOLIC SOLAR COLLECTOR

Noor Adil MOHAMMED

Karabük University
Institute of Graduate Programs
The Department of Mechanical Engineering

Thesis Advisor:
Prof. Dr. Kamil ARSLAN
September 2022, 120 pages

In this study, a three-dimensional analysis of the *PTC* receiver tube containing elliptical dimples, with different ratios *(0.66-1.66)* has been performed. The flow type has been considered turbulent, and the Reynolds number is chosen between *10000* to *30000*. The inlet temperature has been considered to be constant at *500 K*, and *C++* code has also been developed to perform a non-uniform heat flux on the outside of the receiver tube to approximate real life standards. The types of mono and hybrid nanofluids and their combinations with different *NPVF* are *2%TiO_2/Syltherm800, 2%Al_2O_3/Syltherm800, 1.0%TiO_2-1.0%Al_2O_3/Syltherm800 ,1.5%TiO_2-0.5%Al_2O_3/Syltherm800, and 0.5%TiO_2-1.5%Al_2O_3/Syltherm800*. The study provides a detailed analysis of the energy performance, entropy generation, coefficient of friction *(ff)*, Nusselt number *(Nu)* and thermal efficiency of *PTC*. Contours of the velocity and temperature distribution inside the receiver tube for *PTC* are also given.

The results of the study show that hybrid nanofluid *1.5% Al_2O_3-0.5% TiO_2/Syltherm 800* is chosen as the best heat transfer fluid. It was also defined that *PEC* increases by *27%* when *ER= 5/3* elliptical ratio receiver tube is used. With increasing *Re* from *10000* to *30000* reduces the entropy generation rate by *52%*. The lowest entropy generation rate has been obtained for the case of using *0.5%TiO_2-1.5%Al_2O_3/Syltherm800* hybrid nanofluid flowing inside the receiver tube containing dimples with elliptical ratio of *ER=5/3* by *1.25%* when compare it with smooth receiver at *Re =30000*.

Keywords : Parabolic trough collector, dimple, elliptical ratio, hybrid nanofluid, thermal efficiency, entropy, non-uniform heat flux.

Science Code : 91441

ÖZET

Yüksek Lisans Tezi

ELİPTİK ÇUKURLU YÜZEYE SAHİP ALICI TÜPLÜ PARABOLİK GÜNEŞ KOLLEKTÖRÜ İÇERİSİNDEKİ HİBRİT NANOAKIŞKAN AKIŞININ ENERJİ ANALİZİ VE ENTROPİ ÜRETİMİ

Noor Adil MOHAMMED

Karabük Üniversitesi
Lisansüstü Eğitim Enstitüsü
Makine Mühendisliği Anabilim Dalı

Tez Danışmanı:
Prof. Dr. Kamil ARSLAN
Eylül 2022, 120 sayfa

Bu çalışmada, eliptik çukurlu kanatçıklar içeren *PTC* alıcı tüpünün farklı oranlarda (*0.66-1.66*) üç boyutlu analizi yapılmıştır. Akış tipi türbülanslı olarak kabul edilmiş ve Reynolds sayısı *10000* ile *30000* arasında seçilmiştir. Giriş sıcaklığının *500 K*'de sabit olduğu kabul edilmiştir. Ayrıca, gerçek şartların sağlanabilmesi için *C++* kodu kullanarak alıcı tüp yüzeyine düzgün olmayan bir ısı akısı geliştirilmiştir. Mono ve hibrit nanoakışkan türleri ve bunların farklı *NPVF* ile kombinasyonları *2%TiO_2/Syltherm800, 2%Al_2O_3/Syltherm800, 1.0%TiO_2-1.0%Al_2O_3/Syltherm800 ,1.5%TiO_2-0.5%Al_2O_3/Syltherm800, and 0.5%TiO_2-1.5%Al_2O_3/Syltherm800* şeklindedir. Çalışma kapsamında, *PTC*'nin enerji performansı, entropi üretimi, sürtünme katsayısı (*ff*), Nusselt sayısı (*Nu*) ve termal verimliliği hakkında ayrıntılı bir analiz yapılmıştır. *PTC* için alıcı tüp içindeki hız ve sıcaklık dağılımları da sunulmuştur. Çalışmanın sonuçları, hibrit nanoakışkan *%1,5Al_2O_3-%0,5*

TiO_2/Syltherm800'ün en iyi ısı transfer akışkanı olduğunu göstermiştir. Ayrıca *ER=5/3* eliptik oranlı alıcı tüp kullanıldığında *PEC* değerinin *%27* oranında arttığı saptanmıştır. Ayrıca, Reynolds sayısının *10000*'den *30000*'e yükselmesi ile entropi üretim oranının *%52* azaldığı görülmüştür. En düşük entropi üretim oranı, pürüzsüz alıcı ile karşılaştırıldığında, *ER=5/3* eliptik oranlı gamzeler içeren alıcı tüp içerisinde *%1,25* oranında akan *0.5%TiO_2-1.5%Al_2O_3/Syltherm800* hibrit nanoakışkan kullanılması durumunda *Re=30000* için elde edilmiştir.

Anahtar Kelimeler : Parabolik çukur kollektör, çukur kanatçık, eliptik oran, hibrit nanoakışkan, termal verim, entropi, düzgün olmayan ısı akısı.

Bilim Kodu **:** 91441

ACKNOWLEDGMENT

At first, I would like to extend my thanks and gratitude to my supervisors (Prof. Dr. Kamil ARSLAN) for his help, support and constant communication with me throughout the period of my master's studies. I also extend my thanks to (Dr. Recep EKICILER), for shared his information with us about his articles on Parabolic trough collector. And also, I would like to extend my thanks to my family for their constant support (my father, my mother and my sisters). Especially my father (Adil) for helping me teach computer`s programs.

Finally, thanks to my friend (MSc. Hayati Kadir Pazarlıoğlu) for his help .

CONTENTS

Page

APPROVAL ii
ABSTRACT iv
ÖZET vi
ACKNOWLEDGMENT viii
CONTENTS ix
LIST OF FIGURES xii
LIST OF TABLES xv
SYMBOLS AND ABBREVITIONS INDEX xvi

PART 1 1
INTRODUCTION 1
1.1. SOLAR ENERGY AND PRICIPLE OF CONCENTRACTION SOLAR POWER *(CSP)* TECHNOLOGIES 3
1.1.1. Central Receiver System 6
1.1.2. Linear Fresnel Reflectors 7
1.1.3. Parabolic Dishes 8
1.1.4. Parabolic Trough 9
1.2. BRIEF OF PARABOLIC TROUGH COLLECTOR 11
1.3. THERMAL STORAGE FOR (*PTC)* 15
1.3.1. Storage Media or (Storage Mechanism) 16
1.3.1.1. Sensible 16
1.3.1.2. Latent 18
1.3.1.3. Chemical 19
1.3.2. Storage Concepts 19
1.3.2.1. Active Thermal Energy Storage 20
1.3.2.2. Passive Thermal Energy Storage 20
1.4. THESIS OVERVIEW 21
1.5. THESIS OBJECTIVE 22
1.6. THESIS SCOPE 22

Page

PART 2 23
LITERATURE REVIEW..... 23
2.1. LITERATURE REVIEW FOR *PTC*..... 23
2.2. LITERATURE REVIEW FOR *(PTC)* WITH NANOFLUID 25

PART 3 35
NUMERICAL STUDY..... 35
3.1. PHYSICAL MODEL 36
3.2. GOVERING EQUATIONS 38
3.3. MONTE CARLO RAY TRACING (MCRT) METHOD AND STATE OF BOUNDARY FOR GEAT FLOW 41
3.4. BOUNDARY CONDITIONS..... 44
3.5. EQUATIONS OF ENTROPY PRODUCTION..... 44
3.6. THERMO PGYSICAL PROPERTIES OF NANOFLUID..... 45
3.6.1. Thermo-Physical Properties of Mono Type Nanofluid 45
3.6.2. Thermo-Physical Properties of Hybrid Nanofluid..... 46
3.7. NUMERICAL PRODUCE..... 47
3.8. MESH STUDY..... 48

PART 4 50
RESULT AND DISCUSSION 50
٤,١. *CFD* MODEL VALIDATION..... 50
٤.3. FRICTION FACTOR *(ff)*..... 61
4.4. PERFORMANCE EVALUTION CRITERIA *(PEC)*..... 67
4.5. THERMAL EFFICIENCY (η_{th})..... 72
4.6. ENTROPY GENERATION AND THERMODYNAMIC ANALYSIS 78
4.6.1. Irreversible Heat Transfer and Fluid Friction..... 78
4.6.2. Thermodynamic Performance with Nanofluids 97
4.7. THE TEMPERATURE DISTRIBUTION OF DIFFERENT PLACES FOR DIFFERENT RECEIVER..... 103
4.8. THE VELOCITY DISTRIBUTION IN OF DIFFERENT PLACES OF THE RECEIVER OF THE RECEIVER..... 106

Page

PART 5 109
CONCLUSIONS 109

REFRENCES 111

RESUME 121

LIST OF FIGURES

Page

Figure 1.1. Global primary energy consumption by region (2010-2050) 1

Figure 1.2. Monthly crude oil spot prices (2017-2022) 2

Figure 1.3. Renewable energy generation 3

Figure 1.4. The three main components of solar radiation 4

Figure 1.5. Type of *CSP* according to work principle. 5

Figure 1.6. Central receiver systems 6

Figure 1.7. Linear Fresnel reflectors 7

Figure 1.8. Parabolic dishes 9

Figure 1.9. Parabolic trough collector. 10

Figure 1.10. Technical storage options 16

Figure 1.11. Schematic diagram of a parabolic trough solar power plant with a two-tank molten salt storage. 21

Figure 2.1. Collector receiver model : a) Cross-sectional view, b) Thermal resistance network for the cross-section of the receiver 24

Figure 2.2. Geometry of a solar receiver tube with twisted tape inserts 25

Figure 2.3. Experimental setup 27

Figure 2.4. Schematic diagrams of the studied *PTSC*. 33

Figure 2.5. Comparison among basic *PTSC*, novel *PTSC* and re-novel *PTSC* in different eco- nomic, thermal and hydraulic parameters 33

Figure 3.1. *3D* view of parabolic trough collector and numerical parameters. 36

Figure 3.2. Modeled (a)Receiver without dimples (b) Receiver with dimples(c) front view of dimpled receiver. 37

Figure 3.3. Modelling *PTC* in SOLTRACE 42

Figure 3.4. The heat flux distribution of the receiver modelled in *SOLTRACE* 43

Figure 3.5. (a) Validation of local concentration, (b) Heat flux distributed on the outer surface of the receiver tube of *PTC*. 44

Figure 3.6. View of mesh distribution on the receiver tube of *PTC*. 49

Figure 4.1. Validation of outlet temperature according to experimental data of Dudley et al. and Vahidinia et al. 52

Figure 4.2. Validation of current study: (a) *Nu* with correlations of Dittus-Boelter and Gnielinski [105], (b) *ff* with correlations of Petukhov and Blasius 53

Page

Figure 4.3. Variation of *Nu* with *Re* with different nanofluid types for elliptical ratios of dimples for receiver tube: (a) *ER=5/3* (b) *ER=3.3/2* (c) *ER=3/5* (d) *ER=2/3.3* (e) *smooth.* 57

Figure 4.4. Variation of *Nu* with *Re* for elliptical ratios of dimples with working fluids of: (a) *Syltherm800* (b) *2.0% Al_2O_3/Syltherm800* (c) *2%TiO/Syltherm800* (d) *1%Al_2O_3- 1%TiO_2/Syltherm800* (e) *0.5%Al_2O_3-1.5%TiO_2/Syltherm800* (f) *1.5%Al_2O_3-0.5%TiO_2/Syltherm800.* 60

Figure 4.5. Variation of *ff* with *Re* with different nanofluid types for elliptical ratios of dimples for receiver tube: (a) *ER=5/3* (b) *ER= 3.3/2* (c) *ER=3/5* (d) *ER=2/3.3* (e) *smooth.* 63

Figure 4.6. Variation of *ff* with *Re* for elliptical ratios of dimples with working fluids of: (a) *Syltherm800* (b) *2.0% Al_2O_3/Syltherm800* (c) *2% TiO/Syltherm800* (d) *1%Al_2O_3-1%TiO_2/Syltherm800* (e) *0.5%Al_2O_3-1.5%TiO_2/Syltherm800* (f) *1.5%Al_2O_3-0.5%TiO_2/Syltherm800.* 66

Figure 4.7. Variation of *PEC* with *Re* with different nanofluid types for elliptical ratios of dimples for receiver tube: (a) *ER=5/3* (b) *ER= 3.3/2* (c) *ER=3/5* (d) *ER=2/3.3* (e) *smooth.* 69

Figure 4.8. Variation of *PEC* with *Re* for elliptical ratios of dimples with working fluids of: (a) *Syltherm800* (b) *2.0% Al_2O_3/Syltherm800* (c) *2%TiO/Syltherm800* (d) *1%Al_2O_3-1%TiO_2/Syltherm800* (e) *0.5%Al_2O_3-1.5%TiO_2/Syltherm800* (f) *1.5%Al_2O_3-0.5%TiO_2/Syltherm800.* 72

Figure 4.9. Variation of η_{th} with *Re* with different nanofluid types for elliptical ratios of dimples for receiver tube: (a) *ER=5/3* (b) *ER= 3.3/2* (c) *ER=3/5* (d) *ER=2/3.3* (e) *smooth* 75

Figure 4.10. Variation of η_{th} with *Re* for elliptical ratios of dimples with working fluids of: (a) *Syltherm800* (b) *2.0% Al_2O_3/Syltherm800* (c) *2%TiO/Syltherm800* (d) *1%Al_2O_3-1%TiO_2/Syltherm800* (e) *0.5%Al_2O_3-1.5%TiO_2/Syltherm800* (f) *1.5%Al_2O_3-0.5%TiO_2/Syltherm800.* 78

Figure 4.11. Variation of *Irreversible* heat transfer with different nanofluid types for elliptical ratios of dimples for receiver tube: (a) *ER=5/3* (b) *ER= 3.3/2* (c) *ER=3/5* (d) *ER=2/3.3* (e) *smooth.* 81

Figure 4.12. Variation of *Irreversible* heat transfer with *Re* for elliptical ratios of dimples with working fluids of: (a) *Syltherm800* (b) *2.0% Al_2O_3/Syltherm800* (c) *2%TiO/Syltherm800* (d) *1%Al_2O_3-1%TiO_2/Syltherm800* (e) *0.5%Al_2O_3-1.5%TiO_2/Syltherm800* (f) *1.5%Al_2O_3-0.5%TiO_2/Syltherm800.* 84

Figure 4.13. Variation of Irreversible fluid friction with *Re* with different nanofluid types for elliptical ratios of dimples for receiver tube: (a) *ER=5/3* (b) *ER= 3.3/2* (c) *ER=3/5* (d) *ER=2/3.3* (e) *smooth* 87

Page

Figure 4.14. Variation of Irreversible fluid friction with *Re* for elliptical ratios of dimples with working fluids of: (a) *Syltherm800* (b) *2.0% Al_2O_3/Syltherm800* (c) *2%TiO/Syltherm800* (d) *1%Al_2O_3-1%TiO_2/Syltherm800* (e) *0.5%Al_2O_3-1.5%TiO_2/Syltherm800* (f) *1.5%Al_2O_3-0.5%TiO_2/Syltherm800*. 90

Figure 4. 15. Variation of *Be* with *Re* with different nanofluid types for elliptical ratios of dimples for receiver tube: (a) *ER=5/3* (b) *ER= 3.3/2* (c) *ER=3/5* (d) *ER=2/3.3* (e) *smooth* 93

Figure 4.16. Variation of *Be* with *Re* for elliptical ratios of dimples with working fluids of: (a) *Syltherm800* (b) *2.0% Al_2O_3/Syltherm800* (c) *2%TiO/Syltherm800* (d) *1%Al_2O_3- 1%TiO_2/Syltherm800* (e) *0.5%Al_2O_3-1.5%TiO_2/Syltherm800* (f) *1.5%Al_2O_3-0.5%TiO_2/Syltherm800*. 96

Figure 4.17. Variation of total entropy generation with *Re* with different nanofluid types for elliptical ratios of dimples for receiver tube: (a) *ER=5/3* (b) *ER= 3.3/2* (c) *ER=3/5* (d) *ER=2/3.3* (e) *smooth*. 99

Figure 4.18. Variation of total entropy generation with *Re* for elliptical ratios of dimples with working fluids of: (a) *Syltherm800* (b) *2.0% Al_2O_3/Syltherm800* (c) *2%TiO/Syltherm800* (d) *1%Al_2O_3-1%TiO_2/Syltherm800* (e) *0.5%Al_2O_3-1.5%TiO_2/Syltherm800* (f) *1.5%Al_2O_3-0.5%TiO_2/Syltherm800*. 102

Figure 4.19. Temperature distribution at the outlet section of the receiver tube for different *Re* and elliptical ratios. 104

Figure 4.20. Temperature distribution at different sections along the receiver tube for different elliptical ratios. 105

Figure 4.21. Velocity distribution at the outlet section of the receiver tube for different *Re* and elliptical ratios. 107

Figure 4.22. Velocity distribution at different sections along the receiver tube for different elliptical ratios. 108

LIST OF TABLES

Page

Table 1.1. Comparison of the characteristics of *CSP* technologies 5
Table 1.2. Advantages and disadvantages for the *CSP* types..... 11
Table 1.3. Solid Storage Media for *SEGS* Plants 17
Table 1.4. Liquid storage media for *SEGS* plants 18
Table 1.5. Latent Heat Storage Media for *SEGS* Plants..... 19
Table 3.1. The parameters of the numerical study. 35
Table 3.2. Physical properties of the receiver. 38
Table 3.3. Geometrical dimensions of the receiver 38
Table 3.4. The properties of nanoparticles and base fluid 47
Table 3.5. Mesh independency study. 49

SYMBOLS AND ABBREVITIONS INDEX

SYMBOLS

A	: Area, m^2
Be	: Bejan number
C_1, C_2, C_3	: Turbulent model constants
C_P	: Specific heat, $J.kg^{-1}.K^{-1}$
CSP	: Concentrating solar power
d	: Receiver diameter, m
ER	: Elliptical ratio
ΔP	: Pressure drop, Pa
ff	: Darcy friction factor
G_k	: Generation of turbulent kinetic energy due to mean velocity gradients
$H\text{-}Tr$	: Heat transfer rate
HTF	: Heat transfer fluid
h	: Heat transfer coefficient, $W.m^{-2}.K^{-1}$
I	: Direct normal irradiance, $W.m^{-2}$
K	: Turbulent kinetic energy, $m^2.s^{-2}$
k	: Thermal conductivity, $W.m^{-1}.K^{-1}$
L	: Length of the receiver, m
LFR	: Linear Fresnel reflectors
$\dot{m}$	: Mass flow rate, $kg.s^{-1}$
Nu	: Nusselt number
$NPVF$	: nanoparticle volume fraction
PCM	: Phase change material
PEC	: Performance evaluation criteria
PTC	: Parabolic trough collector
Pr	: Prandtl number
q''	: Heat flux, $W.m^{-2}$

Re	: Reynolds number
S_{ij}	: Rate of linear deformation tensor, s^{-1}
S	: Modulus of the mean rate of strain tensor, s^{-1}
S_{gen}	: Entropy generation rate, $W.K^{-1}$
S'	: Entropy generation rate per unit length of the receiver, $W.m^{-1}.K^{-1}$
S'''_{gen}	: Volumetric entropy generation, $W.m^{-3}.K^{-1}$
$\left(S'''_{gen}\right)_F$	: Volumetric entropy generation due to fluid friction, $W.m^{-3}.K^{-1}$
$\left(S'''_{gen}\right)_H$	: Volumetric entropy generation due to heat transfer, $W.m^{-3}.K^{-1}$
$(\grave{S}_{gen})_T$	: Total entropy generation per unit length of the receiver, $W.m^{-1}.K^{-1}$
T	: Temperature, K
t	: Thickness of receiver tube, m
UHF	: Ultrahigh frequency
x_i, x_j	: Spatial coordinates, m
u_i, u_j	: Averaged velocity components, $m.s^{-1}$
u, v, w	: Velocity components, $m.s^{-1}$
$\grave{u}, \grave{v}, \grave{w}$	: Fluctuations of velocity, $m.s^{-1}$
x, y, z	: Cartesian coordinates, m

Greek Letter

δ_{ij}	: Kronecker delta
ε	: Turbulent dissipation rate, $m^2.s^{-3}$
η	: Turbulence model parameter
η_{th}	: Thermal efficiency
θ	: Circumferential angle of receiver,°
θ_r	: Rim angle, °
μ	: Viscosity, $Pa.s$
μ_t	: Eddy viscosity, $Pa.s$
ν	: Kinematic viscosity, $m^2.s^{-1}$
ρ	: Density, $kg.m^{-3}$
$-\rho\ \overline{u_i'u_j'}\frac{\partial u_i}{\partial x_j}$	: Reynolds stress, $N.m^{-2}$
$\sigma_{h,t}$	: Turbulent Prandtl number for energy
σ_k	: Turbulent Prandtl number for k

σ_ε : Turbulent Prandtl number for ε

Subscript

b : Bulk

eff : Effective

hnf : Hybrid nanoparticle

i : inlet

i, j, k : Spatial indices

o : outlet

P : Aperture

p1, p2 : Nanoparticle

w : wall

Superscript

` : Fluctuation from average value

- : Time-averaged value

PART 1

INTRODUCTION

Rapid population growth and industrialization processes have led to an increase in the need for energy use directly [1]. Figure 1.1 indicates the energy consumed by humans and the percentage of energy that is likely to be consumed to 2050 [2]. Where the developments taking place in the eighteenth and nineteenth centuries all over the world led to an increase in factories that consume fossil fuels. Fossil fuels are considered one of the energy systems adopted in the recent times. Fossil fuels were used even before the invention of the Watt steam engine in 1781. Fossil fuels became completely dependable in the Industrial Revolution, where fossil fuels were used in the textile industries as well as in the operation of trains and ships [3].

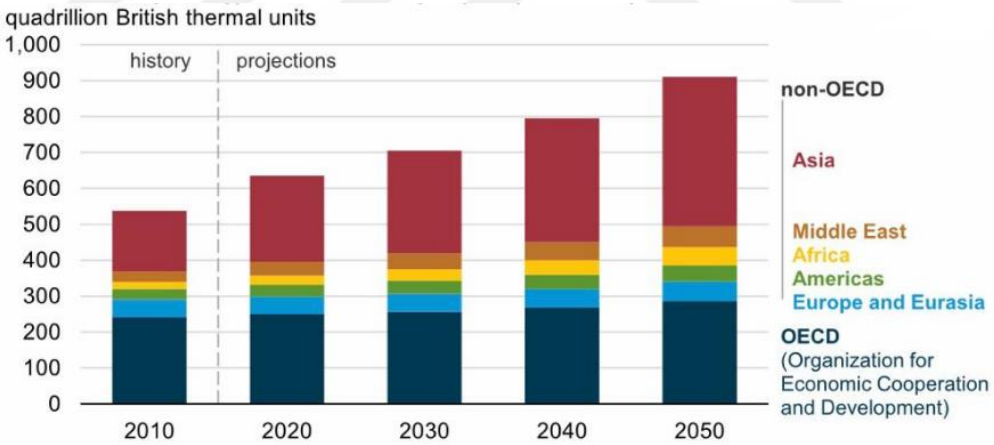

Figure 1.1. Global primary energy consumption by region (2010-2050) [2].

However, the increase in population in the world has led to concern about the possibility of providing fossil fuels sufficient for the population growth that occurs over time, so it was necessary to provide a new type of fossil fuel, as oil was explored [4].

Oil had a heating capacity higher than coal, as oil contributed to the spread of internal combustion engines, which in turn, this led to the emergence of the automobile and aviation industries. As oil replaced coal, but the increase in the price of oil, especially after the oil crisis in 1973, in which he saw the rise in the price of oil led to weak markets (where the nominal prices rose from 12.52 to 22.3 dollars per barrel) and in order to find a solution to this crisis, the Organization for Economic Cooperation and Development was established to limit the impact of this crisis on the supply of factories and companies with oil. Figure 1.2 refers to oil prices from 2017 to 2022. It was necessary to find an alternative energy that can be relied upon in factories and factories [5]. But the alternative energy to fossil fuels should not have come from the source of fossil energy, because the emission of fossil energy CO_2 directly affects the climate and the environment [6].

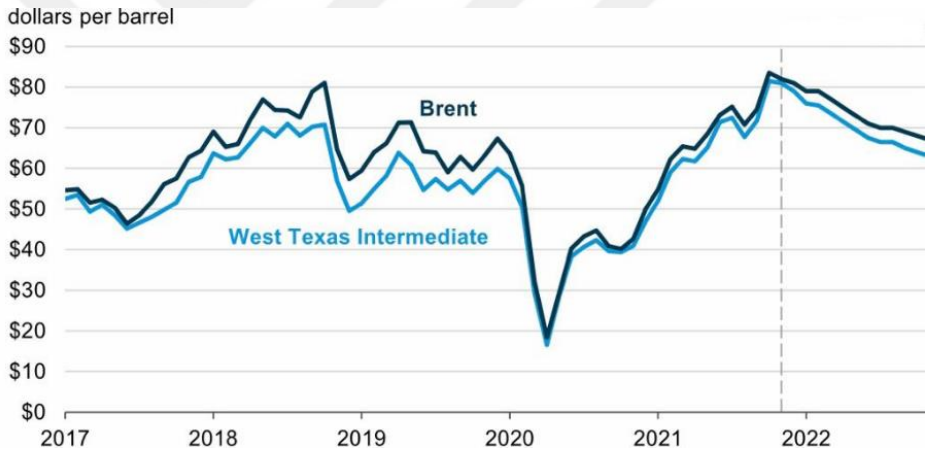

Figure 1.2. Monthly crude oil spot prices (2017-2022) [7].

Therefore, the sources of renewable energies have become attractive because they are considered clean and harmless to the environment and can be stored. They are considered sustainable energy because they are taken from permanent natural sources (such as the sun, wind, and earth). Figure 1.3 indicates the increment in the use of renewable energies over time [8]. One of the most important motives in this thesis is to prove that solar energy can be a reliable source of energy in the future, as. It gives independence to its users where its performance and sustainability can be improved through the use of designs that help on increasing storage and control algorithms [9].

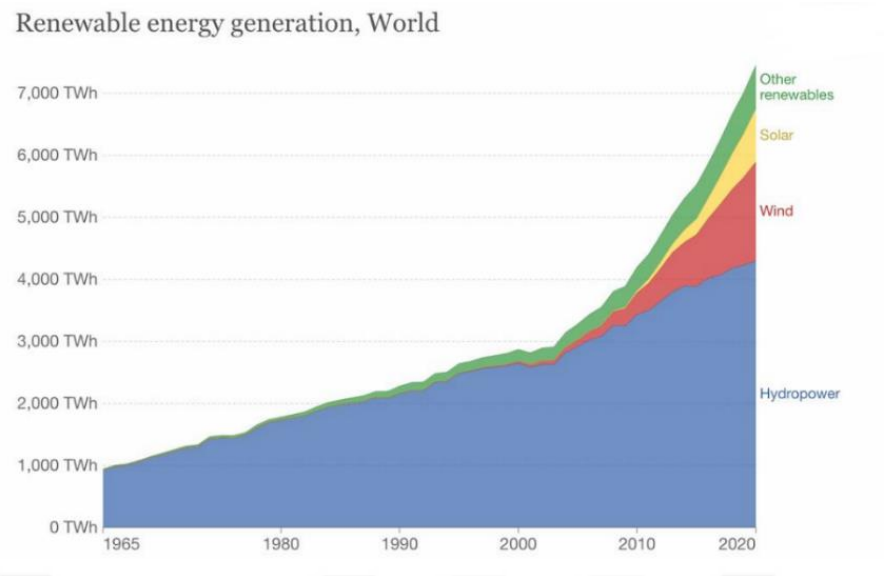

Figure 1.3. Renewable energy generation [8].

1.1. SOLAR ENERGY AND PRICIPLE OF CONCENTRACTION SOLAR POWER *(CSP)* TECHNOLOGIES

Solar energy is a clean, renewable and affordable energy source compared to other renewable energy sources [10]. Whereas, concentrated solar power technology is a favourable method to generate electrical and thermal energy [11]. The principle of solar energy techniques is to focus solar radiation on a smaller surface specified by using mirrors or lenses, so that the surface on which the light is focused the solar radiation can generate electrical energy, so the energy absorbed by the solar radiation is photoelectric energy or these surfaces can be used as a medium for heat for high temperature, which can be used to generate electricity to run the engines of large factories. To clarify the principle of the work of concentrated solar energy systems, it is necessary to know the types of solar radiation coming from the sun towards the earth. Solar radiation is electromagnetic waves transmitted from the sun to the earth at the speed of light. Global solar radiation is radiant energy It has a short wave and is coming from the sun and passing through a horizontal region per unit time in general. Figure 1.4 indicates to the three main components of solar radiation are the direct, the diffused and the reflected solar radiation [12].

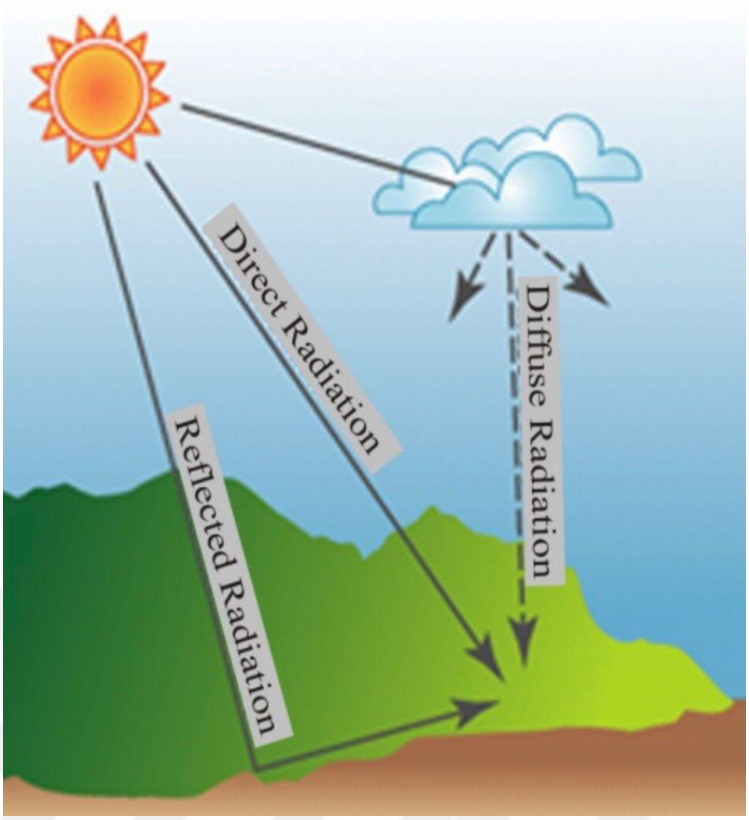

Figure 1.4. The three main components of solar radiation [12].

As for the components of solar radiation, there are three the first is direct solar radiation or the beam is the radiation that falls directly to the earth without scattering in the particles of the atmosphere. The second type is the diffuse solar radiation, which collides with particles such as dust and clouds in the atmosphere before falling on the surfaces. As it can be used to *CSP* Applications, the third type is the reflected solar radiation, which is the radiation that fall on surfaces such as buildings and ground [3].

There are four main techniques of concentrated solar power, which will be discussed to clarify the principles of its work and the pros and cons of each type [13].

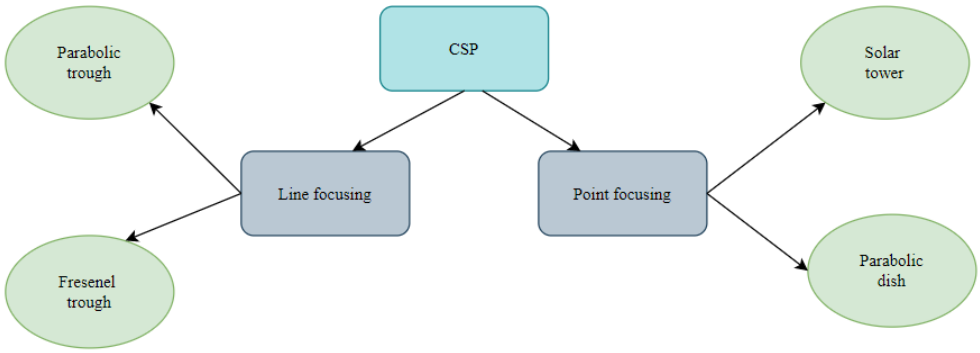

Figure 1.5. Type of *CSP* according to work principle.

As shown in Figure 1.5, there are two types of concentration of solar energy, either linear or point. Where the concentration of solar radiation in the linear focus on two collectors, the path is on one axis and in a linear manner. As for the point focus, the focus in the tracking collectors is on the thickness axis and the height axis and in the Cases where high temperatures are required. Dealing with the linear focusing is easier and cheaper, because the focus is on one axis only. It is preferable to use *PTC* to produce electricity on a large scale. If a cheaper focus device is required, regardless of its efficiency, it is recommended to use Central Receiver Systems (*CRS)*. It is preferable to use Linear Fresnel Reflector (*LFR*) which has added benefit of enabling simple dual use of land as property plants grow under collectors or place collectors on roofs .As for Parabolic Dishes, it does not need cooling water, so it is recommended to use it in dry areas, as well as it can produce high temperatures and high Carnot efficiency [14]. Table 1.1 presents a comparison of the characteristics of *CSP* technologies.

Table 1.1. Comparison of the characteristics of *CSP* technologies [14].

CSP Type	Operating Temperature (***ºC***)	Ratio of Solar Concentration	Thermal Storage Suitability	Average Annual Efficiency	Land Use Efficiency (Total Area/Power)
Parabolic Trough	*20–400*	*15–45*	Suitable	*15%*	*3.9*
Linear Fresnel Reflector	*50–300*	*10–40*	Suitable	*8–11%*	*0.8–1*
Solar Trough	*300–1000*	*150–1500*	Highly suitable	*17–35%*	*5.4*
Parabolic Dish	*120–1500*	*100–1000*	Difficult	*25–30%*	*1.2–1.6*

1.1.1. Central Receiver System

It has many names, including the solar power tower or the central tower as well as the power station (heliostats). It is known as a type of *CSP*. A group of flat and moving mirrors is used for the purpose of focusing the sun on the collecting tower. Early designs use these rays for the purpose of heating water, The steam resulting from it in the operation of the turbines. It was distilled using liquid sodium as well as molten salts (*40%* potassium nitrate, *60%* sodium nitrate) as a working fluid because it is known that these materials work at high thermal capacities and can be used for the purpose of producing energy [15].

This type of *CSP* can generate energy even when the sun is not shining. In recent times, many improvements have been made to this system, including the transition from the current (hot/cold) tank designs to the single tank thermal line systems that are stuffed with quartzites and oxygen blankets, which in turn improve performance and reduce costs. As for the designs of this system, they are multiple, including using flat glass instead of curved glass for reducing costs. Molten salt containers are used in thermal storage for the purpose of continuing to produce electricity during the Brightness of the sun [16]. Figure 1.6 shows the parts that make up the *CSP* (*CRS*) [17].

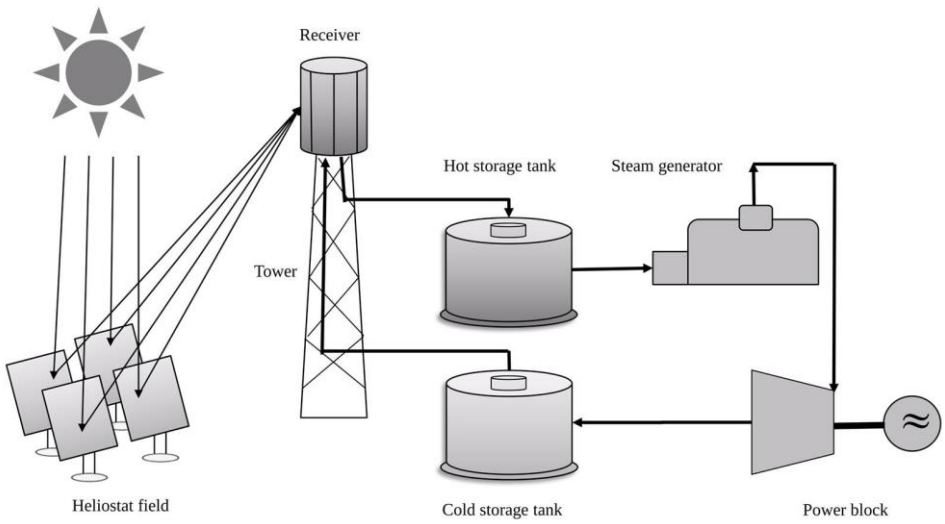

Figure 1.6. Central receiver systems [17].

1.1.2. Linear Fresnel Reflectors

It is also called as a linear compressed Fresnel reflector. It was called by this name because of its similarity to the Fresnel lens, its principle of operation where a group of small, simple, thicker lens fragments are combined. The advantage of this lens is its ability to focus the sun's energy for approximately 30 times its natural intensity. Less expensive than using expensive glass reflectors. The absorbent is immobile. Long and thin sections of mirrors are used to focus the light on the absorber, where the absorber is located at a common focal point for the reflectors. Energy is transferred from the sun to the absorber by means of the absorber to thermal fluids (water - air - oil). It is preferable to use oil because of its ability to maintain heat. At higher temperatures, the liquid is then crossed to run thermal steam through the heat exchanger. The difference between a linear pressurized Fresnel reflector and a conventional linear Fresnel reflector is that a linear pressurized Fresnel reflector is tried on multiple absorbers near the mirrors. Also, the *LFR* can easily accommodate dual-use grounds such as using the land below the collectors for agricultural purposes or locating the pools on the roofs, allowing land costs to be shared with agriculture or very low land costs using ceilings [18]. Figure 1.7 shows the parts of Linear Fresnel Reflectors [19].

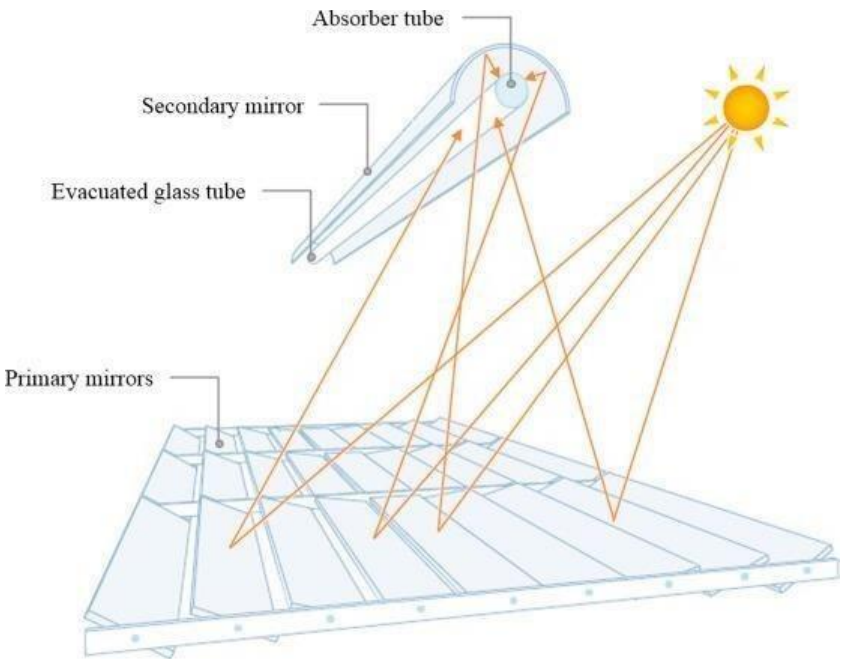

Figure 1.7. Linear Fresnel reflectors [19].

1.1.3. Parabolic Dishes

It is also called a parabolic antenna, and it is one of the types of *CSP*, which is characterized by its high directivity. Parabolic dishes use a parabolic capacitor (area of *50-100* m^2). Concentrates the solar radiation to power the energy conversion unit. They have higher Concentration ratios (*1000-3000*) allowing access to very high temperatures (above $1000\,^{o}C$)a typical parabolic antenna consists of a metal parabolic reflector with a small feed antenna suspended in front of the reflector at its focus, pointed back toward the reflector [20]. The reflector is a metallic surface formed into a paraboloid of revolution and usually truncated in a circular rim that forms the diameter of the antenna. In a transmitting antenna, radio frequency current from a transmitter is supplied through a transmission line cable to the feed antenna, which converts it into radio waves. The radio waves are emitted back toward the dish by the feed antenna and reflect off the dish into a parallel beam. In a receiving antenna the incoming radio waves bounce off the dish and are focused to a point at the feed antenna, which converts them to electric currents which travel through a transmission line to the radio received. It works to direct radio waves in a narrow beam such as a searchlight, or it can be said that it works to receive waves from a certain direction only. But there is a condition to achieve a narrow beam, which is that the length of the reflector used is much greater than the length of the radio waves used, so equivalent dishes are used in the high-frequency part of the radio spectrum at *UHF* and microwave frequencies (*SHF*), where the wavelengths are small enough that it can Use appropriately sized reflectors. For a wide range of power plant, field should be installed parabolic. Since parabolic dishes It does not require active cooling, it can be installed in isolated and remote places such as deserts that result in two advantages: First, deserts are of a very high Direct Nature Insolation (*DNI*), the second generation of off-grid electricity is easy. Figure 1.8 indicates a working principle Parabolic dishes [21].

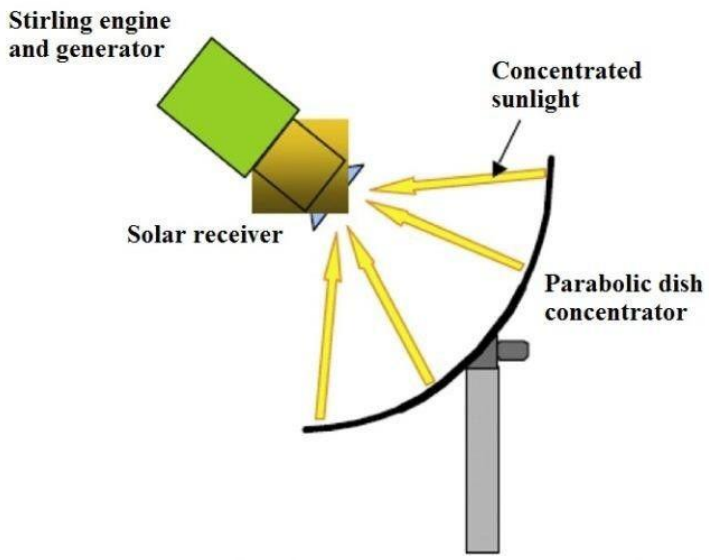

Figure 1.8. Parabolic dishes [21].

1.1.4. Parabolic Trough

It is one of the types of *CSP*, which is a parabolic trough collector consisting of two parts, an absorber, and a parabolic reflector [19]. Usually, the absorber is manufactured from materials with high conductivity such as aluminum or rust-reducing steel and is coated with a selective paint to improve the absorption process of solar radiation waves. The absorber is covered In a vacuum glass envelope of solar energy in order to deal with energy losses in order to reduce heat load and conductive losses from the intake pipe to the air [22].

Working principle, the light is focused in (*25-150 m*) parabolic sectional mirrors into an empty absorber tube closed with glass placed at the focal point of the parabola. The *H-Tr* is heated by sunlight inside the absorber and then pumped into the heat exchanger. The heat exchanger converts it into electrical energy. Or stored. The *H-Tr* used inside the absorber was developed. Previously, it used to use oil, but at the present time, several improvement experiments are being conducted on the working fluid by using nanofluids instead of oil. It has been observed that nanofluids have a great ability to improve the performance of the absorbent tube. Also called the absorbent device. receiver tube. And Figure 1.9 shows the components of *PTC* [23].

The *PTC* uses a single axis tracking system and its operating temperature reaches *400-500* ^{o}C through a long series of thermal collecting elements. As of 2014, the largest solar thermal power systems using parabolic trough technology include the *354 MW* Solar Energy Generating System *(SEGS)* plants in California, the *280 MW* Solana Generating Station with molten salt heat storage, the *250 MW* Genesis Solar Energy Project, the Spanish *200 MW* Solaben Solar Power Station, and the Andasol 1 Solar Power Station [3].

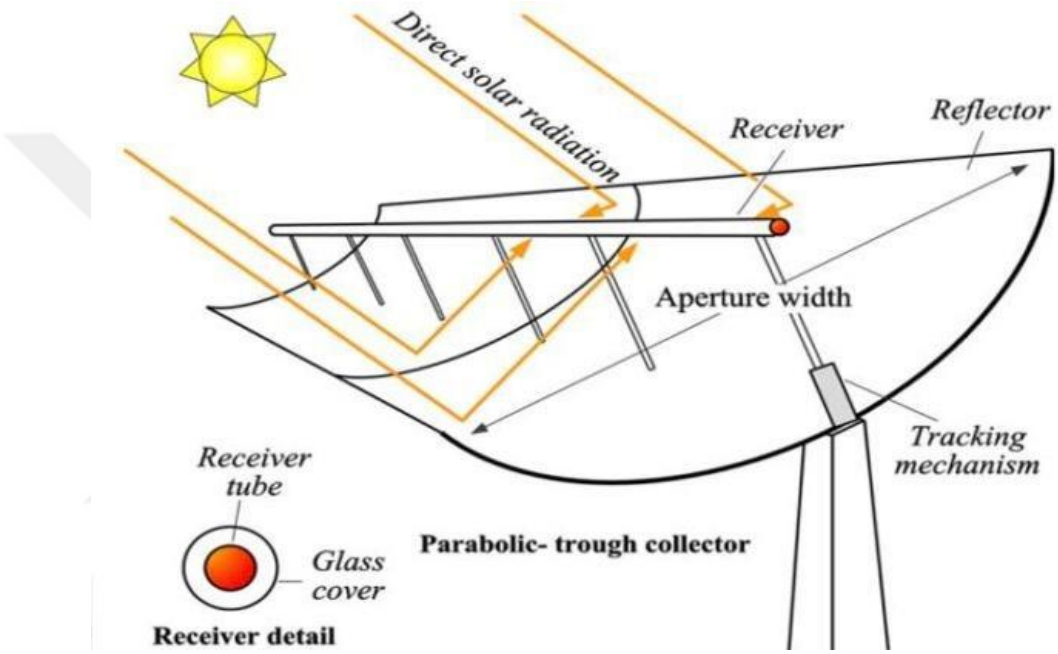

Figure 1.9. Parabolic trough collector [23].

The types of *CSP*, their structure, and their working principle are explained in Table 1.2, which shows the advantages and disadvantages of each type.

Table 1.2. Advantages and disadvantages for the *CSP* types [24].

Type Of Solar Power System	Advantage	Disadvantage
Parabolic Trough	Proven technology- investor confidence. Modular technology. Solar combined cycle system- increase electrical efficiency. Little moving parts. Readily hybridized with fossil fuels.	Flat landed for development. Lower temperatures -> lower efficiency.
Central Receiver	Higher Concentration. More potential energy Storage. Readily hybridized with fossil fuels. Soil Sitting flexibility.	More tracking needed (add moving parts). Higher capital costs. Higher land requirements.
Parabolic Dish	Highest conversion. efficiency simple. Design minimal water requirement. Small, distributed power source -> Self Containing Units.	Little Storage Capability
Linear Fresnel Reflector	Low operating expenses. Little maintenance. Scalable.	Little development -> Low investor confidence. Highest capital costs. Low efficiency -> Largest Area requirement.

1.2. BRIEF OF PARABOLIC TROUGH COLLECTOR

PTC is considered the first type of linear *CSP* system. In 1913, researchers ran a *35 kW* heat engine using solar energy. Despite this success, those responsible for the oil economy stopped working in the field of solar energy. But due to the economic oil crisis in 1974, solar energy was resorted again to and developed, through an initiative of the International Energy Agency (*IEA*), where a group of countries, including the United States of America, Europe, Israel and Japan, launched a campaign to finance and develop solar energy in order to withstand the economic oil crisis that most countries faced. As the development of solar energy started from the United States of America in the mid-seventies, with the establishment of the Ministry of Energy in 1978

to manage research and development in the field of energy, where equivalent complexes were used that can produce energy at temperatures from low to medium (*100-400 ^{o}C)* and applied to produce electricity [25]. It is considered the most important parabolic collector projects in Europe. experimental solar electric trough plant (called the Small Solar Power Systems Project/Distributed Collector System: *SSPS/DCS*) on the test site of the *IEA* at Tabernas (the later Plataforma Solar de Almería) in the Province of Almería/south of Spain in 1981, and its successful test operation as well as test evaluation until the year 1985[26]. Engineers from different cities of the world, mainly from the United States of America, have conducted field experiments and development research to develop and study the parabolic trough collector. Typical electric power for irrigation or water pumping has operated more than *25* basin systems with reflective surfaces ranging from a few hundred square meters to about *5000* $m^{٢}$. The most frequent development of *PTC* was (1977-1982). A great deal of international experimental block has been accumulated. The main manufacturers in this period were Accorx, SunTec and Solar Kinetics in the *USA*, and MAN in Germany in 1979 *LUZ* International Ltd was formed. (*LUZ*) in Israel and in *USA*, with the stated goal of developing and building low-cost solar energy systems industrial heat applications. *LUZ* has conducted a thorough survey of Experience mainly gained through *DOE/Sandia* and *IEA-SSPS/DCS* testing plants to build prototype systems for testing and implementation. 1982 *LUZ*. set up industrial process heating system for the Tabu potato processing plant near Tel Aviv,Israel. *LUZ* started marketing activities in the *USA* in the early 1980s improved solar heating systems. Many industrial companies were interested in it the use of solar energy as a source of hot water, steam , and hot air due to the energy crisis[26]. but *LUZ* found that selling such facilities came with some major downsides despite solar thermal applications, sales are expensive and difficult it is estimated to be a large but untapped market. *LUZ* began operating its first commercial solar thermal power plant in late 1984, which is *13.8 MW SEGS I* (solar electricity generation system) in Daggett, California. *(USA)* because favorable tax provisions and power purchase agreement with Southern California Edison corporation (*SCE*). This was followed by the construction of a series of improvements, the largest *SEGS* plants in California until 1990. Finally, one *13.8 MW*, six *30 MW*, and two *80MW* SEGS plants were commissioned which were provided with peak power in SCE Network. SEGS plants are designed, built, and

operated by *LUZ* for third party stockholders. The specific ownership structure varies from project to project, reflect tax provisions and financial conditions at the time of construction. At the end of 1984 *LUZ* opened its first commercial solar thermal system *13.8 MW SEGS I* in Daggett, California. (United States) because favorable tax regime and power purchase agreement with (*SCE*). Many improvements followed the largest *SEGS* plants were in California until 1990. Ultimately one *13.8 MW* and six *30 MW SEGS* turbines with a capacity of *80 MW* have been commissioned and operated at maximum power *SCE* Network. *SEGS* systems are planned, built, and operated by *LUZ* for third party shareholders. The specific ownership structure varies from project to project, Consider tax regulations and financial terms at the time of construction. Shareholders provided about half of the capital while the rest came from Various sources of debt. Unfortunately, *LUZ's* financial problems stopped in 1991. The existing factories are still operating financially and technically Successful management under local operating companies in Kramer Junction and Lake Harbor. No additional plants were built due to financial uncertainty. Rapid progression of basin collecting technology for solar electricity applications from Perspectives of unit power size and cost reductions in the time period from the end from the seventies to the eighties can be illustrated by the following three examples:

- The *150 kW* facility in Coolidge, Arizona, *USA* (1979) was the first solar thermal power plant full system experience to prove automation in irrigation application.
- *500 kW IEA-SSPS / DCS* Pilot Plant in Almeria, Spain (1981) was designed, built, and operated as a collaborative research and development project under the auspices of international Energy Agency.
- The *SEGS I-IX* plants were in California (1984-1990) with units up to *80 MW* electric. It was commercially built by a group of American, Israeli, German and companies Marketed by *LUZ*. Although *LUZ* failed to survive the financial meltdown in 1991, the factories in Kramer Junction (five 30 *MW* of *SEGS III-VII* plants) and into Lake Harbor (the two the 80 *MW* SEGS *VIII* and *IX* stations are in continuous operation. resulting from their operation great business operation experience accumulated so far. They have fed the plants more than *7 TW.h* in the *SCE* grid over the course of a fixed solar electricity record of more

than 10 years of continuous operation equivalent to about half of the total solar energy electricity generated all over the world so far. Constant availability of solar energy exceeded 98%, operating and maintenance costs succeeded *30%* reduction. At the same time, industries and other companies have been encouraged to push for new designs parabolic basin systems in the Southwest United States, Southern Europe, and the United States the Mediterranean Sea and other parts of the world. project development and preliminary studies for large plants on Crete (Greece), Egypt, India, Morocco, Spain, and other countries in the solar cell belt point to potential cost reductions and semi-commercial applications. The trustee system is also integrated in circuits (gas/steam turbine power plants) show a clear decline investment costs and increased capacity factor, resulting in high attractiveness for companies from the development of new technologies for the new idea about direct steam generation (*DSG*). It is currently being carried out mainly by Germany and Spain, and another push is expected commercial application for solar energy generation. This technology can also be works in combined heat and power plants and solar energy applications, including solar energy the purposes of desalination of water.

There are noticeable activities in the United States of America to commercialization *SEG* by improving the quality and reducing the cost of *PTC* (example: small trough collectors of the Industrial Solar Technology Co. (*IST*) in Denver)[26]. In addition, several research and development activities are carried out in Europe. Research is still underway in order to develop *PTC* and improve its efficiency. The improvement may be through changing the design of the receiving tube for *PTC* or by changing the working fluid for the purpose of increasing *H-Tr*. There are still significant barriers in the market for the use of solar process heat (as in case of solar power generation today), despite the fact that many research and development efforts and marketing activities are continuing, the fact that the heat of solar processing orders are assessed to represent a large untapped market [26].

1.3. THERMAL STORAGE FOR (*PTC)*

When designing a storage tank for thermal energy for *PTC*, its ability to store thermal energy must be considered.

The cost of a thermal energy storge system depends on the following items

- Item that is stored
- Heating and discharging system (heat exchanger)
- Thermal tank area

But from a technical point of view, it must be provided

- High energy density (per unit mass or per unit volume) in the storage material
- Good heat transfer between the heat transfer fluid (*HTF*) and the storage medium
- Mechanical and chemical stability of the material being stored
- Compatibility between *HTF* and heat exchanger and/or storage medium
- Complete reversibility for many charge/discharge cycles
- Capable of heat loss
- Ease of control

As for the design criteria, they are as follows

- Nominal temperature and specific enthalpy reduction at load
- The maximum load it can reach
- Operational strategy
- The ability to integrate into the power plant

Figure 1.10 shows the Technical Storage Options [9].

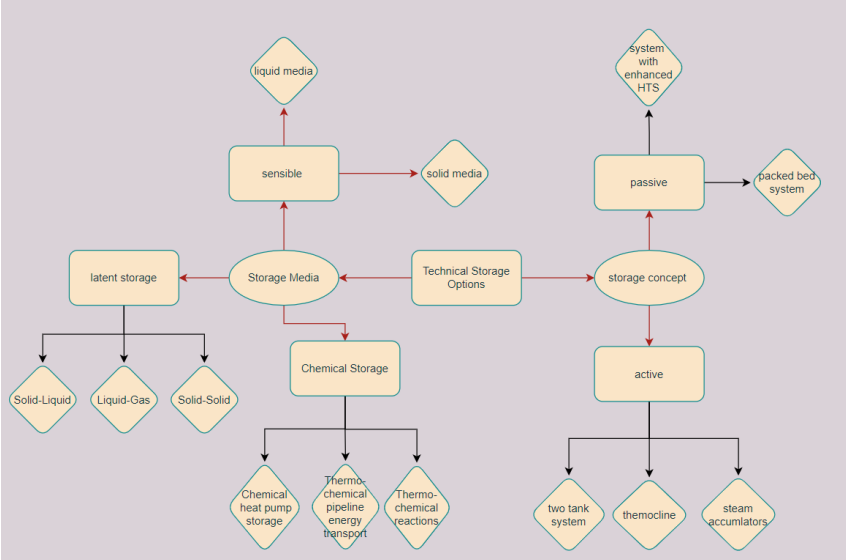

Figure 1.10. Technical storage options [9] .

1.3.1. Storage Media or (Storage Mechanism)

It consists of three mechanisms which are as follows:

1.3.1.1. Sensible

It is a method of storing energy by increasing the temperature of a solid or liquid. can be stored in the sensible heat (temperature change) of substances that experience a change in internal energy. The stored energy can be calculated by the product of its mass, the average specific heat, and the temperature change. Besides the density and the specific heat of the storage material, other properties are important for sensible heat storage: operational temperatures, thermal conductivity, and diffusivity, vapor pressure, compatibility among materials, stability, heat loss coefficient as a function of the surface areas to volume ratio, and cost.

- *Solid Media:* Solid media in packed layers are typically used for heat storage that requires a liquid heat exchange. If the heat capacity of the liquid is very small (e.g. when using air), solid is the only storage material; however, if the liquid is liquid, its capacity can be neglected, the system is called a dual storage system. Crowded families prefer thermals layering with benefits.

- Stored energy can be easily removed warmer layers and cold liquid can be taken from and added to colder layers omnibus area. An advantage of the binary system is the use of inexpensive solid materials such as rock, sand, or the like. Concrete for storage materials in connection with more expensive heat transfer fluids like thermal paste. However, the pressure drops, which means that the parasitic energy consumption can be reduced. Become high in the binary system. This should be considered when designing the memory.

For some of the solid media in Table1.3, the temperature limits from cold to hot are greater than they could be. Parabolic solar panels can be used in SEGS systems as this is limited. The maximum outlet temperatures are approx. *400 ℃.* Table 1.3 shows the effect on solid media by applying this temperature limit to the average storage temperature range, the device heat capacities and media costs [25].

Table 1.3. Solid Storage Media for *SEGS* Plants [25].

Storage Medium	Heat Capacity *KWht/m³*	Media Cost *$/KWht*
Reinforced concrete	*100*	*1*
NaCl (solid)	*100*	*2*
Cast iron	*160*	*32*
Cast steel	*180*	*150*
Silica fire bricks	*60*	*18*
Magnesia fire bricks	*120*	*30*

- *Liquid Media:* Density differences between hot and cold liquids make them maintain their natural thermal layers. One of the most important conditions for applying this feature is to provide the hot liquid to the upper part of the storage system during shipment and to extract the cold liquid from the bottom during unloading, or to avoid mixing another mechanism is used to ensure that the liquid enters the storage at the appropriate level according to its temperature (density). Some splitters are equipped to perform this process (floating entry, cover heat exchange, etc.) the heat transfer fluid in the *SEGS* plant operates between temperatures of about *300 ºC* and *400 ºC.* Applying these temperature

constraints and dropping mineral oil because it cannot operate at higher temperature requirements, gives the results shown in Table 1.٤, both oils and salts are possible. However, salts generally have a high melting point, and parasitic heating is required to keep them liquid at night, during low insolation, or during plant closures. Silicone oil is very expensive, despite its benefits to the environment, but it can be dangerous at times, while synthetic oils can be classified as dangerous substances [27].

Table 1.4. Liquid storage media for *SEGS* plants [27].

Storage Medium	Heat Capacity *kWht/m³*	Media Cost *$/kWht*
Synthetic oil	٥٧	٤٣
Silicone oil	٥٢	٨٠
Nitrite salts	٧٦	٢٤
Nitrate salts	٨٣	١٦
Carbonate salts	١٠٨	٤٤
Liquid sodium	٣١	٥٥

1.3.1.2. Latent

It is a method to store energy by heat transition from the solid state to the liquid state. It is a method of storing energy by transferring heat from the solid to the liquid state. In some materials, e.g., heat of fusion (transition solid to liquid), heat of vaporization (liquid vapor) or heat of transformation of the crystalline solid phase. All materials that exhibit these properties are called phase change materials (*PCMs*). Because the latent heat of fusion between the liquid and solid states of materials is quite high compared to reasonable heat, the volume of storage systems using *PCMs* can be reduced compared to reasonable single-phase heating systems. For example, molten salt has more energy per unit mass than solid salt. For example, molten salt has more energy per unit block of solid salt. Table 1.٥ indicates to Latent Heat Storage Media for *SEGS* Plants [27].

Table 1.5. Latent Heat Storage Media for *SEGS* Plants [27].

Storage Medium	Heat Capacity *KWht/m³*	Media Cost *$/KWht*
$NaNO_3$	١٢٥	٤
KNO_3	١٥٦	٤
KOH	٨٥	٢٤

1.3.1.3. Chemical

It is the third type of storage mechanism and is based on chemical reactions. One of the most important conditions in it that the chemical reactions completely reversible. heat is produced by a solar receiver to catalyze an endothermic chemical reaction. If this reaction is completely reversible and the heat can be completely recovered by reverse reaction. Catalysts are often necessary to release heat. The advantages of this type of storage mechanism are high storage energy densities, indefinitely long storage time in the near vicinity temperature and heat pump capacity. As for its disadvantage, it is first not easy (complexity). Uncertainty in the thermodynamic properties of the reaction components and Reaction kinetics under a wide range of operating conditions, high cost, toxicity, and flammability [27].

1.3.2. Storage Concepts

Storage concepts can be categorized as active or passive systems. Storage characterized by forced convection heat transfer to storage materials is active storage. The storage medium circulates itself through a heat exchanger. This heat exchanger can also be a solar receiver or a steam generator. The main feature of the passive system is the passage of the heat transfer medium by storage only for charging and discharging. Heat transfer the same medium does not distribute [27].

1.3.2.1. Active Thermal Energy Storage

Active thermal systems typically use tank storage. It can be designed as a single tank or two tank systems. Active storage is again divided into direct and indirect systems. In the direct system, a fluid acts as a heat carrier, a heat fluid collects solar heat, and acts as a storage medium, whereas in the indirect system, a second medium is used to store heat [27].

1.3.2.2. Passive Thermal Energy Storage

Passive systems are generally dual medium storage systems. *HTF* transmits power. When charging and receiving energy from storage materials, discharging takes place from the energy source to the storage medium. These systems are also called restorers. The storage medium can be solid, liquid or *PCM*. In general, a chemical storage system uses at least two methods. The main disadvantage of generators is that the temperature of the *HTF* drops during a vacuum as the storage material is cooled. Another problem is the change in internal temperature. In the case of solids in particular, the heat transfer is low and there is usually no direct contact between *HTF* and the storage material since the heat is transferred via a heat exchanger [27].

Tank system uses one tank for *HTF* cooling method coming from steam generator and one tank of hot *HTF* comes out directly from the solar receiver before being fed to the steam generator. The advantage of this system is *HTF* hot and cold storage separately. The main disadvantage is the need for a second tank, which makes it expensive. In this type of system, storage tanks are directly correlated with *HTF* pressure levels (which is not necessarily a defect). The single tank system reduces storage volume and cost by eliminating the second tank. However, it is difficult to separate hot and cold *HTF* in a single tank system. Because of the density difference between hot and cold liquid, *HTF* is naturally broken down in the tank, from the coldest layer at the bottom to the warmest layer at the top. Maintenance of thermal layers requires charge and discharge control. The procedure and appropriate methods or devices to avoid confusion. filling storage tank using a second solid storage material (rock, iron, sand, etc.) can help achieve this stratification. Figure 1.11 shows a process flow schematic for a typical large-scale parabolic trough solar power plant with a two-tank molten salt storage [27].

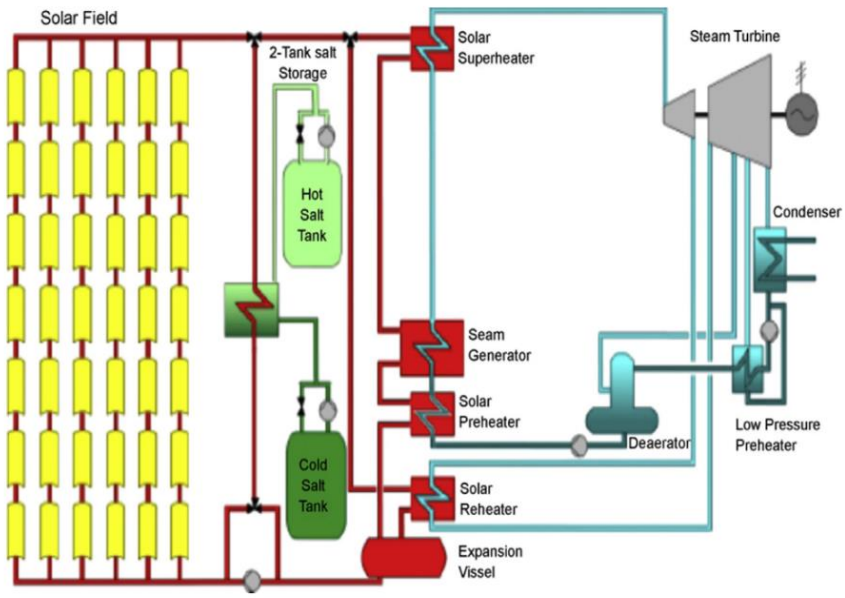

Figure 1.11. Schematic diagram of a parabolic trough solar power plant with a two-tank molten salt storage [27].

1.4. THESIS OVERVIEW

Solar energy is considered one of the cleanest and most suitable types of renewable energy. *PTC* is a type of *CSP*. In this thesis, it is conducted analysing the energy and entropy for the *PTC*'s receiver tube contain the elliptical dimples, which present higher thermal efficiency in comparison with other dimple types [28,29]. The elliptical dimples have been selected with different dimensional parameters *(ER=a/b=0.66-1.66)*. The type of flow has been considered as turbulent, and the *Re* is ranged between *10,000* and *30,000*. The inlet temperature is considered constant at *500 K*. The *C++* code has been developed to perform non-uniform heat flux on the outside of the *PTC*`s receiver tube to approximate real-life standards. Mono and hybrid nanofluid types and their combinations with different *NPVF* have been studied in detail to determine the energy and entropy performance of *PTC*. To explain *H-Tr* and entropy performance of *PTC* comprehensively, the mono and hybrid nanofluid configurations are used as follows; *2%TiO_2/Syltherm800, 2%Al_2O_3/Syltherm800, 1.0%TiO_2-1.0%Al_2O_3/Syltherm800 ,1.5%TiO_2-0.5%Al_2O_3/Syltherm800, and 0.5%TiO_2-1.5%Al_2O_3/Syltherm800*. Hybrid nanoparticles are chosen for the reasons that the

higher level of stability of TiO_2 [30] and higher ability to improve the heat transfer process of Al_2O_3 [31]. Finally, entropy production, *Nu*, *ff*, and thermal efficiency have been analysed section by section.

1.5. THESIS OBJECTIVE

In this thesis, thermal performance and entropy analysing have been studied of the *PTC* receiver tube when adding the dimples on the internal surface of the receiver and passing the mono and hybrid nanofluid through it. The graphs and the fluid flow circumference inside the receiver have been obtained. At the same time, the *ER* for the dimples and the type of the nanofluid which achieve best improvement in the thermal performance of the *PTC* receiver tube have been chosen.

1.6. THESIS SCOPE

This study carried out because of the wide using of the solar energy. The experimental and numerical studies on the parabolic solar collector have a great place in the literature. The present study focuses on a thermal improvement for *PTC* receiver numerically by using *Ansys Fluent 2020R2* commercial program. The *PTC`s* receiver has been studied by adding dimples with different elliptical ratios and seeing their effect on the heat transfer process and measuring its ability to improve the thermal efficiency of the *PTC`s* receiver. Addition, mono and hybrid types nanofluids have been used as working fluids instead of water or other solutions, due to the ability of nanoparticles to increase the heat transfer rate.

PART 2

LITERATURE REVIEW

Concentrated solar power technology is a favorable method to generate electrical and thermal energy. The parabolic trough type solar collectors are used in many fields such as water heating and electricity generation. *PTC* is the most commonly used type of solar collector, because it is the most mature and most capable of optimization. There are several improvements have been made to the *PTCs*, including by adding fins to the collector tubes to increase the surface area, thus increasing the convective heat transfer rate *(H-Tr).* The other method used to improve the collector efficiency is to treat it using nanofluids. The literature review about *PTC* has been divided in two groups as shown below.

2.1. LITERATURE REVIEW FOR *PTC*

Ghassemi et al. [32]numerically carried out a study to determine *H-Tr* characteristics of receiver tube inserted ring turbulators in the parabolic trough collector (*PTC*) using *Syltherm-800* as working fluid. The distances between two rings have been taken in four cases (*140-70-105-52.5 mm*) and ratio of ring diameter to inner diameter (D_{in}*=70 mm*) have been taken in six cases (smooth receiver-*0.6-0.7-0.75-0.8-0.*9). *Re* has been considered between *30000* and *251000*. It has been found that the ring type of fin increases the ability of the receiver tube to absorb solar energy. Then, reducing the distance between the rings increases the *H-Tr*. The best thermal efficiency has been obtained when the distance between two rings is *170 mm* at *Re=30000.*

Kalogirou [33] performed an analytical study to provide an accurate explanation about the heat transfer inside the receiver tube of the parabolic trough complex, where the heat transfer of the model is studied in all transfer modes. The convection is between the fluid and the receiver tube wall and from the cover glass to the surrounding air,

then the heat conduction is between the ring wall (the receiver tube) and then the radiation and convection together. The radiation is between the metal receiver tube and the surfaces of the metal glass cover to the metal glass cover and the sky, respectively as shown in Figure 2.1 the analytical process was carried out using the geometric equations analyzer and the results that were reached through the known performance of the current complexes were compared. The results were obtained using a *12.2m* tube placed in the laboratory surface and the collector can work up to *200 °C,* where it was reached that the collector is able to give a thermal efficiency of about *58%* at *200 °C,* which is a good thing. These results were obtained at a solar irradiance of *900 W/m²*, a wind speed of *0.45 m/s,* a flow rate of *8.8 kg/s,* an ambient temperature of *25 °C,* and ambient air at atmospheric pressure in the receiver loop.

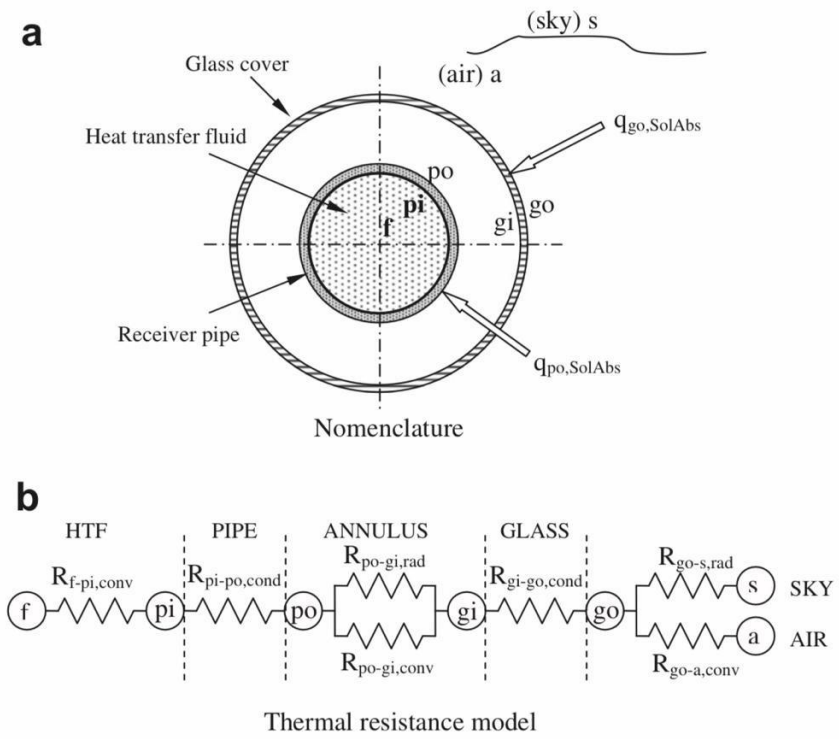

Figure 2.1. Collector receiver model : a) Cross-sectional view, b) Thermal resistance network for the cross-section of the receiver [33].

Chang et al. [34] numerically studied the effect of inserting a twisted tape into the receiver tube of *PTC* As shown in Figure 2.2. The twist ratios have been designed as *2.5º, 5.0º, 12.5º, 15.6º, 25º, 41.7º*. *Re* has been considered between *7485* and *30553*. The results show that inserting a twisted tape into the receiver tube can significantly

improve *H-Tr*. Whereas, lower *C* clearance rate and torsion rate can improve heat transfer effectively. Especially when the clearance rate is C = *0, E*. But at the same time, the lower filtering rate and the torsion rate also increase the friction factor. These methods and results can be extended to improve the heat transfer of all *CSP* receivers.

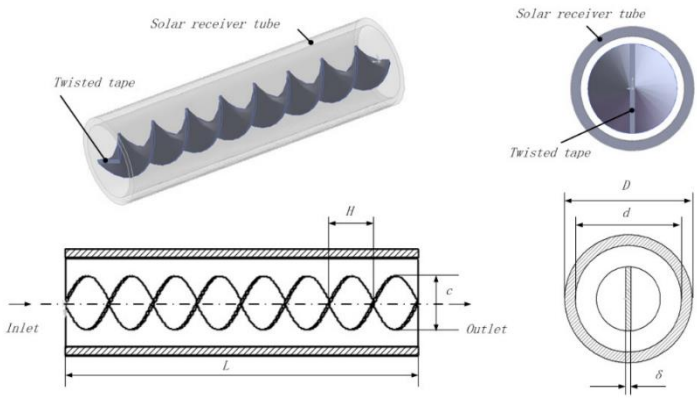

Figure 2.2. Geometry of a solar receiver tube with twisted tape inserts [34].

Khanjian et al. [35] numerically studied the effect of using vortex generator in a rectangular channel. The lower wall is equipped with two rectangular vortex generators. The working fluid is air. Also, the effect of vortex generator angle *(20°≤β≤90°)* on the flow characteristics and heat transfer has been studied. *Re* has been ranged from *456* to *911*. The best result has been obtained using *β=70°* at *Re=911* and the *H-Tr* increased by *13.9%* compared to the base case.

2.2. LITERATURE REVIEW FOR *(PTC)* WITH NANOFLUID

Heat transfer efficiency can be used through different methods such as the use of extended surfaces and vibration for heat transfer surface and use of small channels [36]. In addition, heat transfer efficiency for devices can also be developed with environmental improved characteristics such as labor liquid, especially thermal conductivity and specific heat [37]. Special mineral solid particles have a hundred times thermal conductivity higher than traditional fluids [38]. Therefore, different studies have been implemented on the thermal performance of solid molecules that have become hanging in fluids. The size of the first outstanding particles had

millimeters or micrometers [39,40]. Nanometer particles are set in a base liquid are suspended in the liquid and the term "neophile" was for the first time discovered by Choi in 1995 [41]. The most appropriate nanotechnology of fluids obtained with molecules of small size particles, has higher thermal conductivity, which caused reduced pumping strength and has better rheological properties [34–37]. The surface of the fluid and thermal surface is increasing with the disintegration of nanoparticles in fluid. In addition, the interactions and collision among nanoparticles are increased from fluid surface and flow transmission. Addition, the dispersion process increases disorder and intensity in fluid. This phenomenon increases the rate of convection heat transfer [42–45].

Nanofluids can be divided into two parts, metallic and non-metallic. Metallic nanofluids consist of basic fluids (ethylene glycol, water, oil), metal nanoparticles *(Fe)* and non-metallic nanoparticles *(Al_2O_3, CuO, SiC, ZnO, TiO_2)*. Addition, nanofluids can be produced using carbon nanotubes in various structures (single-walled, multi-walled), nanoparticles in composite structures (such as alloys), and other nano-sized materials [46–49]. Compared with conventional solid and liquid suspensions, nanofluids have obvious advantages in heat transfer behavior. These advantages can be explained as follows [50–54]:

- A smaller precipitate diameter of nanoparticles results is lower precipitation than conventional solid-liquid solutions.
- Brownian behavior of nanoparticles is more stable.
- Thermal conductivity and larger surface area where nanofluids can be produced with different nanoparticle sizes and surface modifications. It has adjustable features like this, that allows us to get the nanofluid with the required performance.
- It has a lower pumping capacity than the primary fluid for the same amount of heat transfer.

As can be understood from the above explanations, nanofluids are a promising heat transfer fluid. For this reason, studies on nanofluids are continuing rapidly in many scopes [36].

Sheikhzade et al. [55] studied the effect of using nanofluid such as *Ag/water*, *Cu/water*, and TiO_2*/water* with the various nanoparticle volume fractions (*NPVF)* $(0 \leq \varphi \leq 4\%)$ in a micro-channel and assumed that the type of flow in the channel is turbulent flow $(20000 \leq Re \leq 100000)$. The maximum amount of *H-Tr* has been obtained using a TiO_2*/water* nanofluid by *10.27%* compared to the base fluid (water). Finally, it has been concluded that increasing the *NPVF* reduces entropy production, the total entropy generation increases with the increasing of *Re*.

Farajallah et al. [56] conducted an experimental study on the effect of turbulent nanofluid flow in a heat exchanger Figure 2.3 shows the flow loop of constructed system. The nanofluids have been selected as TiO_2*/water* and Al_2O_3*/water*. The *NPVF* of γ-Al_2O_3*/water* and TiO_2*/water* are arranged in the range of *0.3–2%* and *0.15–0.75%*, respectively. Finally, it is concluded that *H-Tr* of TiO_2*/water* at the highest *NPVF* is greater than γ-Al_2O_3*/water* at the highest *NPVF* by *18.7%*.

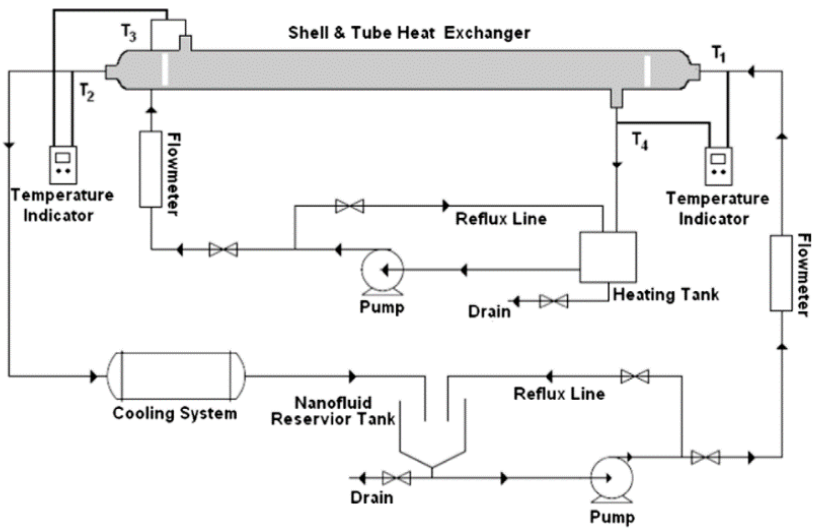

Figure 2.3. Experimental setup [56].

Fard et al. [57] conducted studies on the effect of using *ZnO/water* nanofluid *(0.5 vol.%)* in a heat exchanger with the configuration of single and double pipes. Also, the type of flow in the study is laminar flow $(Re \leq 2300)$. The findings support that the use of nanofluid in a double tube heat exchanger has a greater effect than the single tubes.

It also has been reached that the heat transfer coefficient *(h)* increases by *12%* when using a nanofluid instead of the base fluid in the heat exchanger. In the same conditions, the heat transfer coefficient increases by *14%* in the double-tube heat exchanger.

Akhtari et al. [58] performed experimental and numerical study on the heat transfer using α-Al_2O_3/*water* nanofluid with different *NPVF* $(0.2 \leq \varphi \leq 0.5\%)$ flowing through clam-tube heat exchangers. The flow system was considered as laminar flow $(Re \leq 2300)$. Finally, the heat transfer coefficients of the nanofluid in the shell-and-tube paired tubes are *13.2%* higher than that of water. The heat transfer coefficients of the nanofluid in the shell-and-tube heat exchangers are *21.3%* higher than that of water. In the shell and tube heat exchanger is *26.2%* higher than in the double tube heat exchanger. It was concluded that the use of nanofluid instead of pure water increases *H-Tr* in the heat exchanger by *45.37%*. The validity of the obtained results was compared with the experimental data.

Rangbarzad et al. [59] experimentally studied to investigate the effect of using water/graphene oxide nanofluid on the thermo-hydraulic behavior of a copper receiver tube of *PTC*. The ratio of nanofluid concentration was $0 \leq \varphi \leq 0.1\%$ and *Re* was chosen between 5250 and 36500. It was found that there is a 28.15% increment in *H-Tr* at the maximum *NPVF*.

Al-Khatib et al. [60] performed a numerical study about the effect of spherical grooves in the pipe on *H-Tr* in the *PTC*. Different heights of grooves *(1.5-2.5-3.5 mm)* have been used and the flow type has been considered as turbulent flow regime. The working fluid has been utilized as *MWCNT*-Al_2O_3/*water* nanofluid $(\varphi=3\%)$ and the range of *Re* is between *5000 -20000*. As a result, it is found that the groove height of *3.5 mm* shows enhancement in *H-Tr* by *16.99%* compared to height groove of *1.5 mm* at $\varphi=3\%$ and *Re=20000*.

Parsaiemehr et al. [61] numerically investigated to the elucidate hydrothermal performance of a rectangular channel passed nanofluid. Al_2O_3/*water* nanofluid has been passed through the rectangular channel. The range of *Re* is between *15000 - 30000* and the volume fraction of nanoparticles is $0 \leq \varphi \leq 4\%$. The rectangular shape of

Rib changing of their angles from *0°* to *180°* has been added to the bottom side of the channel. The maximum performance of system has been obtained using nanofluid and rib of *60º*.

Muhammad et al. [62] numerically conducted a study using computational fluid dynamics (*CFD*) to investigate the effect of using magnetized nanofluids (Fe_3O_4 and *CuO/Therminol66*) flowing in *PTC* inserted fins. The range of *Re* is between *30000 - 250000* and the volume fraction onanoparticles is $2 \leq \varphi \leq 4\%$. The different magnetic field magnitude $(0 \leq B \leq 0.3T)$ has been applied to the *PTC*. It is found that the use of small *NPVF* leads to an increase in *H-Tr*.

Amina et al. [63] conducted a numerical study about *PTC*. The main aim of these analyses is to determine the effect of the presence of triangular and rectangular fins in the receiver tube of *PTC*, the working fluid used is synthetic oil. *Re* range is between *25700* and *257000*. This investigation has been conducted at a constant inlet temperature of *573 K*. It is reported that the use of the fin leads to an increase in Nusselt number (*Nu*) directly associated with *H-Tr*. Then, it is reached that the friction factor (*ff*) is doubled when using triangular fins compared to the absence of fin in the receiver tube.

Rios et al. [64] experimentally studied on the *H-Tr* performance of Al_2O_3*/water* nanofluid with the *NPVF* of $0 \leq \varphi \leq 3\%$ flowing in the receiver tube of *PTC*. The main purpose of the study is to determine the optimum angle of a collector from *0°* to *20°* to increase thermal efficiency. As a result, the use of the highest *NPVF* with the angle of the collector of *10°* provides the maximum thermal efficiency.

Khakrah et al. [65] carried out a numerical study on how to reduce the entropy production of the receiver tube of *PTC* using synthetic *oil/*Al_2O_3 nanofluid $(0 \leq \varphi \leq 8\%)$ as working fluid. The investigations have been applied under different inlet temperature conditions from *320 K* to *550 K*. The *Re* has been ranged from *3560* to *115000*. Finally, it is shown that the use of nanofluid by 4% improves the thermal efficiency of the receiver by up to *7.6%*.

Bellos et al. [66] numerically studied on the performance of *PTC* by using different types of fluids (pressurized water, *Terminol VP-1*, molten nitrate salt, liquid sodium, air, carbon dioxide and helium) to observe the extent of their effect on thermal efficiency. The type of flow was turbulent regime, and the analyses were carried out at high temperatures as the temperatures ranged between *300 K* and *1500 K*. Finally, it was reached that liquid sodium leads to the maximum effective efficiency (*47.48%*) at inlet temperature of *800 K*. Pressurized water is the best working medium for low and medium temperature levels of up to *550 K*, while carbon dioxide and helium have the priority for temperatures greater than *1100 K*.

Minea et al. [67] performed a numerical study on the effect of using hybrid nanofluids *(Ag–MgO/water, GO–Co_3O_3/60EG: 40 W, Cu–Al_2O_3/water)* on *H-Tr*. *Re* range is between *100* and *3000* and *NPVF* is ranged $0 \leq \varphi \leq 2\%$. The results of the study showed that the use of *Cu-Al_2O_3/water* hybrid nanofluid having the highest viscosity compared to other types of hybrid nanofluid used in this study reduces the *H-Tr*. However, using the *Ag-MgO/Water* hybrid nanofluid with the *NPVF 2%* increases the *H-Tr* up to *14%*.

Ekiciler et al. [68] numerically carried out a study that searching *H-Tr* performance of several types of hybrid nanofluids *(Ag-ZnO/Syltherm 800, Ag-TiO2/Syltherm 800, and Ag-MgO/Syltherm 800)* in the *PTC*. While the *NPVF* has been planned as $0 \leq \varphi \leq 4\%$, the working range has been studied from *10000* to *80000*. The inlet temperature of the working fluid is kept as *500 K*. As a result, the *H-Tr* and thermal efficiency enhance with increasing nanofluid's concentration in base fluid and *Re*. However, thermal efficiency, which is one of the important parameters of *PTC*, decreases with the increase of the *Re*. Then, it is obtained that the use of *Ag-MgO/ Syltherm 800* with *4%* is the one that achieves the best result on *H-Tr*.

Bellos et al. [69] analytically carried out a study to find out the effect of using nanofluids in *PTC* receiver. The nanoparticles (*Al_2O_3 and CuO*) were used in thermal oil (*Syltherm 800*) with constant *NPVF* of *4%* and the type of flow was considered as turbulent regime. The model was developed using *EES* (*Engineering Equator Solver*). Finally, it was found that the use of nanofluids increases *H*-Tr up to *50%*. Also, using (*Syltherm 800 - CuO*) achieves better results than using *Syltherm 800*. As the use of

Syltherm 800-CuO increases the thermal efficiency at a rate of *1.26%*, while the use of *Syltherm 800-*Al_2O_3 is able to increase the thermal efficiency at a rate of *1.13%*.

Vahidinia et al. [70] numerically studied the effect of using Al_2O_3/SiO_2*-Syltherm 800* hybrid nanofluid $(1.5 \leq \varphi \leq 3\%)$ in receiver tube of *PTC*. The range of Re is between 10000 and 22000 and the inlet temperature has been considered in the variety of *550-660 K*. The results show that the energy and strain energy efficiencies of the Al_2O_3/SiO_2*-Syltherm 800* hybrid nanofluid are always the highest, with the maximum improvements compared to those of the base liquid being *5.22%* and *5.49%*, respectively; While for SiO_2 nanofluid they are *1.71%* and *1.75%* and for Al_2O_3 monofluid they are *1.19%* and *1.36%* respectively. Moreover, the hybrid nanofluid is the most suitable with the highest concentration up to *1.76*. The best thermal efficiency of the receiver tube can be obtained using the hybrid nanofluid with the *NPVF 3.0 vol.%* at inlet temperature *600 K* and *Re=10000*.

Bellos et al. [71] has conducted to increase the heat transfer coefficient between the working fluid and the dimpled absorber tube for *PTC* that was designed by using Solid works program. The study has been conducted on three different liquids (thermal oil, thermal oil with nanoparticles and pressurized water) and within the *Re* ranging between *1000-25000*. Finally, it was noted that the use of nanofluids increases the efficiency of the collector by *4.25%* and that improving the geometric shape increases the efficiency of the collector by *4. 55%*.

Bellos et al. [72] numerically carried out a study, evaluating *H-Tr* performance of mono and hybrid nanofluids *(3 vol.%* Al_2O_3*/Oil, 3 vol.%* TiO_2*/Oil, 1.5 vol.%* Al_2O_3*-1.5 vol.%* TiO_2*/Oil)* in the LS-2 type of *PTC*. The inlet temperature of the working fluid is varied from *300* to *650 K*. It is concluded that the use of mono nanofluid positively increases the *H-Tr* performance of the receiver tube compared to pure water while the highest increment in *H-Tr* performance has been acquired using hybrid nanofluid compared to others.

Alnaqi et al. [73] conducted numerical study to examine the hydro-thermal performance of *PTC's* receiver tube inserted two types of twisted tapes (*LCRW-*

LWRC). The receiver tube of *PTC* has been filled with *MgO-MWCNT (80%:20%)/thermal oil (0≤φ≤2%)* hybrid nanofluid and *Re* has been considered between *2500* and *100000*. It is concluded that using the *LCRW* model in the receiver tube and filled with hybrid nanofluid is suggested as the best at *Re<30.873* with *NPVF* of *2%*. However, the use of *the LWRC* model filled with a hybrid nanofluid with *NPVF* of *2%* is proposed as the optimum design for *Re>30.873*.

Bellos et al. [74] numerically studied has been conducted to find out the effect of using longitudinal fins on the heat transfer process in the *PTC* receiver tube. The working fluid *Syltherm 800* has been accepted. Longitudinal fins of different length *(0≤p≤20mm)* and thickness *(0≤t≤6mm)* have been used. The *Re* range between *5000* to *150,000* and the range of inlet temperature is *(400-600 K)*. Finally, the optimum condition of the receiver has been obtained at *t= 4mm* and *p= 6mm* where the thermal efficiency was improved by *0.82%*, and the *Nu* was increased to *65.6%* when using the longitudinal finned receiver tube compared to the smooth receiver tube.

Al-Rashed et al. [75] numerically studied to improve the thermal performance of the *PTC* equipped with turbulator as shown in Figure 2.4 the working fluid was accepted as Al_2O_3*-MWCNT/thermal oil (80%-20%)* hybrid nanofluid. The inlet temperature is *390 K* and solar radiation=*73,000 W/m*^{2}. The *Re* ranges from *10,000 to 100,000*. Finally, the results obtained showed that the use of a finned turbine is beneficial for regeneration less than *12000* and should not be used at values greater than *Re*. The overall hydrothermal performance of *PTSC* is impaired. In addition, the economic analysis revealed that the new engineering can save *14%* of the use of materials as shown in Figure 2.5.

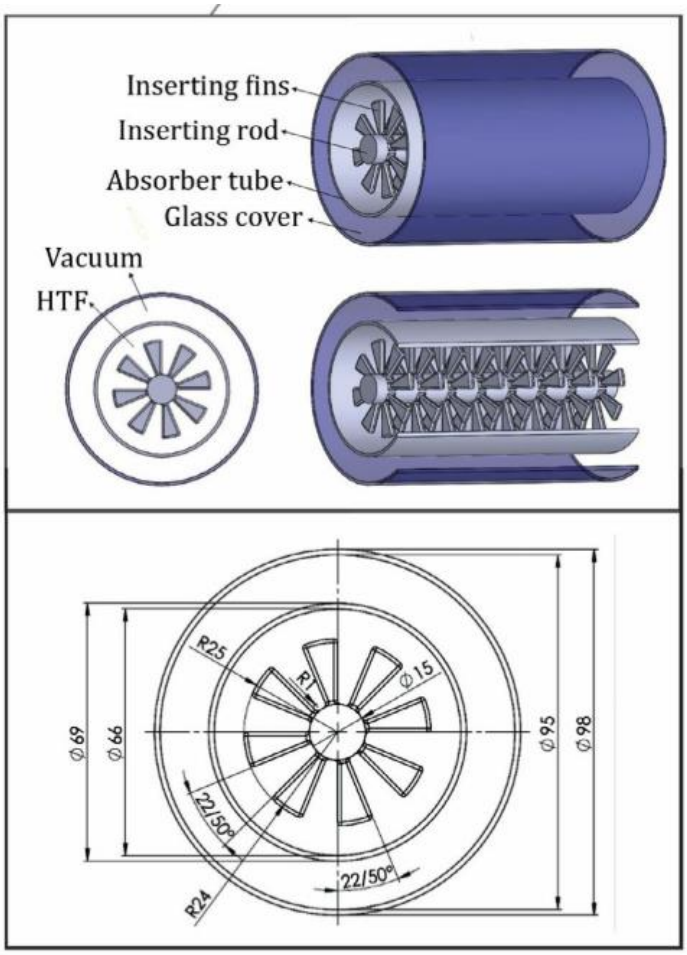

Figure 2.4. Schematic diagrams of the studied *PTSC* [75].

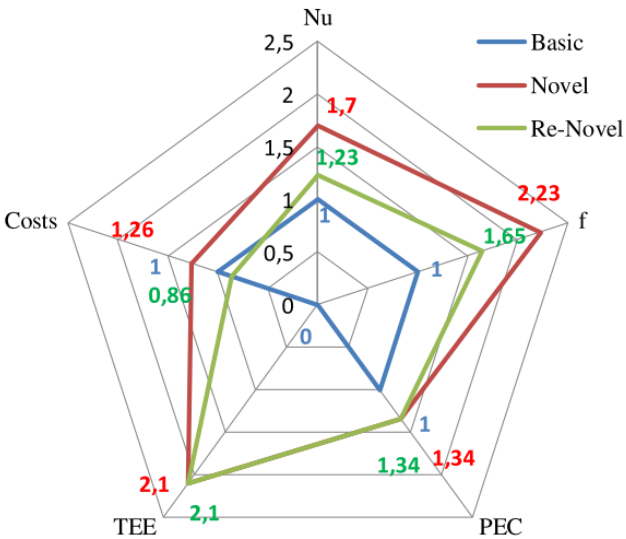

Figure 2.5. Comparison among basic *PTSC*, novel *PTSC* and re-novel *PTSC* in different eco- nomic, thermal and hydraulic parameters [75].

Samiezadeh et al. [76] numerically carried out a study to deal with the thermal performance of *Cu-Al_2O_3/aqueous* hybrid nanofluid *(0-0.02%)* in a *PTC* receiver tube containing longitudinal inner fins. The range of *Re* is between *5,000* and *500,000*. The use of copper nanoparticles in the base liquid is three times more efficient in the process of gaining thermal performance than the Al_2O_3 nanoparticles in it. The volume fraction of *Cu* nanoparticles and Al_2O_3 increased by *0.02* at lower *Re* was found to increase the thermal efficiency *12.2%* with *5.2%* adverse effects on the friction factor; Copper nanoparticles were found to be three times more effective than Al_2O_3 nanoparticles. For Darcy's numbers between *0.01* and *0.1*, high permeability is found to have a slight negative effect on thermal efficiency, but it can reduce the friction factor to a third of its original value. These results can be used to improve the efficiency of solar collectors.

According to the literature review about the use of a hybrid nanofluid in the receiver tube of *PTC* is limited, although studies in which a hybrid nanofluid is used establish better results than using a mono type nanofluid. Therefore, this study is performed using a hybrid nanofluid. As it is explained above, many researchers have been using nanofluids in the fields of solar energy, where nanoparticles have been used inside a *PTC*'s receiver since it is known that nanoparticles have a high ability to improve the *H-Tr*. However, there are few studies on seeing the effect of a change in the receiver's design tube of *PTC*, such as inserting fin types. In this study, it is conducted that an energy and entropy analysis for the *PTC*'s receiver tube containing elliptical dimples, which present higher thermal efficiency in comparison with other dimple types, with different dimensionless parameters (*0.66-1.66*). The type of flow has been considered as turbulent, the *Re* is ranged between *10000* and *30000*. The inlet temperature is considered as constant at *500 K*. The *C++* code has been developed to perform non-uniform heat flux on the outside of the *PTC*'s receiver tube. Mono and hybrid nanofluid types and their combinations with different *NPVF*s have been studied in detail to determine the energy and entropy performance of *PTC*.

PART 3

NUMERICAL STUDY

In this chapter, numerical solution procedure is defined in detail. *ANSYS Fluent 2020R2* commercial program has been used for the numerical calculations. It is conducted that an energy and entropy analysis for the *PTC's* receiver tube containing elliptical dimples, which present higher thermal efficiency in comparison with other dimple types [44,45], with different dimensionless parameters *(ER=0.66-1.66)*. The type of flow has been considered turbulent, the *Re* is ranged between *10000* and *30000*. The inlet temperature is considered as constant at *500 K*. The C++ homemade code has been developed to perform non-uniform heat flux on the outside of the *PTC's* receiver tube to approximate real-life standards. Mono and hybrid nanofluid types and their combinations with different *NPVF (TiO2/Syltherm800, Al_2O_3/Syltherm800)* have been studied in detail to determine the energy and entropy performance of *PTC*. To explain *H-Tr* and entropy performance of *PTC* comprehensively, the mono and hybrid nanofluid configurations are designed as follows; *2%TiO_2/Syltherm800, 2%Al_2O_3/Syltherm800, 1.0%TiO_2-1.0%Al_2O_3/Syltherm800 ,1.5%TiO_2-0.5%Al_2O_3/Syltherm800,and 0.5%TiO_2-1.5%Al_2O_3/Syltherm800.* Figure 3.1 indicates *3D* view of parabolic trough collector and parameters. Parameters of the numerical study are also shown in Table 3.1.

Table 3.1. The parameters of the numerical study.

Working fluid	*TiO_2/Syltherm800, Al_2O_3/Syltherm800, TiO_2-Al_2O_3/Syltherm800*
Nanoparticle volume fraction (*NPVF*)	*0.5%, 1%, 1.5%, 2%*
Reynolds number (*Re*)	*10000, 20000, 30000*
Dimples elliptical ratio (*ER*)	*5/3, 3/2, 3/5, 2/3*

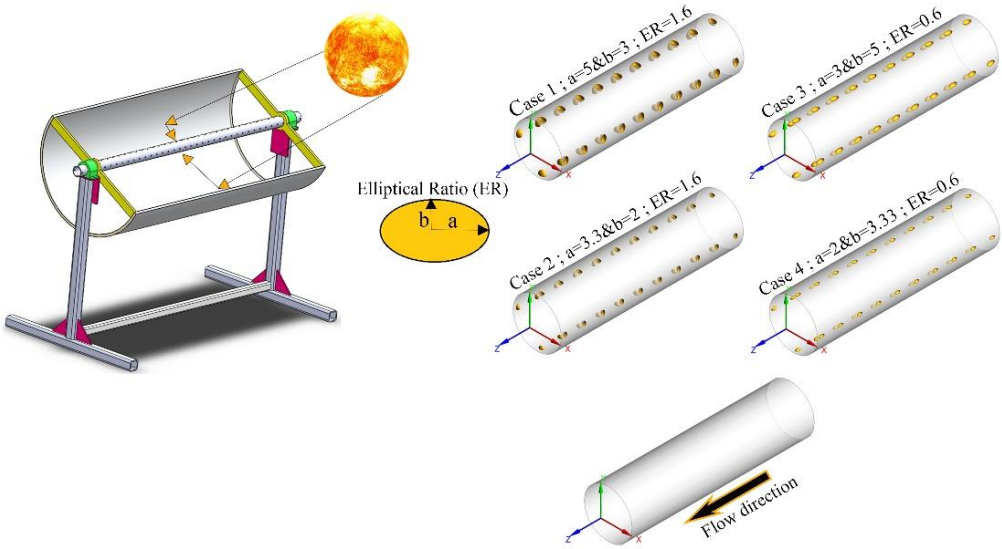

Figure 3.1. *3D* view of parabolic trough collector and numerical parameters.

3.1. PHYSICAL MODEL

The physical shape of the *PTC* type *LS-2* comprises a reflective surface with a parabolic shape and the receiver. The receiver is made of 316L steel with a length of *7.8 m*, the inner and outer diameters are *0.066* and *0.070 m*, respectively [77]. It has been analyzed for five different configurations including four different elliptical dimple designs and one smooth receiver. The design of dimples has been defined with elliptical ratio (*ER*=a/b), where (a) is the horizontal radius and (b) represents the vertical radius of the elliptical dimple. Also, it is taken two values for the elliptical ratio (0.66 and1.66) of the dimples, which exist in the receiver tube as shown in Figure 3.2 the distance between each dimple is *0.485 m.* Table 3.2 indicates the physical properties of the receiver. The type of flow has been considered turbulent and steady state. It has been considered that the fluid is incompressible. The effect of buoyancy has been neglected in this study [78,79]. It has been considered that the fluid is incompressible. The effect of buoyancy has been neglected in this study. Several studies can be seen that ignore the effect of buoyancy [78,79]. Table 3.3 also indicates the receiver geometrical dimensions [77].

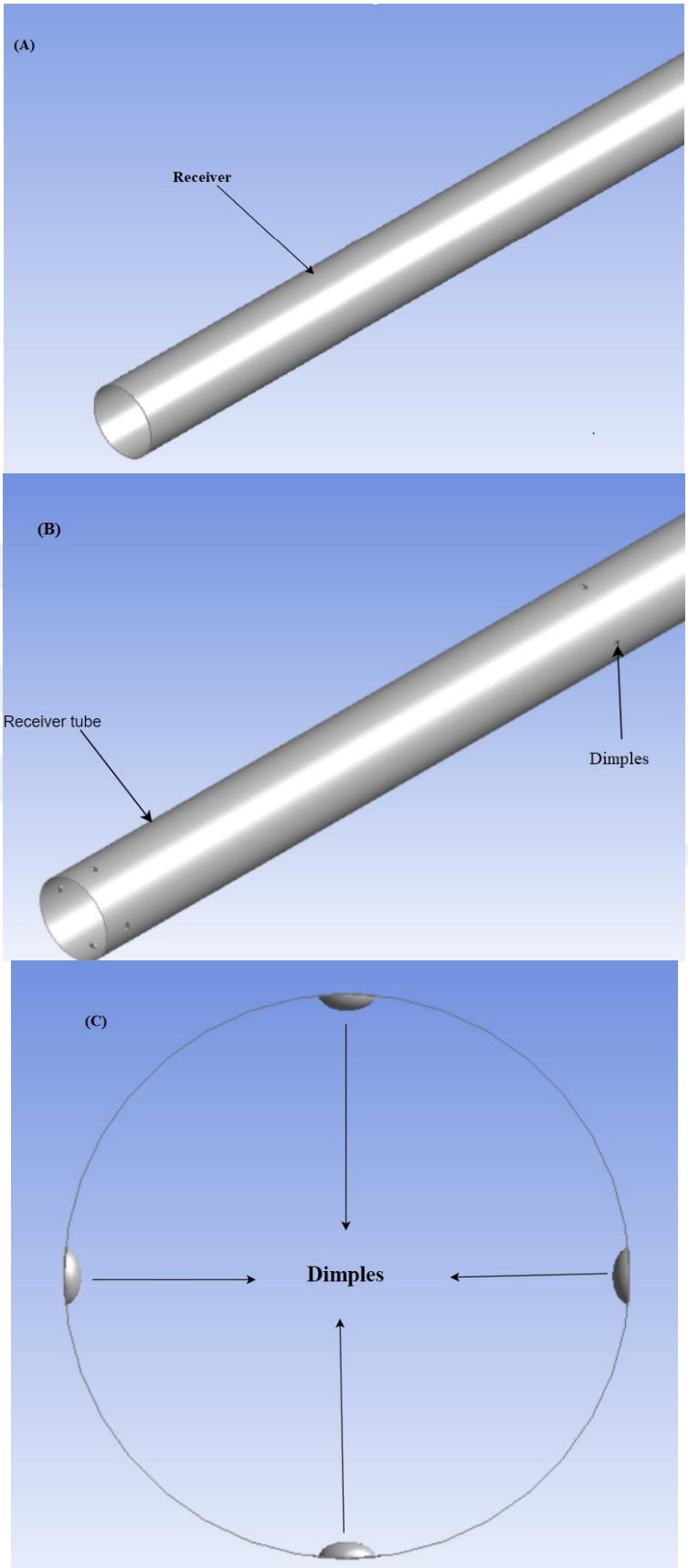

Figure 3.2. Modeled (a)Receiver without dimples (b) Receiver with dimples(c) front view of dimpled receiver.

Table 3.2. Physical properties of the receiver [80].

k [W/m.K]	***C_P [J/kg.K]***	***ρ [kg/m^3]***
24.92	502.48	8030

Table 3.3. Geometrical dimensions of the receiver [77].

Outer diameter (*m*)	Inner diameter (*m*)	Length of receiver (*m*)
0.07	*0.066*	*7.8*

3.2. GOVERING EQUATIONS

The equations that used in three-dimensional turbulent flow numerical simulations are as follows [81];

Continuity:

$$\frac{\partial \rho}{\partial t} + \frac{\partial(\rho u_i)}{dx} = 0 \tag{3.1}$$

Momentum:

$$\frac{\partial(\rho u_i)}{\partial t} + \frac{\partial(\rho u_i u_j)}{\partial x_j} = -\frac{\partial P}{\partial x_i} + \frac{\partial}{\partial x_j}[\mu(\frac{\partial u_i}{\partial u_j} + \frac{\partial u_j}{\partial x_i} - \frac{2}{3}\delta_{ij}\frac{\partial u_i}{\partial x_j})] + i\frac{\partial}{\partial x_j}(-\rho\overline{u'_i u'_j}) \tag{3.2}$$

Energy:

$$\frac{\partial}{\partial t}(\rho E) + \frac{\partial}{\partial x_i}\left[u_i(\rho E + \Pr)\right] = \frac{\partial}{\partial t}\left[\left(k + \frac{C\mu_i}{\Pr_t}\right)\right]\frac{\partial T}{\partial x_j} + \mu_i(\tau_{ij})_{eff} \tag{3.3}$$

Because of the Boussinesq hypothesis, Reynolds stress has been expressed by the following equation [82]:

$$-\rho\overline{u'_i u'_j} = \mu_t\left(\frac{\partial u_i}{\partial x_j}+\frac{\partial u_j}{\partial x_i}\right)-\frac{2}{3}\left(\rho k+\mu_t\frac{\partial u_i}{\partial x_j}\right)\delta_{ij} \tag{3.4}$$

where k represents the turbulent kinetic energy as it is in the following equation:

$$k=\frac{\left(\overline{u'^2}+\overline{v'^2}+\overline{w'^2}\right)}{2} \tag{3.5}$$

Most of the internal flow type analyses that have turbulent flow type carrying out k–ε to get accurate and more correct results [82–84]. To apply the k–ε turbulence model, Eq. (3.6) and Eq. (3.7) are used. The kinetic energy transfer of the turbulent (k), as well as the turbulent dissipation equations (ε) are given in Eq. (3.6) and Eq. (3.7), respectively.

$$\frac{\partial}{\partial t}(\rho k)+\frac{\partial}{\partial x_j}(\rho k u_j)=\frac{\partial}{\partial x_j}\left[\left(\mu+\frac{\mu_t}{\sigma_k}\right)\frac{\partial k}{\partial x_j}\right]+G_k+G_b-\rho\varepsilon-Y_M+S_k \tag{3.6}$$

$$\frac{\partial}{\partial t}(\rho\varepsilon)+\frac{\partial}{\partial x_j}(\rho\varepsilon u_j)=\frac{\partial}{\partial x_i}\left[\left(\mu+\frac{\mu_t}{\sigma_\varepsilon}\right)\frac{\partial\varepsilon}{\partial x_j}\right]+\rho C_1 S\varepsilon-\rho C_2\frac{\varepsilon^2}{k+\sqrt{\nu\varepsilon}}+C_{1\varepsilon}\frac{\varepsilon}{k}C_{3\varepsilon}G_b+S_\varepsilon \tag{3.7}$$

$$G_K=-\rho\overline{u'_i u'_j}\frac{\partial u_i}{\partial x_j} \tag{3.8}$$

where, σ_ε and σ_k show Prandtl number when the flow is turbulent, that relating of k and ε in Eq. (3.6) and Eq. (3.7), respectively. The production of turbulent kinetic energy is calculated from Eq. (3.8) and is symbolized by G_K.

The Re is calculated by the equation [81]:

$$Re=\frac{\rho V D}{\mu} \tag{3.9}$$

where, $\rho[kg.m^{-3}]$ shows fluid density, V $[m.s^{-1}]$ represents the average fluid velocity, D $[m]$ is the hydraulic diameter of the receiver tube, μ $[Pa.s]$ is the viscosity of the working fluid.

Eq. (3.10) expresses to convection heat transfer coefficient [81]:

$$h = \frac{q''}{(T_w - T_b)_{avg}} \tag{3.10}$$

where, q'' $[W.m^{-2}]$ is the value of non-uniform heat flux that applied on the outer surface of the receiver, T_W $[K]$ shows the wall temperature, T_W $[K]$ is also obtained through $(T_{inlet}+T_{outlet})/2$.

Nu is expressed in Eq. (3.11) [81]:

$$Nu = \frac{hD}{k} \tag{3.11}$$

where k $[W.m^{-1}.K^{-1}]$ is represented to the fluid thermal conductivity, h $[W.m^{-2}.K^{-1}]$ is convection heat transfer coefficient.

Eq. (3.12) shows the definition of ff [81]:

$$ff = \frac{\Delta P}{\left(\frac{L}{D}\right)\cdot\left(\frac{\rho \cdot V^2}{2}\right)} \tag{3.12}$$

where ΔP $[Pa]$ is the pressure loss and L $[m]$ is the length of the receiver tube.

Thermal efficiency of the receiver is calculated from the formula given below [67]:

$$\eta_{th} = \frac{\left(\dot{m} C_p \Delta T\right)_{eff.}}{I A_p} \tag{3.13}$$

where $\dot{m}$ [$kg.s^{-1}$] is the mass flow rate value of the working fluid, C_P [$kJ.kg.K^{-1}$] is the specific heat of the fluid, ΔT [K] is the temperature difference and A_P [m^2] is the aperture area of the receiver tube.

The Performance Evaluation Criterion (*PEC*) is a dimensionless number, and it is expressed by the ratio of the convection heat transfer to the hydraulic performance for thermal applications. It is measured by the following equation [68]:

$$PEC=\frac{\left(Nu_{hnf}/Nu_{bf}\right)}{\left(ff_{hnf}/f_{bf}\right)^{\frac{1}{3}}} \tag{3.14}$$

where, Nu_{hnf} and ff_{hnf} defines elliptical dimpled tube. Also, Nu_{bf} and f_{bf} explain smooth tube.

3.3. MONTE CARLO RAY TRACING (MCRT) METHOD AND STATE OF BOUNDARY FOR GEAT FLOW

One of the most important factors in the numerical analysis of *PTC* performance is the modelling of sunlight falling on the absorber. As is known, the intensity of sunlight reflected from the parabola reflector to the absorber is much higher than the intensity of sunlight that falls directly on the absorber. Therefore, the outer plane of the absorber facing the reflecting surface is parabolically heated more than other surfaces. Due to this situation, a heterogeneous distribution of heat flow occurs over the surface of the absorber tube. Here, the open source and free *SOLTRACE* package software is used to obtain a heterogeneous heat flux around the perimeter of this absorber. *SOLTRACE* is a software tool developed at the National Renewable Energy Laboratory (*NREL*) to model (*CSP*) systems and analyse their optical performance [85]. It is using the Monte Carlo optical ray tracing method to model and analyse intensive solar energy systems developed by *NREL* [86]. The parabolic reflector, absorption tube and reflected rays generated in *SOLTRACE* software are shown in Figure 3.3 the value of direct solar radiation (850 W/m^2) distributed asymmetrically along the circumference of the *PTC*`s

receiver, which is used in the *ANSYS Fluent 2020R2* program, has been obtained from the SOLTRACE program. A curve fitting method was used for the heat flow distribution. Considering the data obtained by the method of fitting the curve, the equation of the heat flow distribution curve was found. The equation for the curve found is coded in the *C++* programming language and this code is given in the *C* annotations. The encoded heat flow curve equation has been moved to *ANSYS Fluent* with User Defined Function (*UDF*). in the numerical study [36]. Figure.3.5 (a) indicates to the Local Concentration Ratio (*LCR*). The diagram of the condition of the heat flow limits to be used and the heat angle distribution on the absorber tube (with dimples) obtained in program is shown in Figure. 3.5 (b).

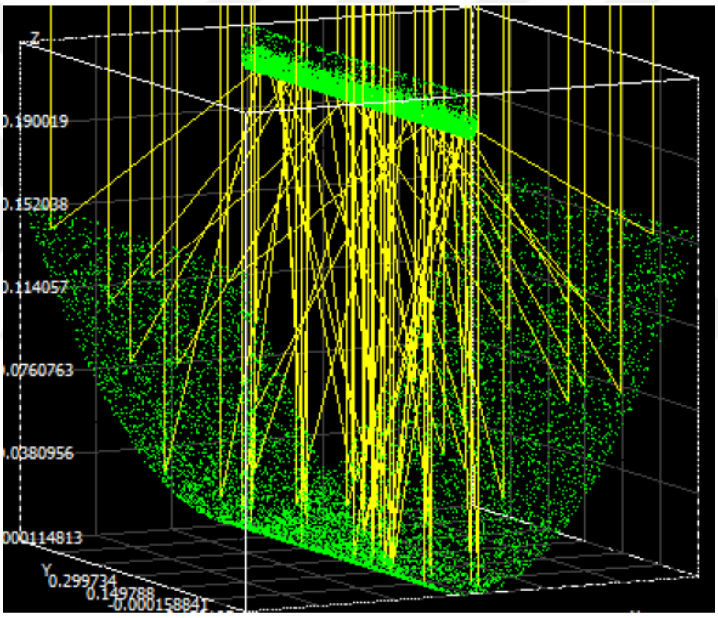

Figure 3.3. Modelling *PTC* in SOLTRACE [36].

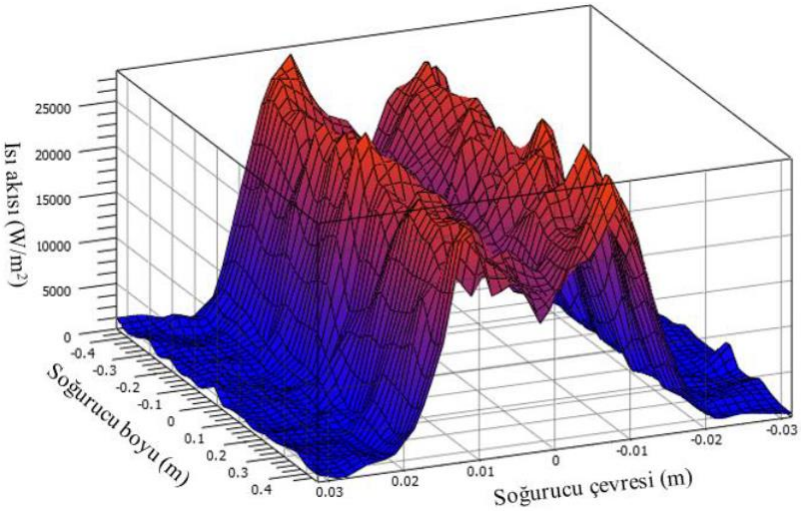

Figure 3.4. The heat flux distribution of the receiver modelled in *SOLTRACE* [36].

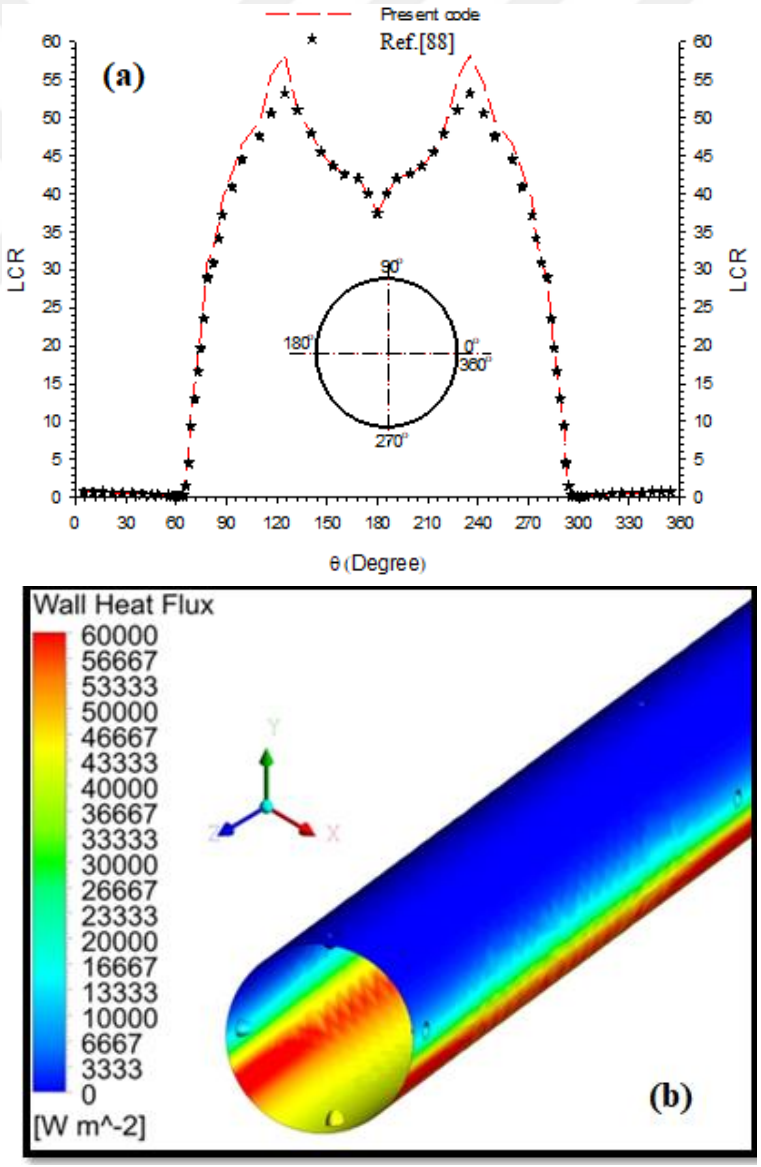

Figure 3.5. (a) Validation of local concentration [87], (b) Heat flux distributed on the outer surface of the receiver tube of *PTC*.

3.4. BOUNDARY CONDITIONS

- The uniform velocity and temperature are taken at the inlet section.
  $T=T_i=500\ K,\ u=V_{in},\ v=w=0$
- At the outlet of the receiver the pressure is equal to the atmospheric pressure:
  $P=P_{gage}=0$
- The non-uniform heat flux profile has been created using Monte Carlo Ray Tracing (MCRT) method used in this study [88]. Also, C++ code in-home made has been written for the whole surface of the receiver regarding the non-uniform heat flux profile.
- Because the analyses done in the study will be only for the receiver, the radiation emitted by the receiver has been ignored [68,89,90].
- The ambient temperature is 22 ^oC [91].

3.5. EQUATIONS OF ENTROPY PRODUCTION

The entropy generation has been calculated as the sum of the heat transfer and the frictional entropies, respectively [68].

$$S'''_{gen} = \left(S'''_{gen}\right)_H + \left(S'''_{gen}\right)_F \tag{3.15}$$

The entropy generation of frictional and heat transfer entropies are determined by [92,93]:

$$\left(S'''_{gen}\right)_F = \frac{\mu}{T}\left(\frac{\partial \overline{u}_i}{\partial x_j} + \frac{\partial \overline{u}_j}{\partial x_i}\right)\frac{\partial \overline{u}_i}{\partial x_j} + \frac{\rho\varepsilon}{\overline{T}} \tag{3.16}$$

$$\left(S'''_{gen}\right)_H = \frac{k}{\overline{T}^2}\left(\nabla\overline{T}\right)^2 + \frac{\alpha_t}{\alpha}\frac{k}{\overline{T}^2}\left(\nabla\overline{T}\right)^2 \tag{3.17}$$

Eq. (3.15) – (3.17) determine the local entropy production rate sourced from heat transfer and frictional irreversibility. Where, α [$m^2.s^{-1}$] represents the thermal diffusivity. Eq. (3.18) indicates the volumetric integral of the entropy generation rate of the whole calculation domain of the fluid.

$$S_{gen} = \iiint_{v} S_{gen}^{'''} dv \tag{3.18}$$

Eq. (3.19) consists of two parts, the first section expresses the entropy generation because of the heat transfer irreversibility and the second section represents the entropy generation because of the frictional irreversibility [94].

$$S^{'} = \frac{q^2}{\pi \lambda T_{bulk}^2 Nu} + \frac{32 \dot{m}^3 c_f}{\pi^2 \rho^2 . T_{bulk} D^5} \tag{3.19}$$

where, $c_f = (-dp/dx)\rho D/2G^2 c_f = (-dp/dx)\rho D/2G^2$

The Bejan number (*Be*) represents the ratio of entropy generation due to the heat transfer irreversibility to the total entropy generation [94]:

$$Be = \left(S_{gen}'''\right)_H / S_{gen}''' \tag{3.20}$$

The condition of *Be* is close to unity refers the dominant heat transfer irreversibility in the flow domain while *Be* is close *0* means that the frictional irreversibility is dominant [94].

3.6. THERMO PGYSICAL PROPERTIES OF NANOFLUID

3.6.1. Thermo-Physical Properties of Mono Type Nanofluid

The following Eq. (3.21) – (3.24) show the method to calculate the thermophysical properties (like density, specific heat, thermal conductivity, and dynamic viscosity of mono type nanofluids.

Pak's and Cho's study indicate to calculate density [95]:

$$\rho_{nf} = (1-\varphi)\rho_{bf} + \varphi\rho_{np} \tag{3.21}$$

Eq. (24) indicate of the specific heat of mono type nanofluid [96]:

$$(\rho c_p)_{nf} = (1-\varphi)(\rho c_p)_{bf} + \varphi(\rho c_p)_{np} \tag{3.22}$$

The dynamic viscosity of mono type -nanofluid is acquired from [97].

$$\mu_{nf} = \frac{\mu_{bf}}{(1-\varphi)^{2.5}} \tag{3.23}$$

The thermal conductivity of mono type -nanofluid can be calculated from [98]:

$$\frac{k_{nf}}{k_f} = \frac{k_{np} + 2k_{bf} - 2\varphi(k_{bf} - k_{np})}{k_{np} + 2k_{bf} + \varphi(k_{bf} - k_{np})} \tag{3.24}$$

3.6.2. Thermo-Physical Properties of Hybrid Nanofluid

The following equations show how to calculate the thermophysical properties (density, heat capacitance, dynamic viscosity, and thermal conductivity) of hybrid nanofluids [99]:

$$\rho_{hnp} = \frac{\rho_{p1}\varphi_{p1} + \rho_{p2}\varphi_{p2}}{\varphi} \tag{3.25}$$

ρ_{hnp} ($kg.m^{-3}$) indicate to hybrid nanofluid density, φ is nanoparticle volume fraction, p_1, p_2 are nanoparticle types [100].

$$C_{p_{hnp}} = \frac{C_{p_{p1}}\varphi_{p1} + C_{p_{p2}}\varphi_{p2}}{\varphi} \tag{3.26}$$

$C_{P\ hnp}$ ($J.kg^{-1}.K^{-1}$) is the specific heat of hybrid nanofluid density [101].

$$k_{hnp} = \frac{k_{p1}\varphi_{p1} + k_{p2}\varphi_{p2}}{\varphi} \tag{3.27}$$

k_{hnp} ($W.m^{-1}.K^{-1}$) is thermal conductivity of hybrid nanofluid density [101].

$$\varphi = \varphi_{p1} + \varphi_{p2} \tag{3.28}$$

$$\mu_{nf} = \frac{\mu_{bf}}{(1-\varphi)^{2.5}} \tag{3.29}$$

Table 3.4. Indicates the thermophysical properties of the nanoparticle that are used to calculate the physical properties of nanofluids that are used in the formation of hybrid nanofluids.

Table 3.4. The properties of nanoparticles and base fluid [68,102].

	ρ(kg/m³)	***C_P(J/kg.K)***	***λ(W/m.K)***	***μ (pa s)***
Syltherm 800	*747.2*	*1962*	*0.0961*	*0.00084*
Al_2O_3	*3970*	*765*	*40*	-
TiO_2	*4175*	*692*	*8.4*	-

3.7. NUMERICAL PRODUCE

ANSYS Fluent 2020R2 program has been used to get numerical solutions by solving *RANS* equations considering the boundary conditions. Firstly, the receiver has been drawn for a *PTC* containing smooth and elliptical dimpled receiver, separately. *Ansys Design Modeler* module has been used to implement the first step, after which a mesh

structure has been created. The mesh structure consists of approximately *4000000* elements. In the third step, boundary conditions have been applied to the receiver tube, where the *k-e* turbulence model has been used, and to achieve better results, the enhanced wall treatment (*EWT*) has been used, as well as the application of *UDF* on the wall of the receiver tube to obtain results closer to the in-real-life conditions, the *COUPLED* method has been chosen since it is known that it is used for heat transfer application and gives realistic results [82]. The numerical iterations continue until the residuals are equal to 10^{-6}.

3.8. MESH STUDY

The correctness of the formation of the mesh structure has a very big impact on the validity of the results that will be obtained at the end of the numerical analysis. The more dense the network is in the areas near the wall exposed to penetration, the better the results will be due to changes in pressure and temperature that will affect the other data results on place near the wall [103].

It has been concluded that more accurate and realistic results can be obtained when applying inflation to areas near the wall, because when applying inflation, it can specify the thickness layers that near the wall, can make the mesh dense in the areas near the wall. In this numerical study, applied five thickness layer inflation to the surface of the tube where *k-e* turbulence model was used to get better results. Because the researchers found that it can get more realistic results with y + when using *k-e* turbulence model [86]. All mesh studies have been done at *Re= 30000* with smooth pipe. Table 3.5 indicate the results have been obtained from the study of the mesh structure. As it was shown from Table 3.5. That the mesh structure *1894500* is the best and fastest in giving the result. As it was noticed that after mesh *No. 13*, the values of the exit temperature and pressure are almost constant, so *1894500* is the optimum amount of mesh. Figure 3.6 shows the formation of the mesh on the receiver tube of the *PTC*.

Table 3.5. Mesh independency study.

Mesh No	Mesh Number	y+	Pressure Drop	T_{wall}	T_{outlet}
1	336180	8.474648	300.7161	525.7951	512.6994
2	460800	6.397361	303.2021	526.1975	512.6891
3	620000	4.319669	310.5754	529.4393	512.6891
4	736100	3.662190	302.7889	530.7561	512.6826
5	905250	3.192372	299.5044	530.7223	512.6774
6	1089000	3.197772	299.8580	530.6959	512.6727
7	1341900	2.827879	295.8429	529.7535	512.6660
8	1524400	2.827349	295.3995	529.7692	512.6634
9	1816700	2.536792	292.9497	528.4251	512.6592
10	2380950	2.105942	290.8069	526.5214	512.6561
11	3165000	1.683221	289.7866	526.1884	512.6527
12	1616400	1.802110	289.6151	526.1007	512.6592
13	**1894500**	**0.575876**	**289.0000**	**526.3413**	**512.6592**
14	2694000	0.679811	288.9389	526.2160	512.6592
15	2345000	0.484312	289.2145	526.4674	512.6561
16	2534000	0.482409	288.6069	526.5113	512.6561

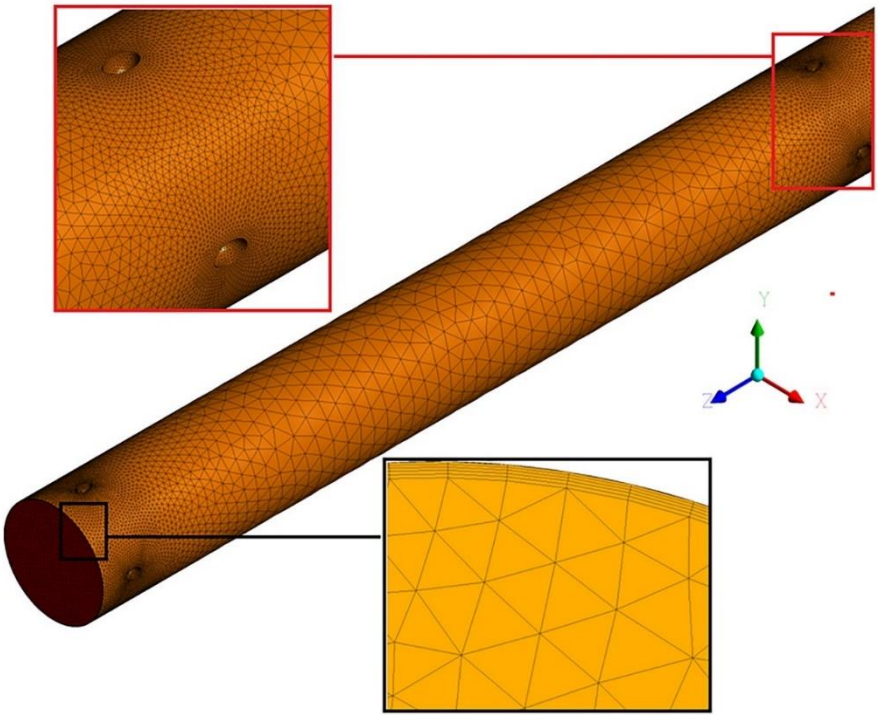

Figure 3.6. View of mesh distribution on the receiver tube of *PTC*.

PART 4

RESULT AND DISCUSSION

In this section, the thermal properties and heat flow are investigated as well as energy and entropy analysis to determine the effects of using hybrid nanofluid as working fluid and elliptical dimples located on the receiver surface on the thermal performance of the *PTC*. In the numerical analyses six different working fluids with different *NPVF* have been used (*Syltherm800, 2%TiO_2/Syltherm800, 2%Al_2O_3/Syltherm800, 1.0%TiO_2-1.0%Al_2O_3/Syltherm800 ,1.5%TiO_2-0.5%Al_2O_3/Syltherm800, and 1.5%Al_2O_3-0.5%TiO_2/Syltherm800*). On the other side, five different receiver types have been investigated with using different elliptical dimple ratios (*ER=a/b=5/3, 3.3/2, 3/5, 2/3.3*) located on the receiver surface. After that the graphs have been presented for each of (*Nu, ff, PEC,* $\left(S_{gen}'''\right)_F$, $\left(S_{gen}'''\right)_H$, S_{gen}, *Be).* Then the best working fluid and *ER* for the receiver that helped to increase thermal efficiency have been determined. The temperature and velocity distribution at outlet of *PTC`s* receiver have been drawn for best case (*ER* of *PTC`s* receiver and working fluid). Finally, the velocity distribution for the best case at different places of the receiver length has been illustrated.

٤,١. *CFD* MODEL VALIDATION

To verify the validity of the results obtained in the study, some of the previous experimental study and well-known correlations in the literature has been selected. Experimental studies of Vahidinia et al. [70] and Dudley et al. [91] are used to verify the numerical results. When comparing the data of Vahidinia et al. [70] and Dudley et al. [91] with the current study using *Syltherm 800* as working fluid, it is clearly seen that the numerical study results are harmonious with literature as shown in Figure 4.4. It is found that the error rate does not exceed *0.42%*. When comparing the current study results with Dudley's [91] data, it is noticed that the error rate does not exceed

0.5%. Then, the *Nu* is compared with the correlation of Dittus–Boelter [104] and Gnielinski [105]. As can also be seen in Figure 4.2 (a), the error rates are *1.8%* and *0.98%* for Dittus–Boelter [104] and Gnielinski [105] relations, respectively.

Dittus-Boelter correlation[104]:

$$Nu = 0.023\,\mathrm{Re}^{0.8}\,\mathrm{Pr}^{0.4} \tag{4.1}$$

Gnielinski correlation [105]:

$$Nu = \frac{(f/8)(\mathrm{Re}-1000)\mathrm{Pr}}{1+12.7(f/8)^{0.5}(\mathrm{Pr}^{2/3}-1)} \tag{4.2}$$

Gnielinski correlation is valid for $0.5 \leq Pr \leq 2000$ and $3000 \leq Re \leq 5000000$ [105]. The numerical results for ff have also been compared with correlations of Petukhov [106] and Blasius. It is determined that the error rates between the present study and Petukhov [106] and Blasius [107]correlations are *0.4%* and *1.78%*, respectively. Figure 4.2 (b) indicates the validation of numerical results of ff with literature correlations given below.

Petukhov correlation[106];

$$ff = (0.790\ln \mathrm{Re} - 1.64)^{-2} \tag{4.3}$$

Blasius correlation [107]:

$$ff = 0.316\,\mathrm{Re}^{-0.25} \tag{4.4}$$

Blasius correlation is approved for $4000 \leq Re \leq 100000$ [107].

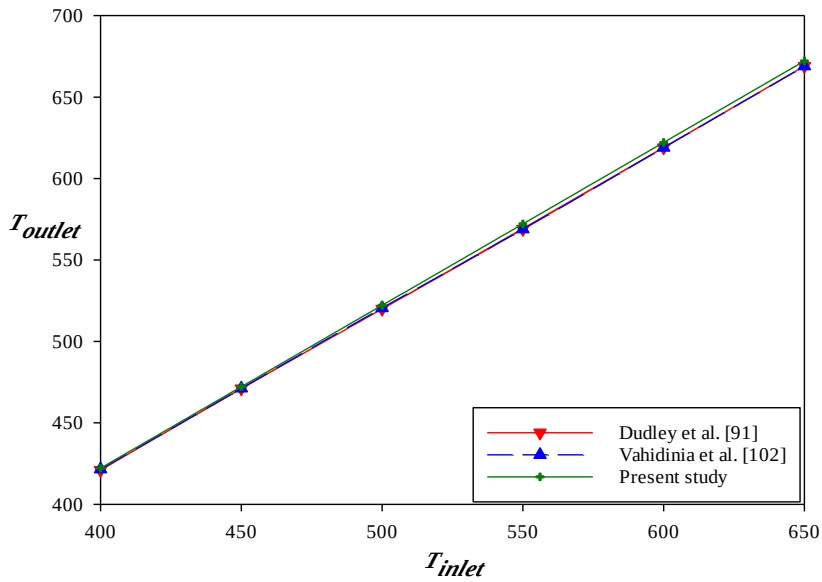

Figure 4.1. Validation of outlet temperature according to experimental data of Dudley et al. [91] and Vahidinia et al. [102].

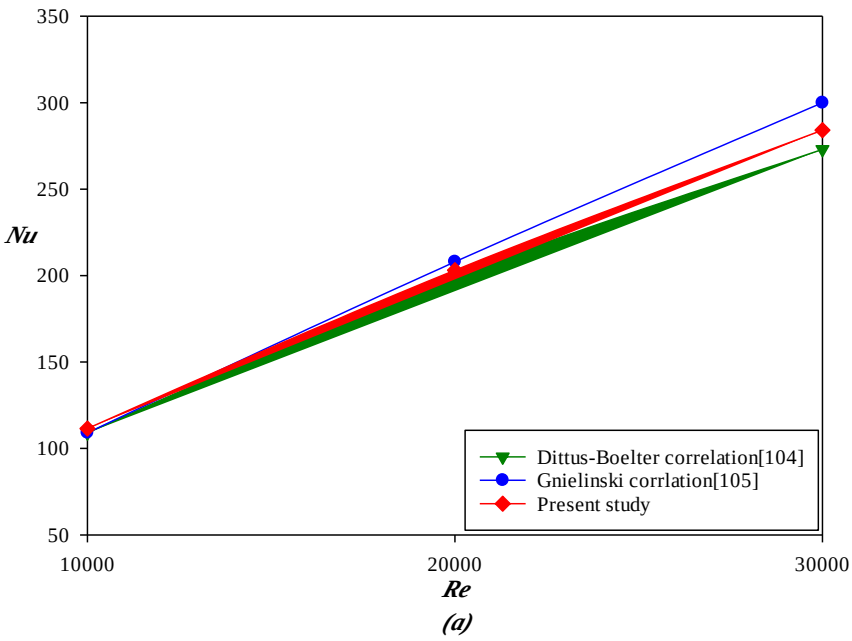

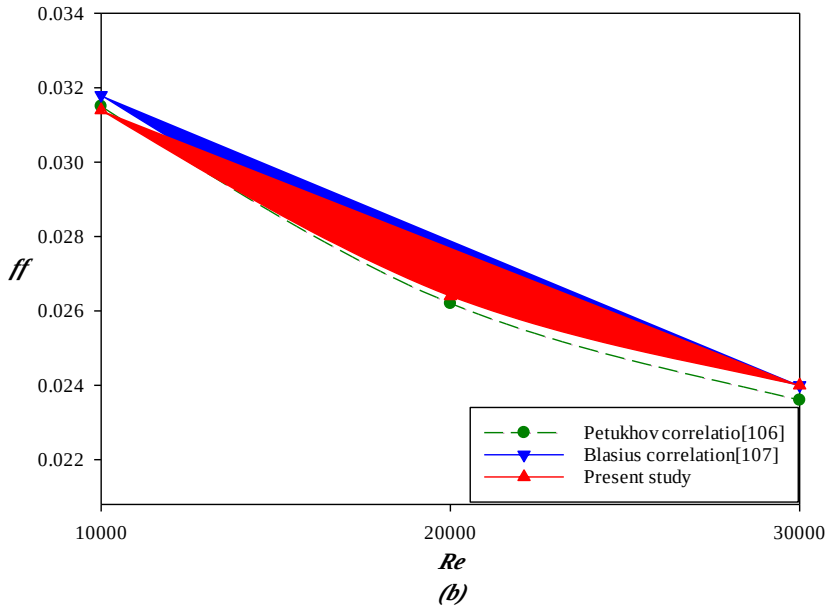

Figure 4.2. Validation of current study: (a) *Nu* with correlations of Dittus-Boelter [104] and Gnielinski [105], (b) *ff* with correlations of Petukhov [106] and Blasius [107].

٤.2. NUSSELT NUMBER

The Nusselt number is defined as the ratio of convection to heat transfer at a boundary in nanofluid. In this section, the *Nu* has been calculated for each *NPVF* with different

elliptical ratio of the receiver tubes for *PTC*. On the other hand, the highest value that the *Nu* reached has been determined, and the type of hybrid nanofluid with its fraction volume have been chosen. At the same time, the best case of elliptical ratio for the receiving tube for *PTC* has been chosen. In Figure 4.3, the Nusselt number for mono nanofluids and hybrid nanofluids with different concentrations has been studied, and inside each receiving tube contains dimples with different elliptical ratio separately. It is determined that the highest Nusselt number is achieved when the hybrid nanofluid of *1.5 %*Al_2O_3*-0.5%*TiO_2*/Syltherm800*.

Since the high stability level of TiO_2, And the Al_2O_3 has a high ability to improve the heat transfer process. As the heat transfer in the nanofluid increases when it is an increase in the Nusselt number. The same is the case in the smooth tube as shown in Figure 4.3 (e) where obtained the highest value of Nusselt number at the hybrid nanofluid of *1.5 %*Al_2O_3*-0.5%*TiO_2*/Syltherm800*.

This means that the best nano-hybrid fluid has been identified and can achieve a greater heat transfer process. It`s been noticed that the Nusselt number increases with increasing Reynolds number, as the result *Nu* rise in the smooth tube by *62%*, while in the receiving tubes containing dimples the number Nusselt increases with Increasing the Reynolds number by ratio *57%*. The increase in the Reynolds number means an increase in the velocity between the nanoparticles and the increase in the movement of the nanoparticles leads to an increase in the energy exchange in the nanofluid with the presence of the effect of shear stress on the wall and in the end all this leads to an improvement in the thermal dispersion of the nanofluid.

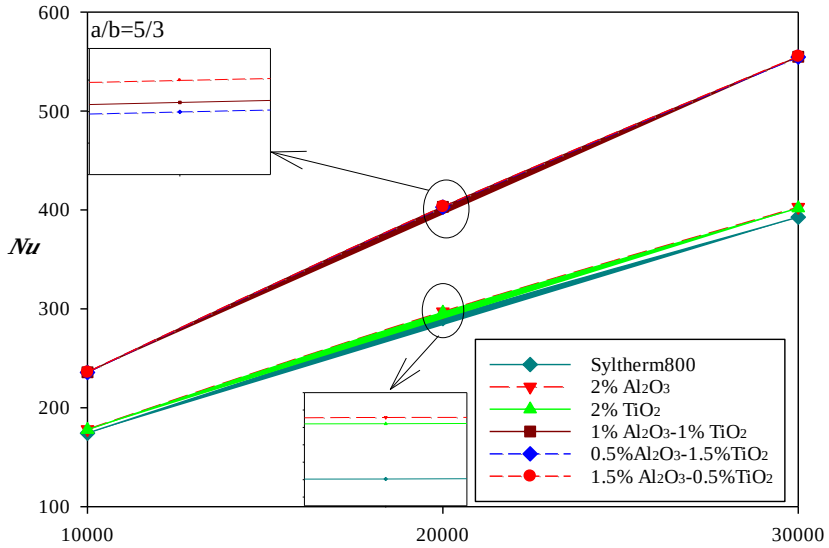
a/b=5/3
600
500
400
300
200
100
Nu
10000
20000
30000
Re
Syltherm800
2% Al2O3
2% TiO2
1% Al2O3-1% TiO2
0.5%Al2O3-1.5%TiO2
1.5% Al2O3-0.5%TiO2

(a)

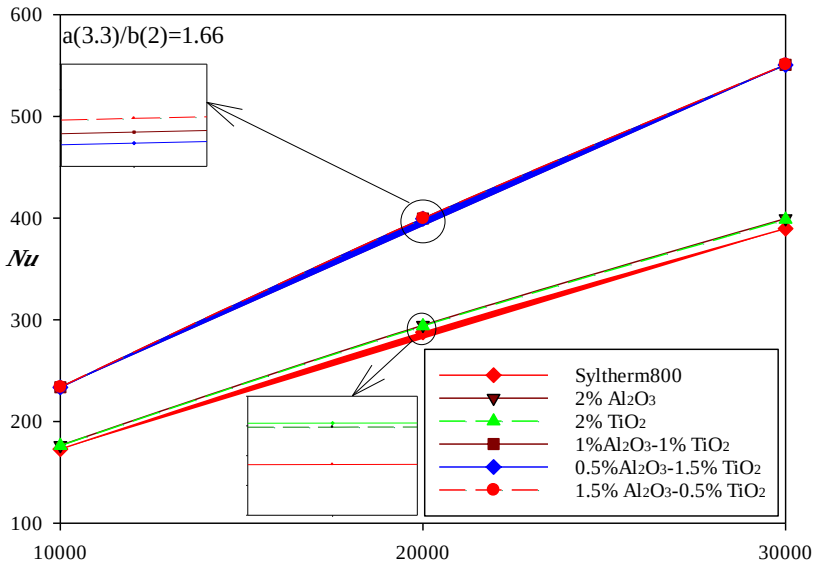
a(3.3)/b(2)=1.66
600
500
400
300
200
100
Nu
10000
20000
30000
Re
Syltherm800
2% Al2O3
2% TiO2
1%Al2O3-1% TiO2
0.5%Al2O3-1.5% TiO2
1.5% Al2O3-0.5% TiO2

(b)

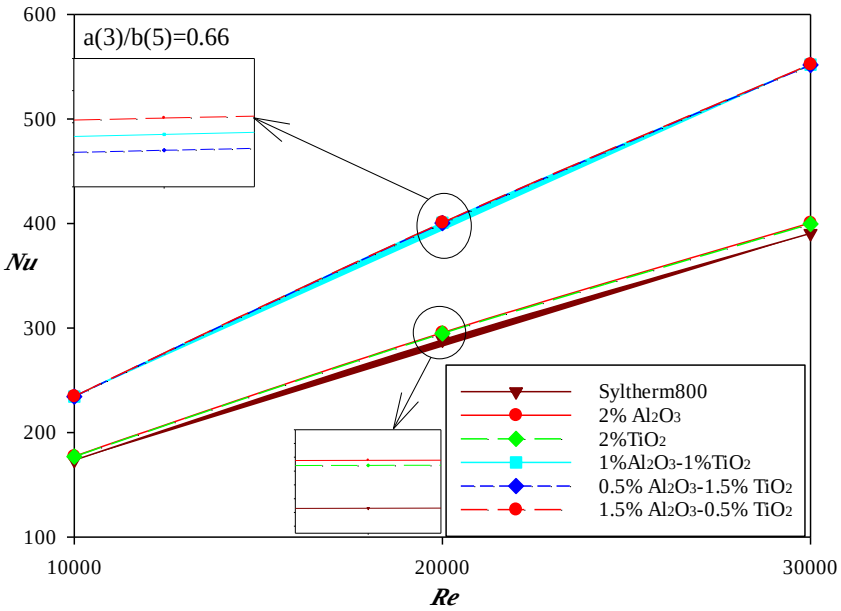
a(3)/b(5)=0.66
600
500
400
300
200
100
Nu
10000
20000
30000
Re
Syltherm800
2% Al2O3
2%TiO2
1%Al2O3-1%TiO2
0.5% Al2O3-1.5% TiO2
1.5% Al2O3-0.5% TiO2

(c)

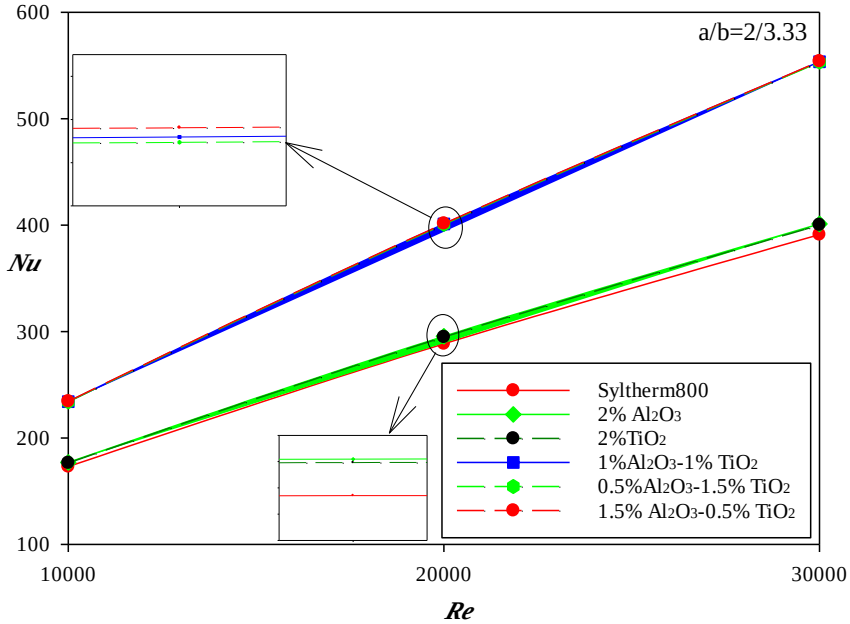
a/b=2/3.33
600
500
400
300
200
100
Nu
10000
20000
30000
Re
Syltherm800
2% Al2O3
2%TiO2
1%Al2O3-1% TiO2
0.5%Al2O3-1.5% TiO2
1.5% Al2O3-0.5% TiO2

(d)

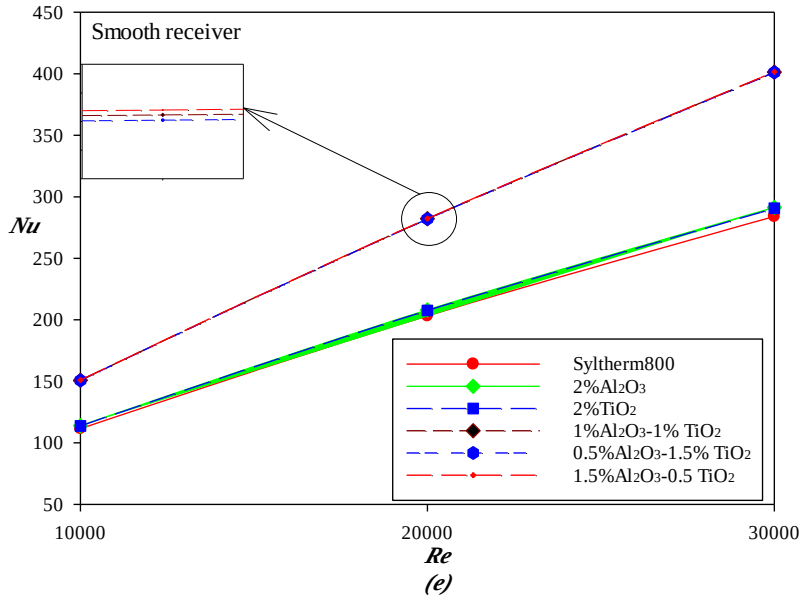

Figure 4.3. Variation of *Nu* with *Re* with different nanofluid types for elliptical ratios of dimples for receiver tube: (a) *ER=5/3* (b) *ER=3.3/2* (c) *ER=3/5* (d) *ER=2/3.3* (e) *smooth.*

The *Nu* has been studied for each nanofluid within the receiver that containing dimples with different elliptical ratios as shown in Figure 4.4 it has been found that the *Nu* increases with the increase in the elliptical ratio for *PTC*`s receiver. The highest *Nu* that was achieved is *555* at an *ER= 5/3* when *Re=30000*. That means the increasing *Nu* increases the fluid flow and thus helps the process of heat transfer. The *Nu* obtained in the smooth receiver with the receiver that containing dimples with *ER= 5/3* was compared. It has been found that the percentage of increase in *Nu* was *27%*.

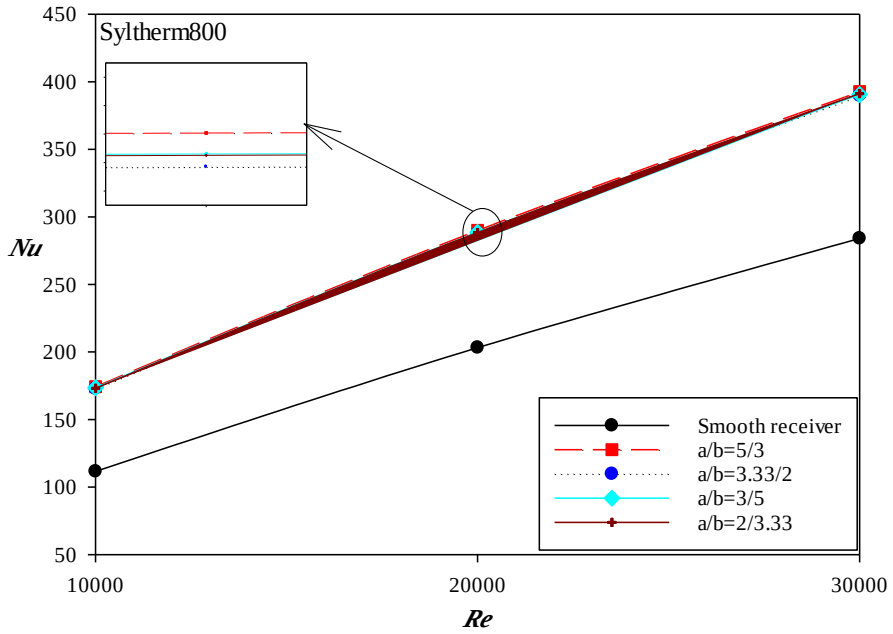
Syltherm800
450
400
350
300
250
200
150
100
50
Nu
10000
20000
30000
Re
Smooth receiver
a/b=5/3
a/b=3.33/2
a/b=3/5
a/b=2/3.33

(a)

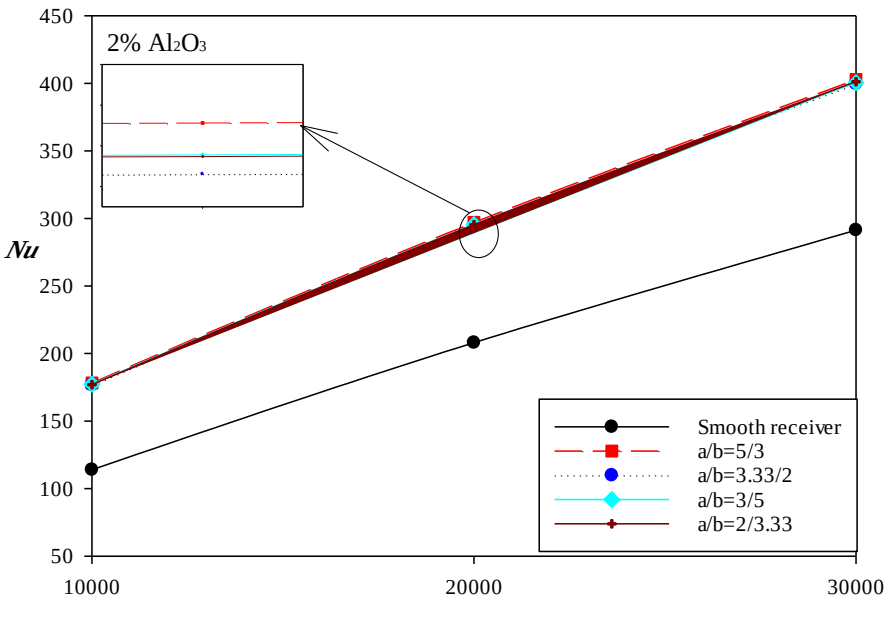
2% Al2O3
450
400
350
300
250
200
150
100
50
Nu
10000
20000
30000
Re
Smooth receiver
a/b=5/3
a/b=3.33/2
a/b=3/5
a/b=2/3.33

(b)

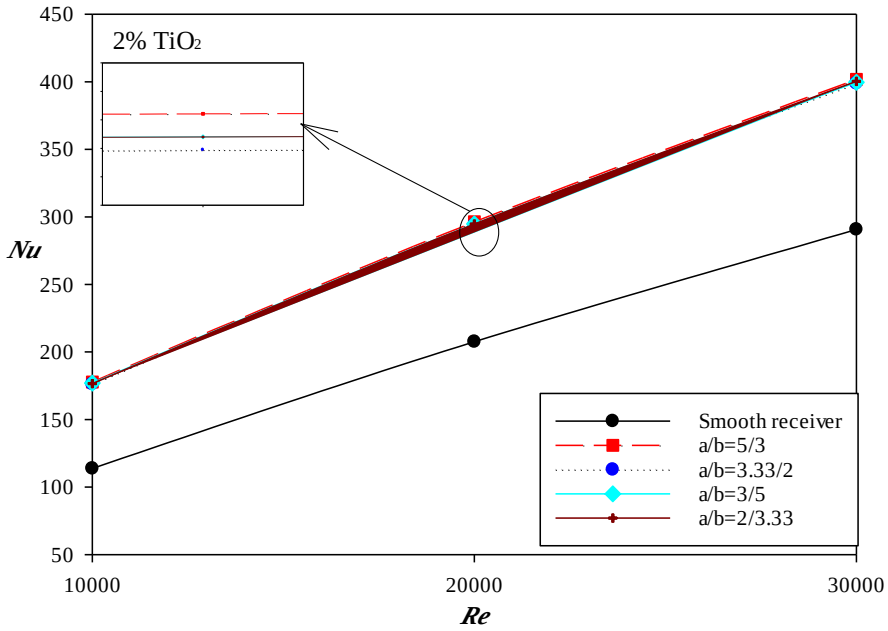
2% TiO2
Nu
Re
Smooth receiver
a/b=5/3
a/b=3.33/2
a/b=3/5
a/b=2/3.33

(c)

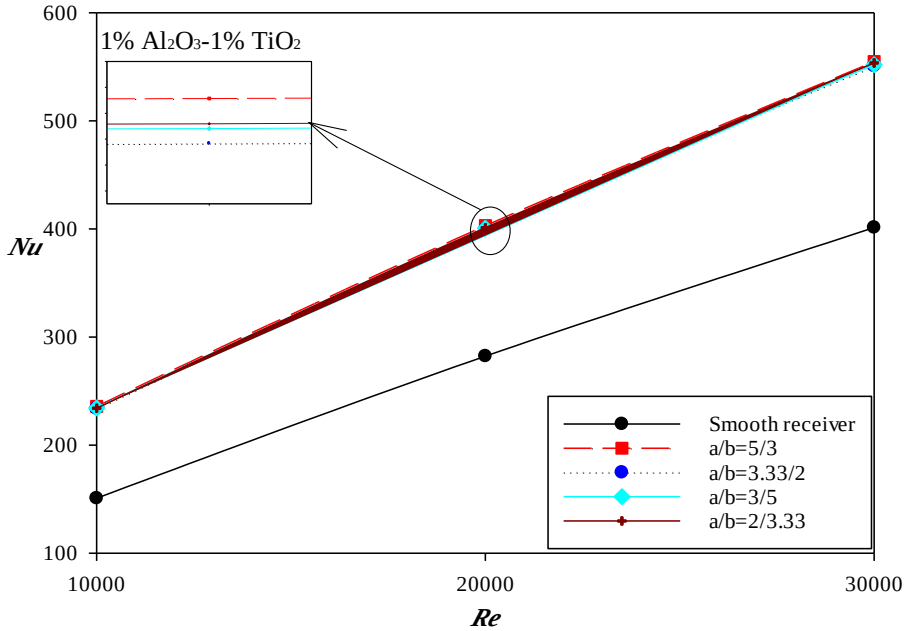
1% Al2O3-1% TiO2
Nu
Re
Smooth receiver
a/b=5/3
a/b=3.33/2
a/b=3/5
a/b=2/3.33

(d)

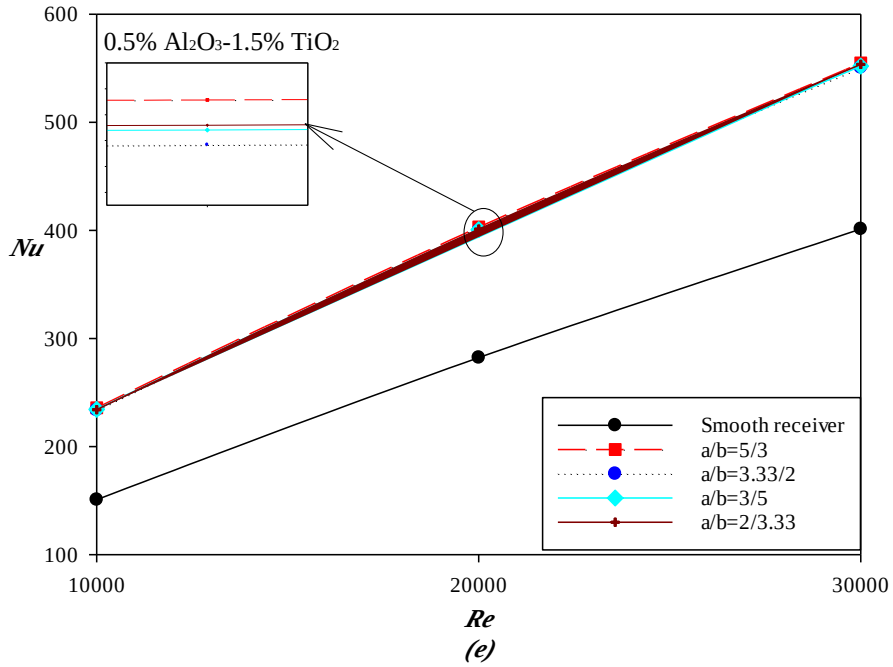

(e)

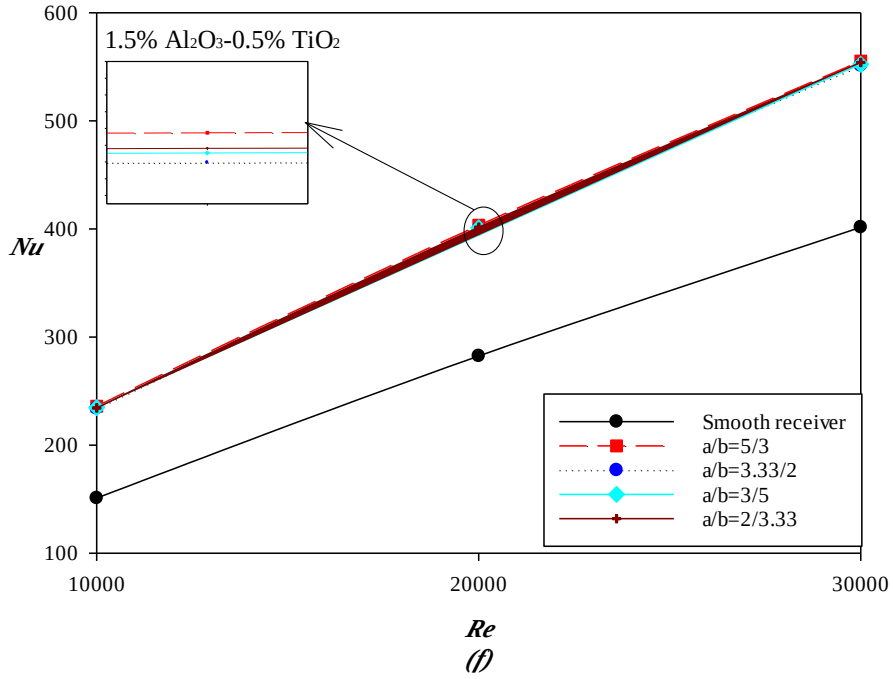

(f)

Figure 4.4. Variation of *Nu* with *Re* for elliptical ratios of dimples with working fluids of: (a) *Syltherm800* (b) *2.0% Al_2O_3/Syltherm800* (c) *2%TiO/Syltherm800* (d) *1%Al_2O_3- 1%TiO_2/Syltherm800* (e) *0.5%Al_2O_3-1.5%TiO_2/Syltherm800* (f) *1.5%Al_2O_3-0.5%TiO_2/Syltherm800*.

٤.3. FRICTION FACTOR *(ff)*

The nanofluids have been compared with different concentrations inside each *PTC`s* receiver separately as shown in Figure 4.5 also, each nanofluid has been studied individually inside the receiving tubes containing dimples of different dimensions as shown in Figure 4.6 to determine the minimum value of the friction factor of the fluid flow. It has been found that increasing the Reynolds number reduces the average friction factor in all the nanofluid and in each case of the receiving tube by *25%*. On the other side, it has been noted that the adding of dimples in the receiver increases the friction factor of the fluid flow, so the lowest value of *ff* has been obtained when using the smooth receiver, the ratio of the increase for the friction factor between the smooth receiver and the receiver that containing the dimples was *32%*. The lowest rate of friction factor has been achieved when using the hybrid nanofluid of *1.5 %Al_2O_3-0.5%TiO_2/Syltherm800*.. When comparing the friction coefficient inside the receiver tubes with different elliptical ratios, it was found that even though the results are very close to each other, but the lowest friction coefficient can be obtained after smooth receiver when using the receiver at *ER= 5/3*.

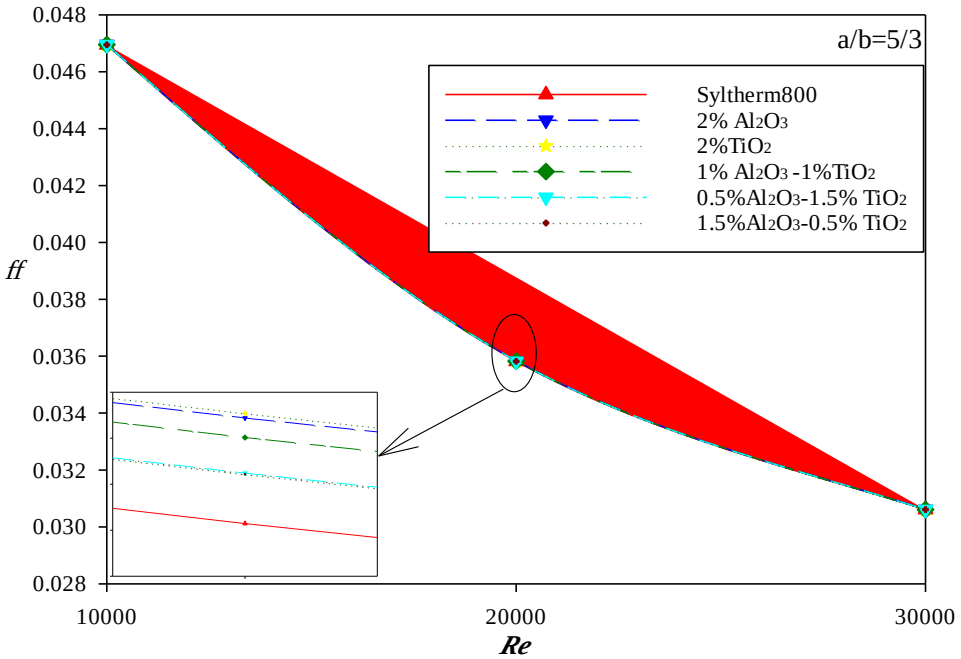

(a)

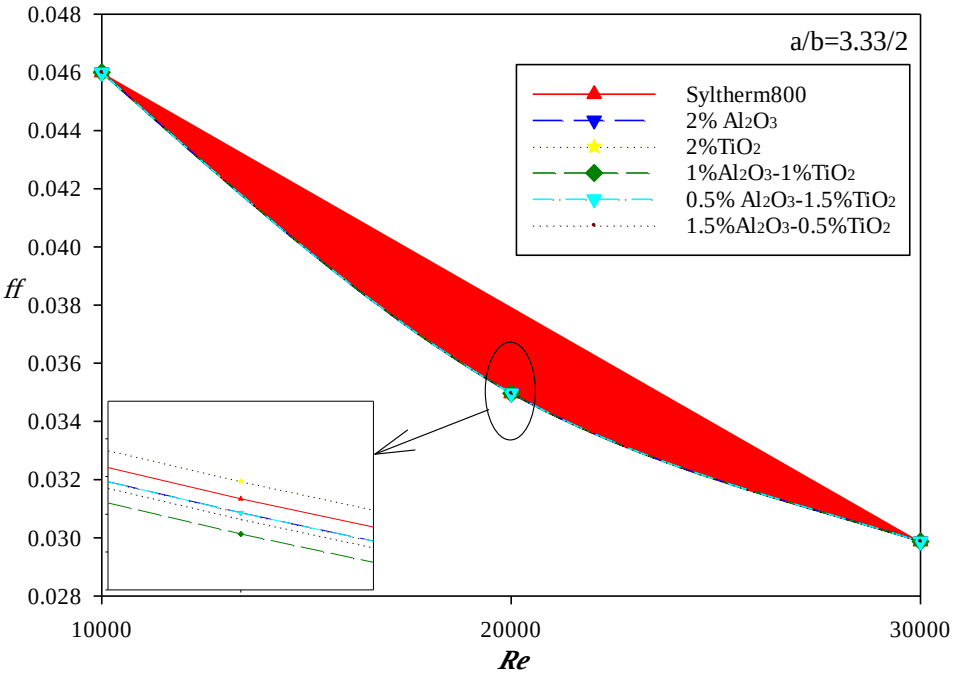
a/b=3.33/2
Syltherm800
2% Al2O3
2%TiO2
1%Al2O3-1%TiO2
0.5% Al2O3-1.5%TiO2
1.5%Al2O3-0.5%TiO2
ff
0.048
0.046
0.044
0.042
0.040
0.038
0.036
0.034
0.032
0.030
0.028
10000
20000
30000
Re

(b)

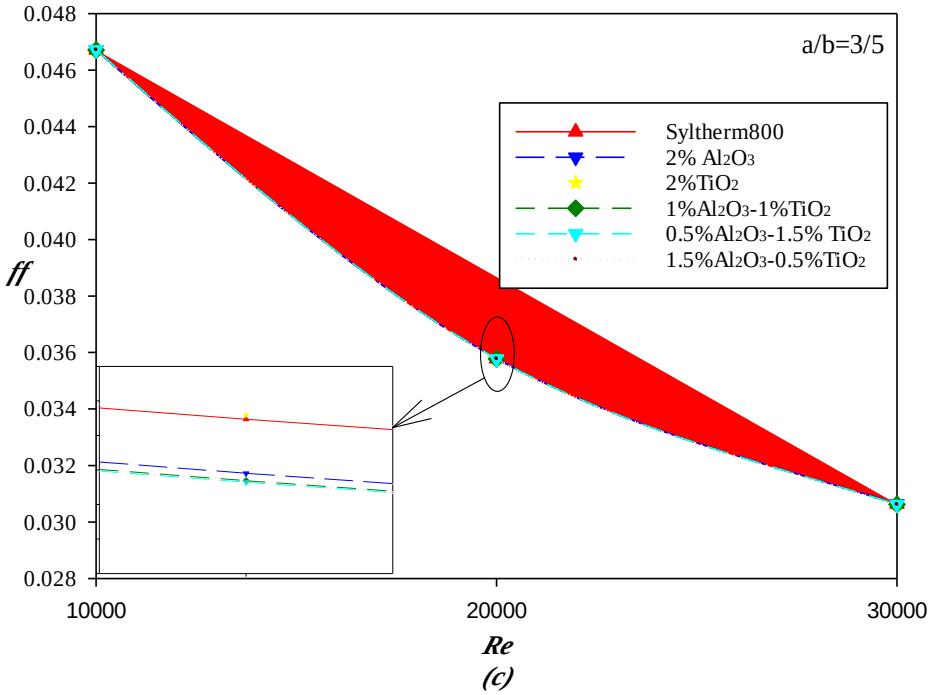
a/b=3/5
Syltherm800
2% Al2O3
2%TiO2
1%Al2O3-1%TiO2
0.5%Al2O3-1.5% TiO2
1.5%Al2O3-0.5%TiO2
ff
0.048
0.046
0.044
0.042
0.040
0.038
0.036
0.034
0.032
0.030
0.028
10000
20000
30000
Re

(c)

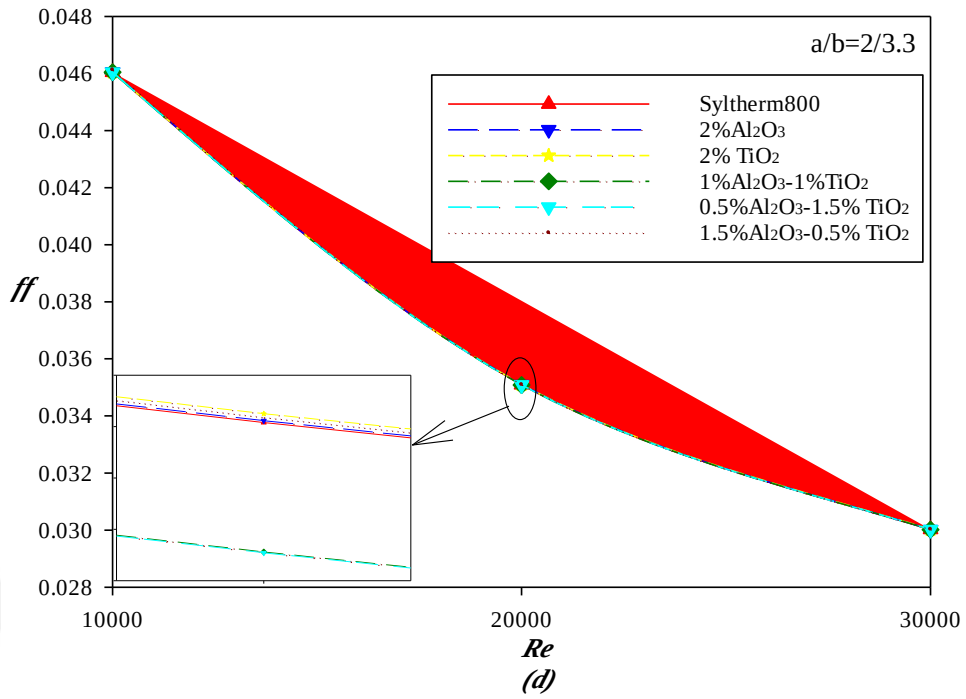

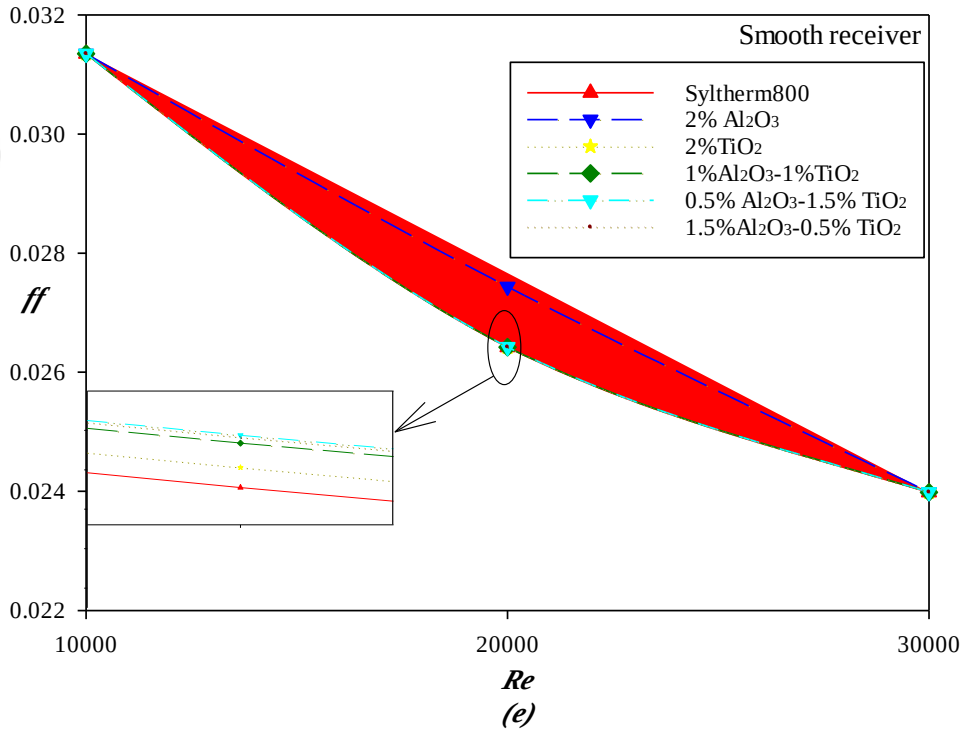

Figure 4.5. Variation of *ff* with *Re* with different nanofluid types for elliptical ratios of dimples for receiver tube: (a) *ER=5/3* (b) *ER= 3.3/2* (c) *ER=3/5* (d) *ER=2/3.3* (e) *smooth.*

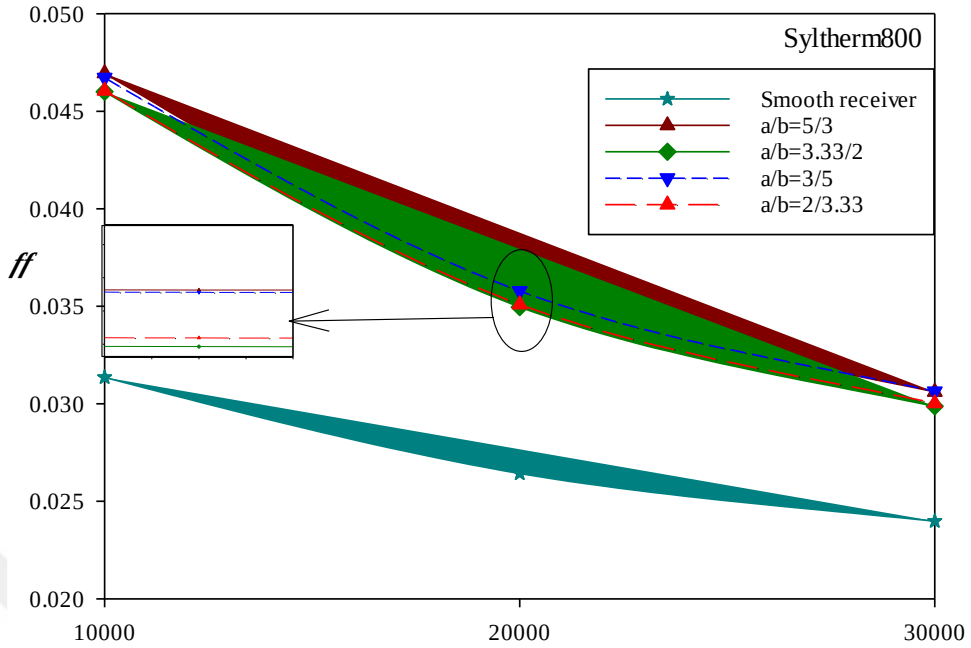
Syltherm800
Smooth receiver
a/b=5/3
a/b=3.33/2
a/b=3/5
a/b=2/3.33
ff
0.050
0.045
0.040
0.035
0.030
0.025
0.020
10000
20000
30000
Re

(a)

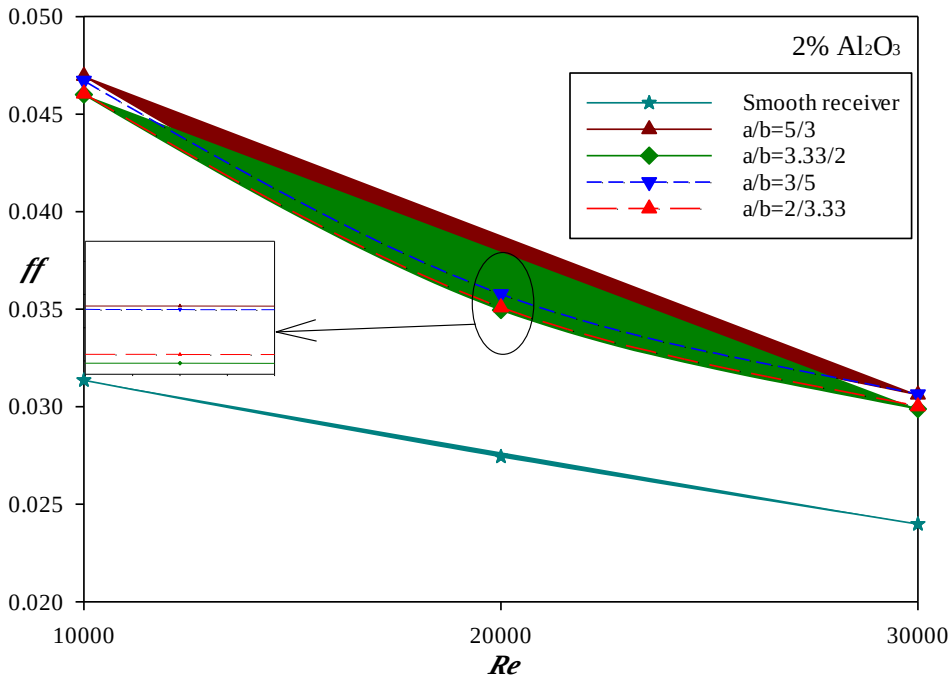
2% Al2O3
Smooth receiver
a/b=5/3
a/b=3.33/2
a/b=3/5
a/b=2/3.33
ff
0.050
0.045
0.040
0.035
0.030
0.025
0.020
10000
20000
30000
Re

(b)

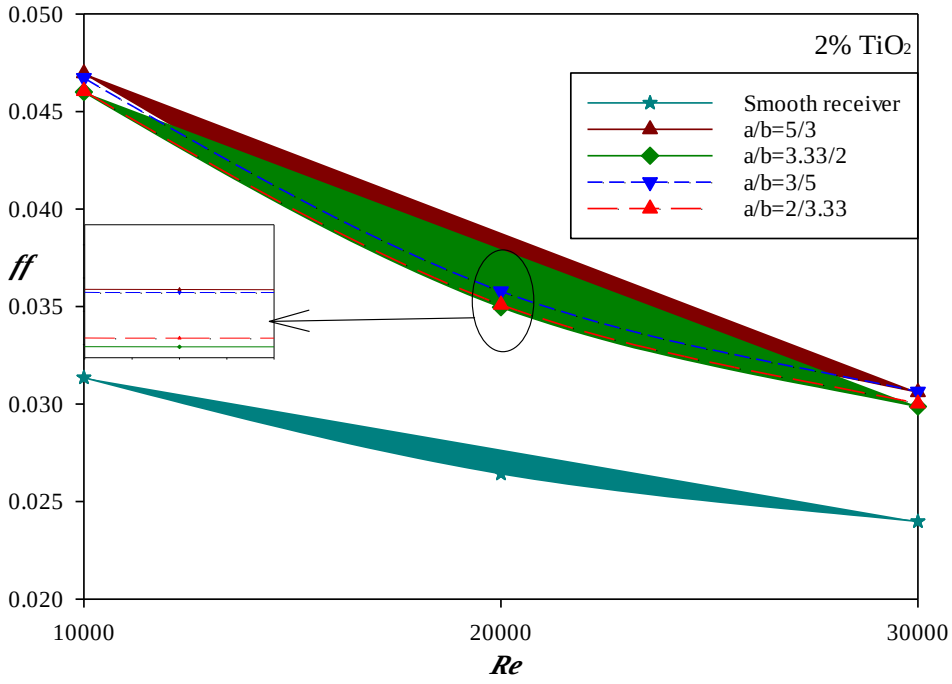
2% TiO2
Smooth receiver
a/b=5/3
a/b=3.33/2
a/b=3/5
a/b=2/3.33
ff
0.050
0.045
0.040
0.035
0.030
0.025
0.020
10000
20000
30000
Re

(c)

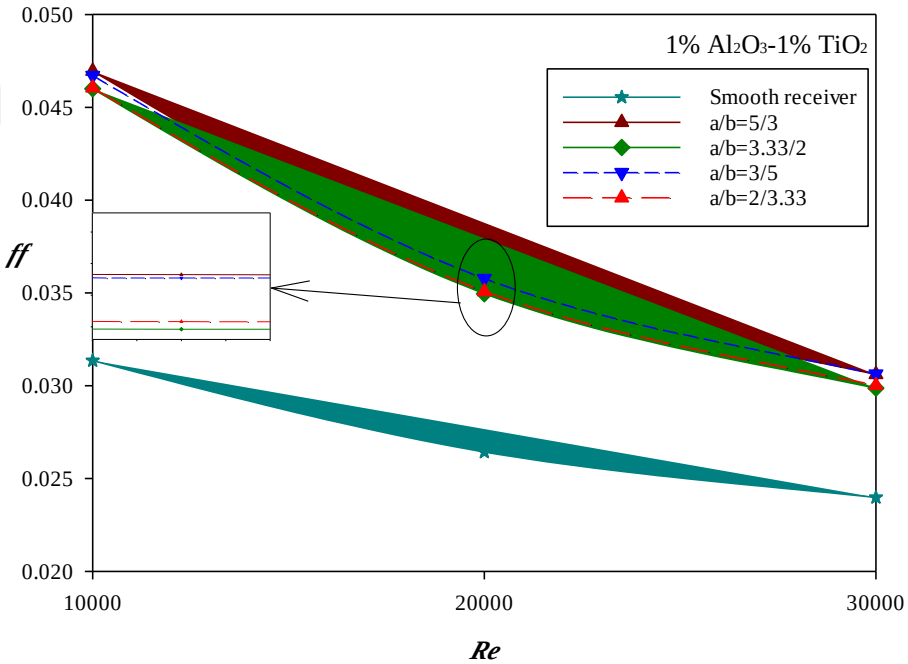
1% Al2O3-1% TiO2
Smooth receiver
a/b=5/3
a/b=3.33/2
a/b=3/5
a/b=2/3.33
ff
0.050
0.045
0.040
0.035
0.030
0.025
0.020
10000
20000
30000
Re

(d)

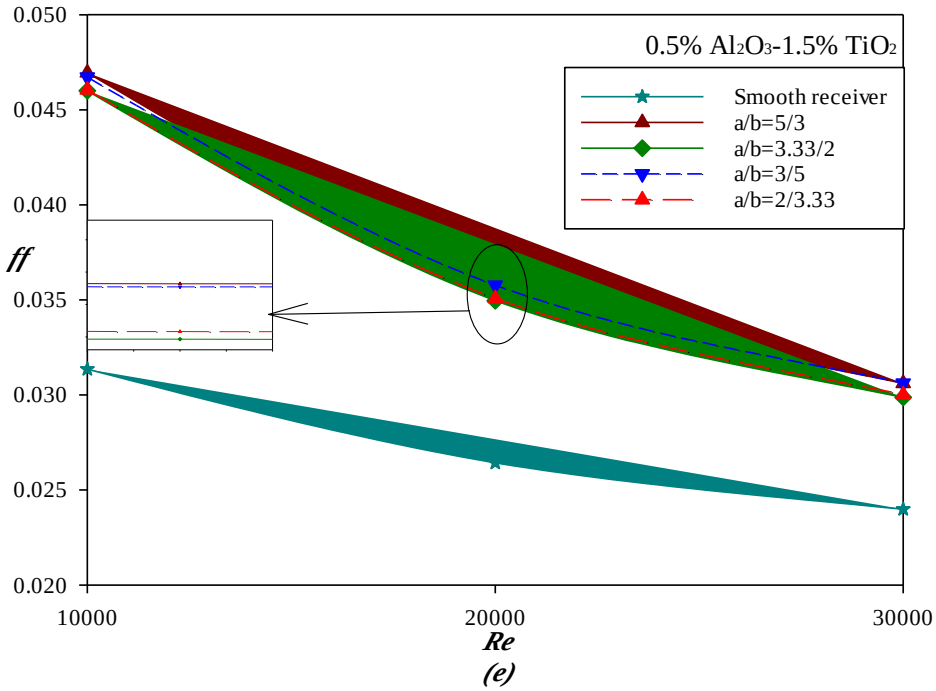

(e)

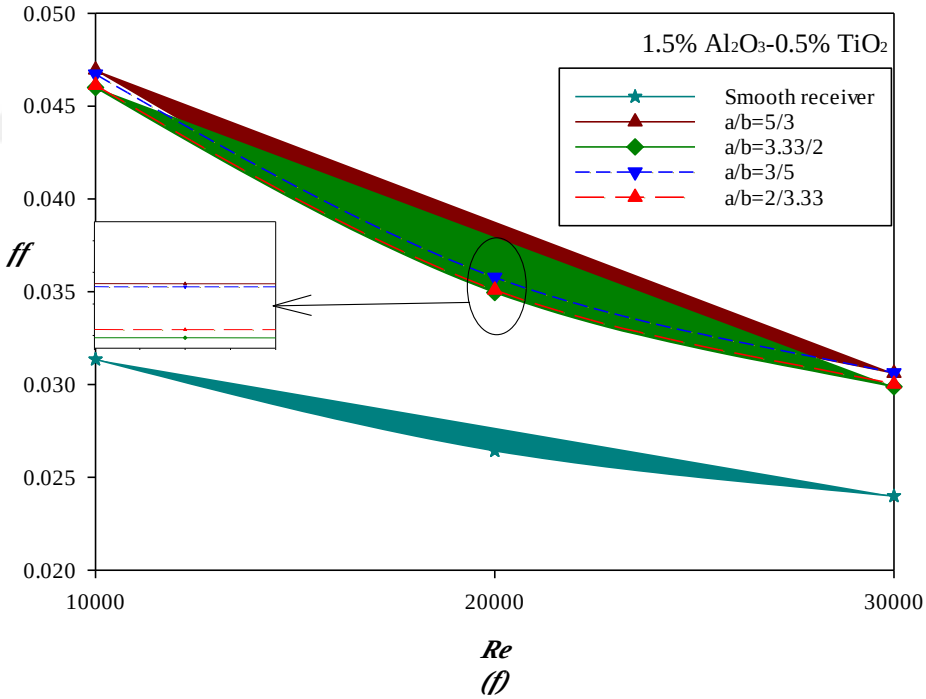

(f)

Figure 4.6. Variation of *ff* with *Re* for elliptical ratios of dimples with working fluids of: (a) *Syltherm800* (b) *2.0% Al_2O_3/Syltherm800* (c) *2% TiO/Syltherm800* (d) *1%Al_2O_3-1%TiO_2/Syltherm800* (e) *0.5%Al_2O_3-1.5%TiO_2/Syltherm800* (f) *1.5%Al_2O_3-0.5%TiO_2/Syltherm800*.

4.4. PERFORMANCE EVALUTION CRITERIA *(PEC)*

The nanofluids have been studied and compared with different concentrations inside each receiving tube separately as shown in Figure 4.7 also, each nanofluid was analyzed individually inside the receiving tubes containing dimples of different dimensions as shown in Figure 4.8 to evaluate the performance criteria of the improved heat transfer surface. The main condition is to ensure that the surface of the working fluid is helping to heat transfer surface to have a *PEC* value greater than 1. This condition has been achieved at all cases of the *PTC`s* receiver, as well this condition has been achieved for All fluid types that used in this study. The highest *PEC* value has been obtained *(PEC=1.85*) when using a receiver tube that containing dimples at elliptical ratio of 5/3 and when using the hybrid nanofluid of *1.5 %*Al_2O_3*-0.5%*TiO_2*/Syltherm800*. When Comparing the *PEC* of a smooth tube with a receiver tube that containing dimples at *ER=5/3,* it has been found that the *PEC* percentage increases by *27%*. This means that the addition of dimples with different dimensions improves the performance of the carrier surface and helps the heat transfer process.

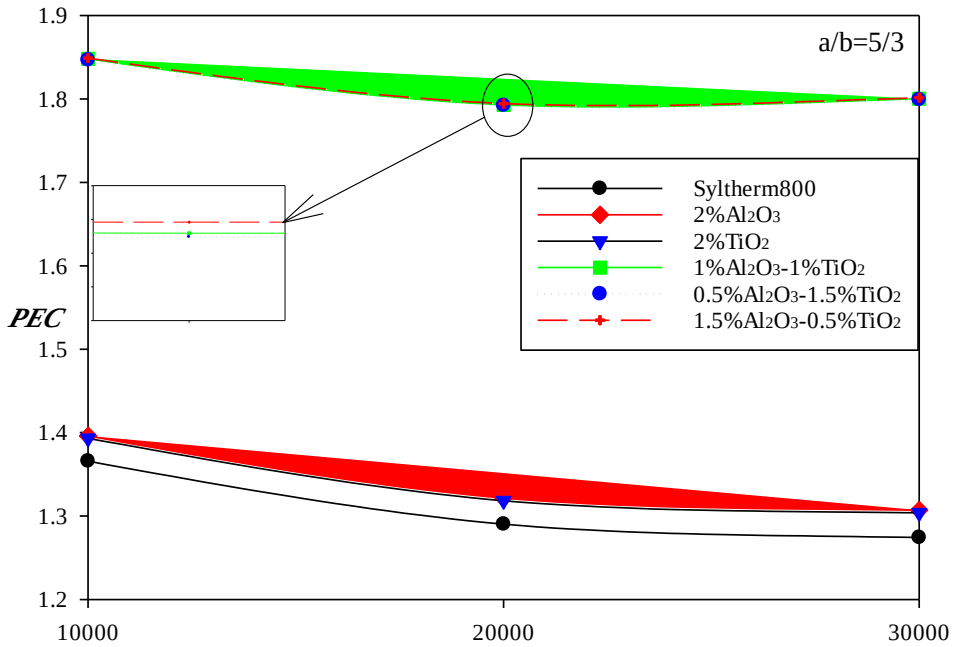
a/b=5/3
PEC
Re
Syltherm800
2%Al2O3
2%TiO2
1%Al2O3-1%TiO2
0.5%Al2O3-1.5%TiO2
1.5%Al2O3-0.5%TiO2
1.9
1.8
1.7
1.6
1.5
1.4
1.3
1.2
10000
20000
30000

(a)

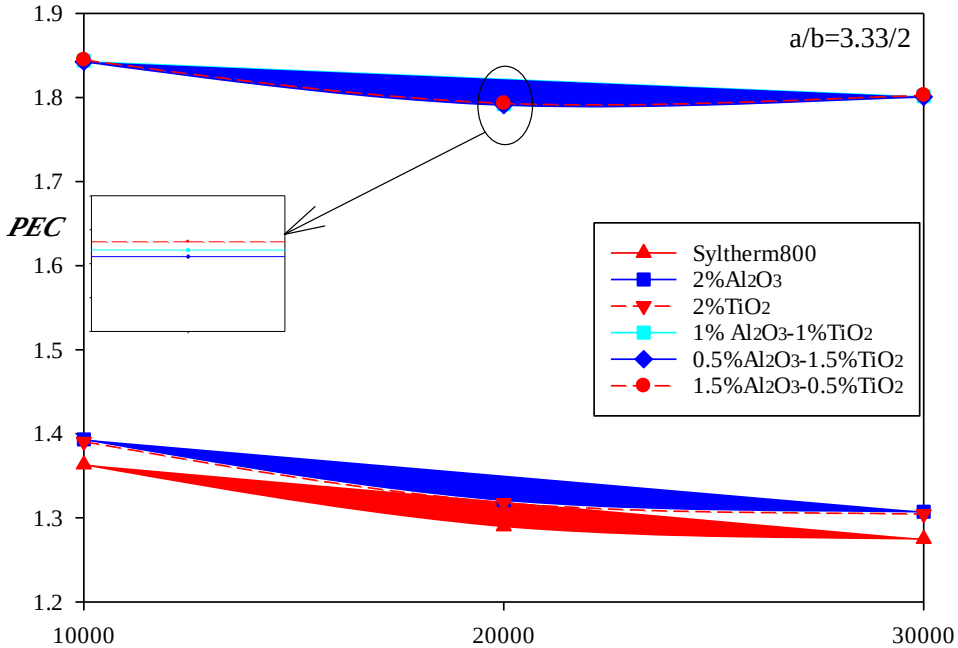
a/b=3.33/2
PEC
Re
Syltherm800
2%Al2O3
2%TiO2
1% Al2O3-1%TiO2
0.5%Al2O3-1.5%TiO2
1.5%Al2O3-0.5%TiO2
1.9
1.8
1.7
1.6
1.5
1.4
1.3
1.2
10000
20000
30000

(b)

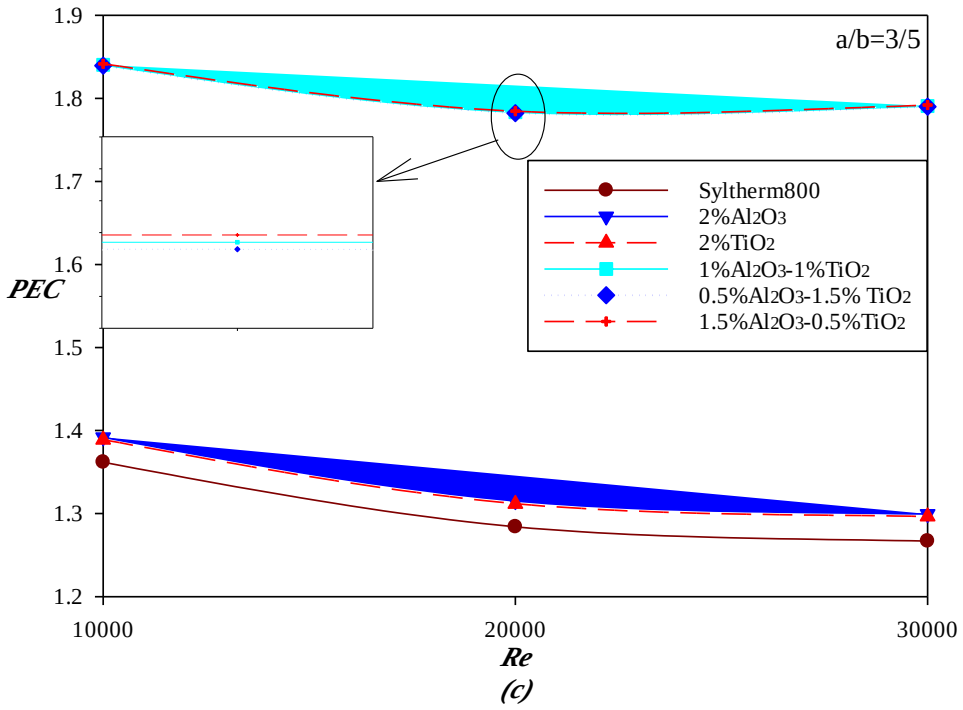

(c)

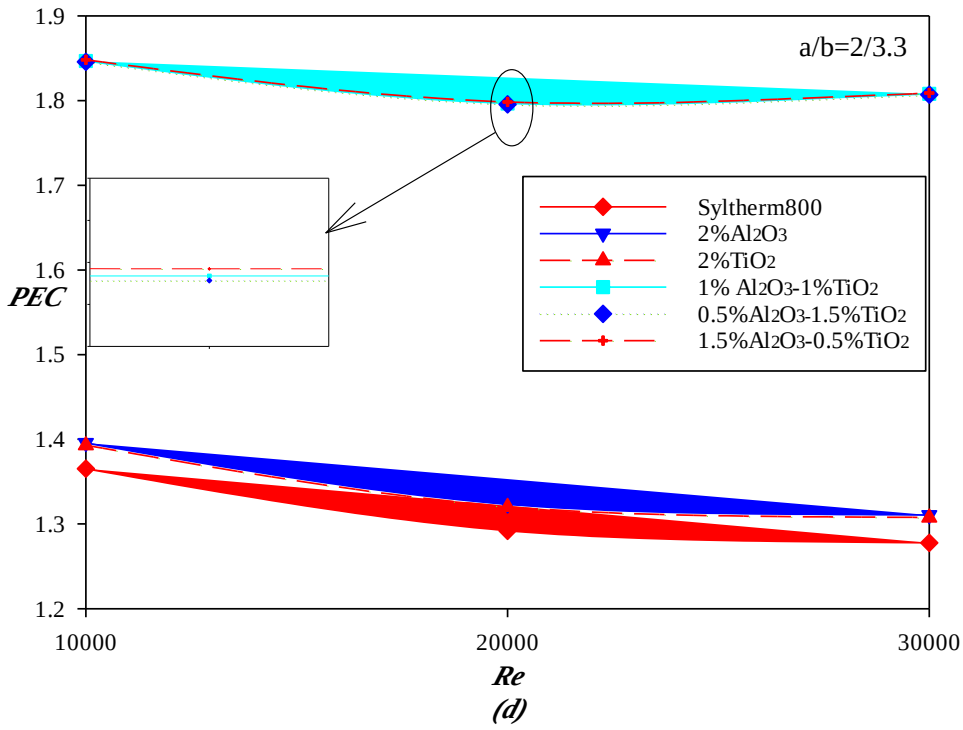

(d)

Figure 4.7. Variation of *PEC* with *Re* with different nanofluid types for elliptical ratios of dimples for receiver tube: (a) *ER=5/3* (b) *ER= 3.3/2* (c) *ER=3/5* (d) *ER=2/3.3* (e) *smooth.*

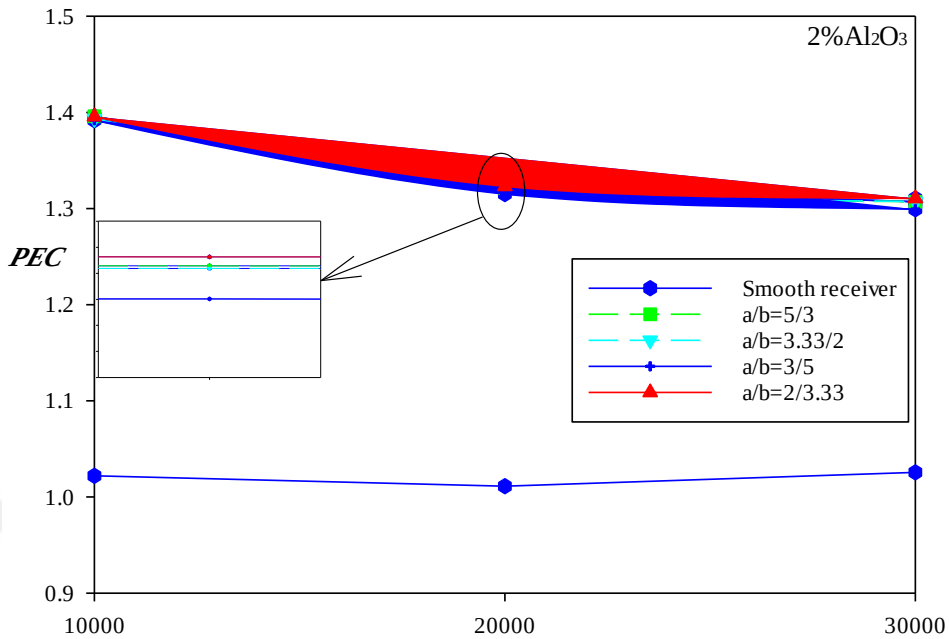
2%Al2O3
1.5
1.4
1.3
1.2
1.1
1.0
0.9
PEC
10000
20000
30000
Re
Smooth receiver
a/b=5/3
a/b=3.33/2
a/b=3/5
a/b=2/3.33

(a)

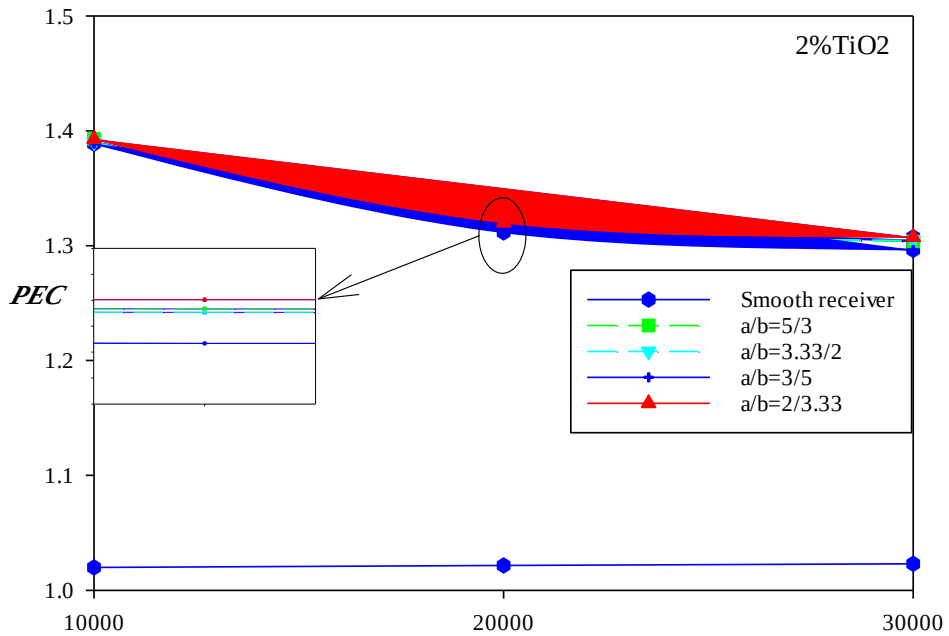
2%TiO2
1.5
1.4
1.3
1.2
1.1
1.0
PEC
10000
20000
30000
Re
Smooth receiver
a/b=5/3
a/b=3.33/2
a/b=3/5
a/b=2/3.33

(b)

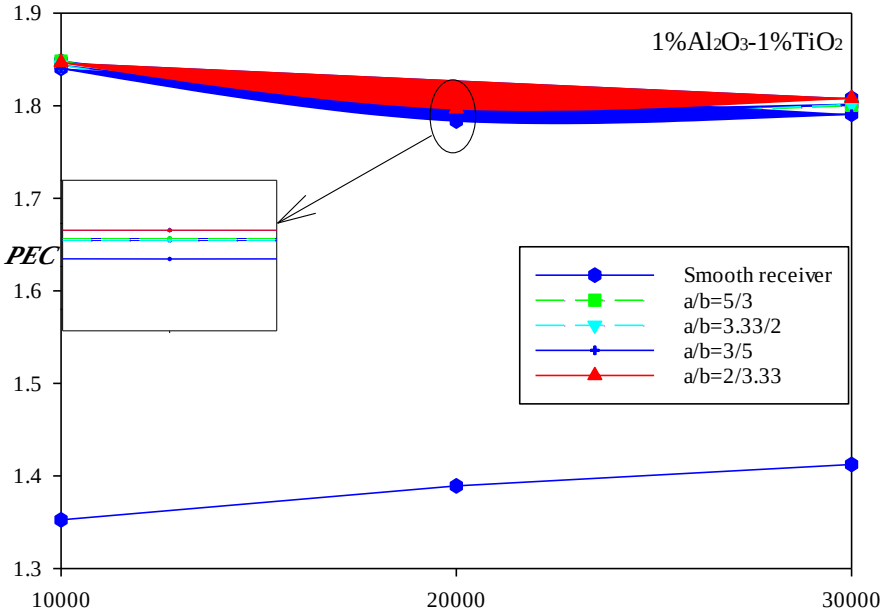
1%Al2O3-1%TiO2
PEC
Re
Smooth receiver
a/b=5/3
a/b=3.33/2
a/b=3/5
a/b=2/3.33
1.9
1.8
1.7
1.6
1.5
1.4
1.3
10000
20000
30000

(c)

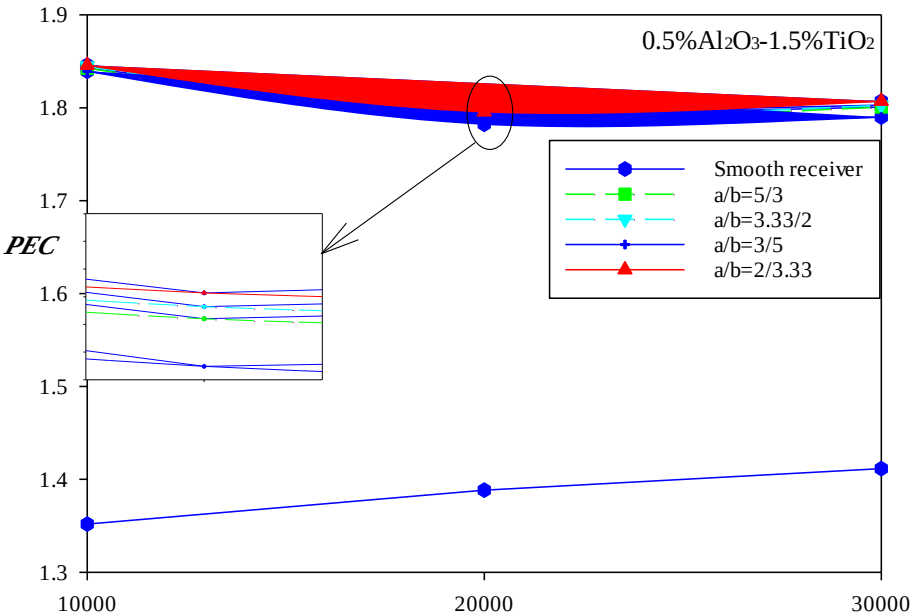
0.5%Al2O3-1.5%TiO2
PEC
Re
Smooth receiver
a/b=5/3
a/b=3.33/2
a/b=3/5
a/b=2/3.33
1.9
1.8
1.7
1.6
1.5
1.4
1.3
10000
20000
30000

(d)

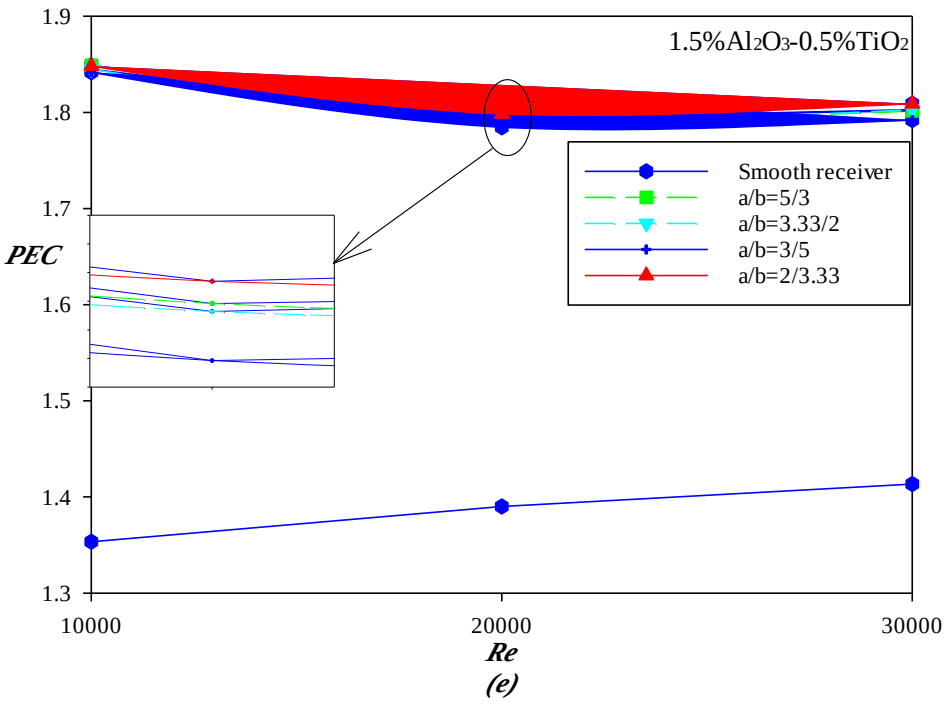

Figure 4.8. Variation of *PEC* with *Re* for elliptical ratios of dimples with working fluids of: (a) *Syltherm800* (b) *2.0% Al_2O_3/Syltherm800* (c) *2%TiO/Syltherm800* (d) *1%Al_2O_3-1%TiO_2/Syltherm800* (e) *0.5%Al_2O_3-1.5%TiO_2/Syltherm800* (f) *1.5%Al_2O_3-0.5%TiO_2/Syltherm800*..

.

4.5. THERMAL EFFICIENCY (η_{th})

The different *NPVF* have been compared in each *PTC`s* receiver separately as shown in Figure 4.9 also, each nanofluid has been examined individually within the *PTC`s* receiver that containing dimples of different dimensions as shown in Fig. 4.10. To see the effect of adding dimples inside *PTC`s* receiver and passing nanofluids on thermal efficiency. The highest value of thermal efficiency *(η_{th}=80%)* has been obtained when using a hybrid nanofluid inside a receiver tube containing dimples with elliptical ratio *ER=5/3* at *Re=10000*. In other hand, increasing the elliptical ratio for *PTC`s* receiver and decreasing the Reynolds number was decreased the velocity of the nanofluids that It has been found that the highest value of thermal efficiency was obtained when using hybrid nanofluid of *1.5 %Al_2O_3-0.5%TiO_2/Syltherm800*. Reducing *Re* from *30000* to *10000* led to increase the thermal efficiency of the working fluids by *6.25%*. When

comparing the thermal efficiency in the receiver tube that contains dimples and the smooth receiver tube, it was found that the thermal efficiency increased by *7.5%*.

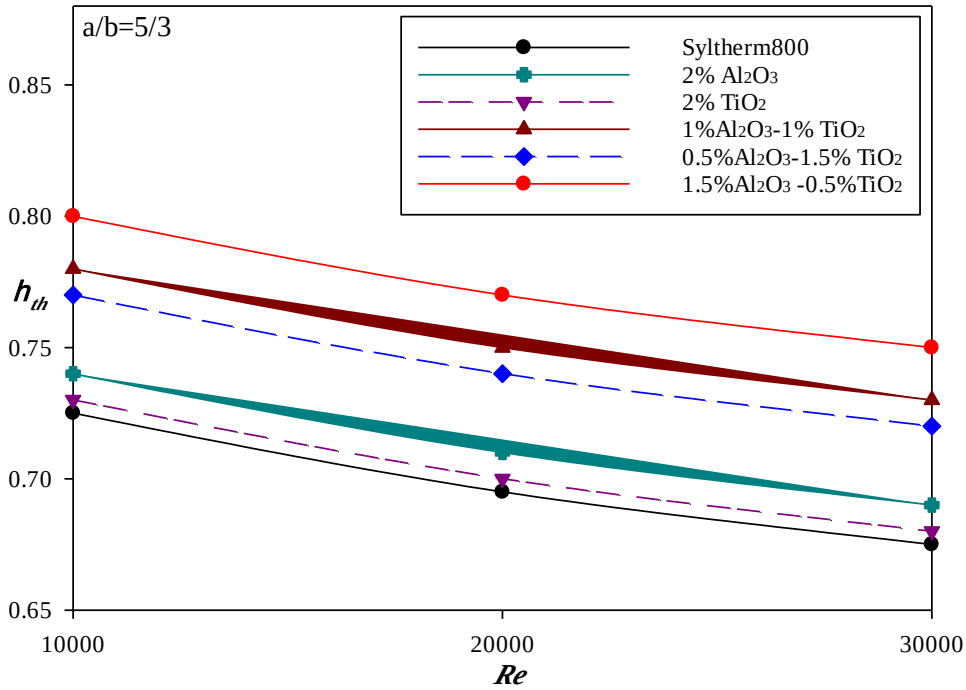

(a)

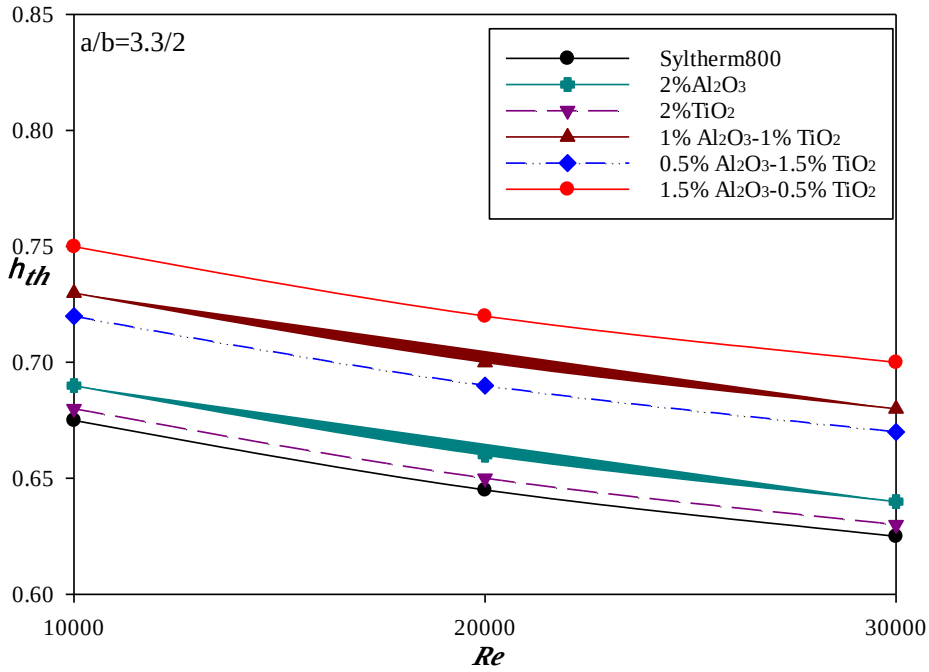

(b)

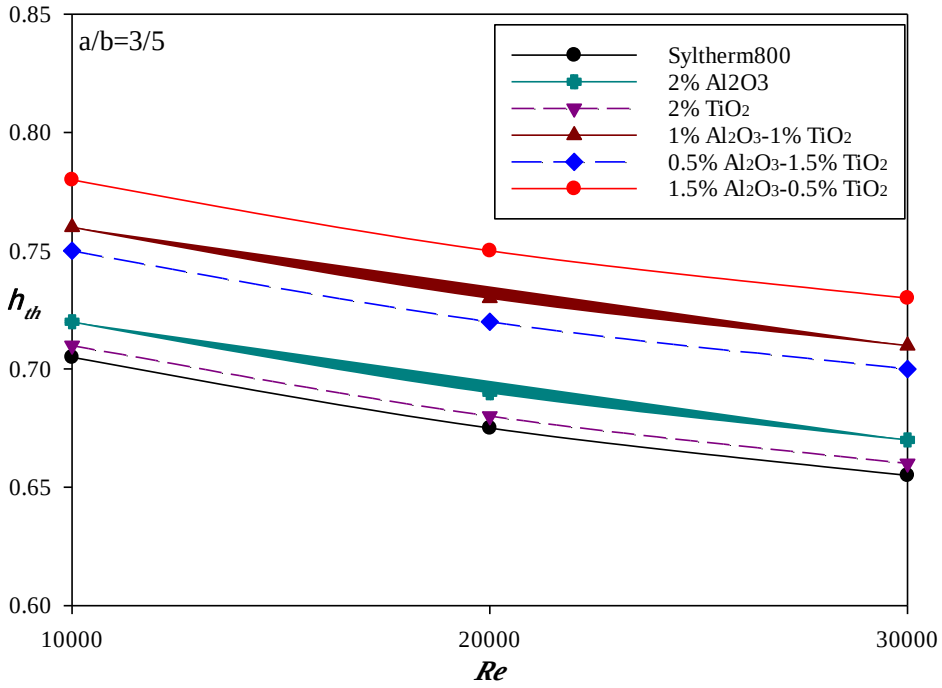
a/b=3/5
Syltherm800
2% Al2O3
2% TiO2
1% Al2O3-1% TiO2
0.5% Al2O3-1.5% TiO2
1.5% Al2O3-0.5% TiO2
0.85
0.80
0.75
0.70
0.65
0.60
h_th
10000
20000
30000
Re

(c)

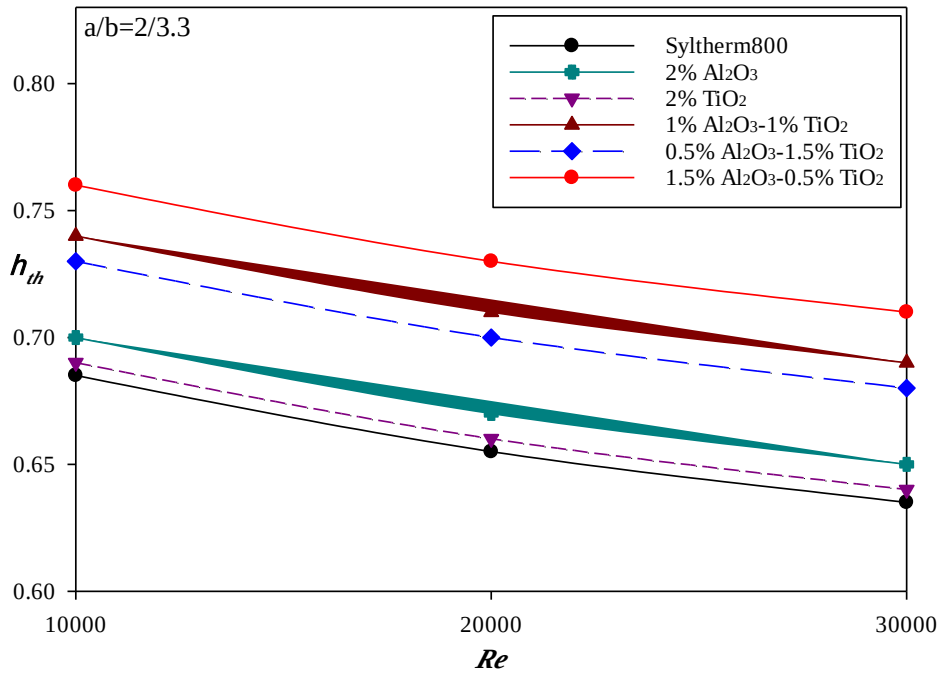
a/b=2/3.3
Syltherm800
2% Al2O3
2% TiO2
1% Al2O3-1% TiO2
0.5% Al2O3-1.5% TiO2
1.5% Al2O3-0.5% TiO2
0.80
0.75
0.70
0.65
0.60
h_th
10000
20000
30000
Re

(d)

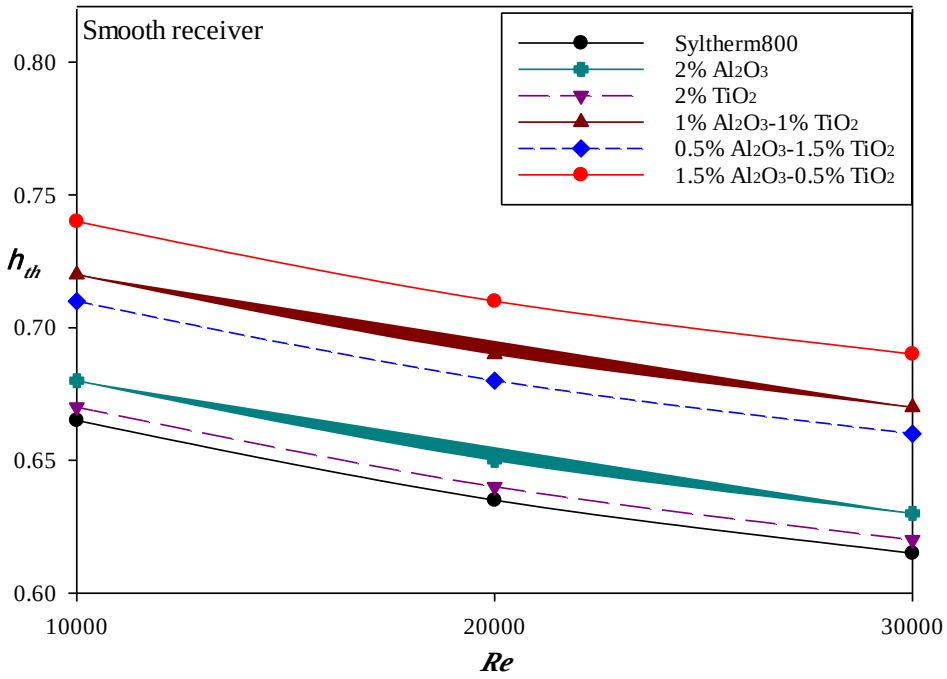

(e)

Figure 4.9. Variation of η_{th} with *Re* with different nanofluid types for elliptical ratios of dimples for receiver tube: (a) *ER=5/3* (b) *ER= 3.3/2* (c) *ER=3/5* (d) *ER=2/3.3* (e) *smooth*

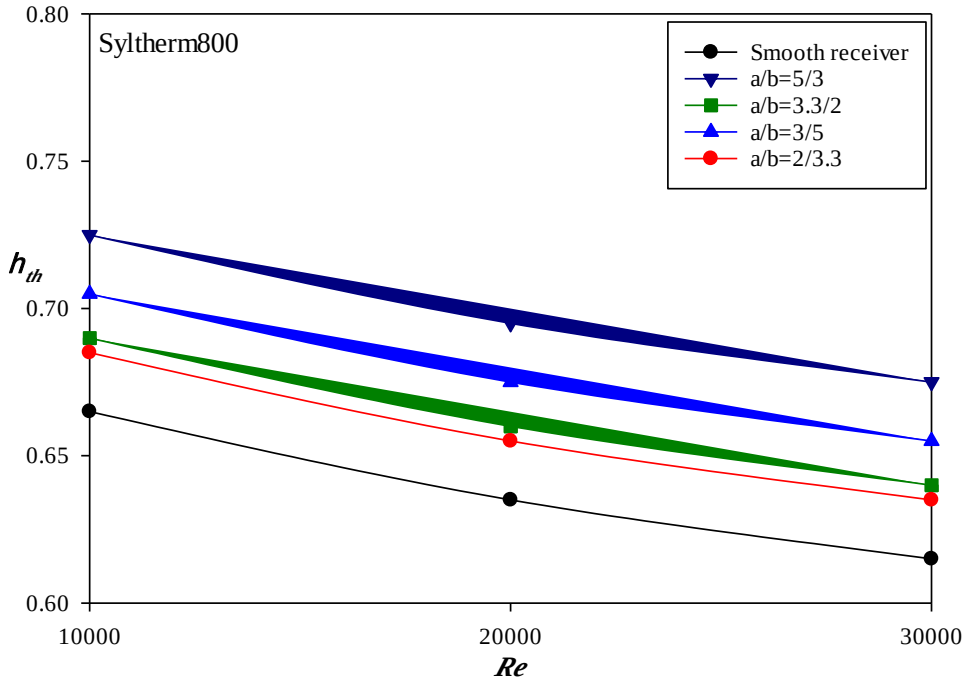

(a)

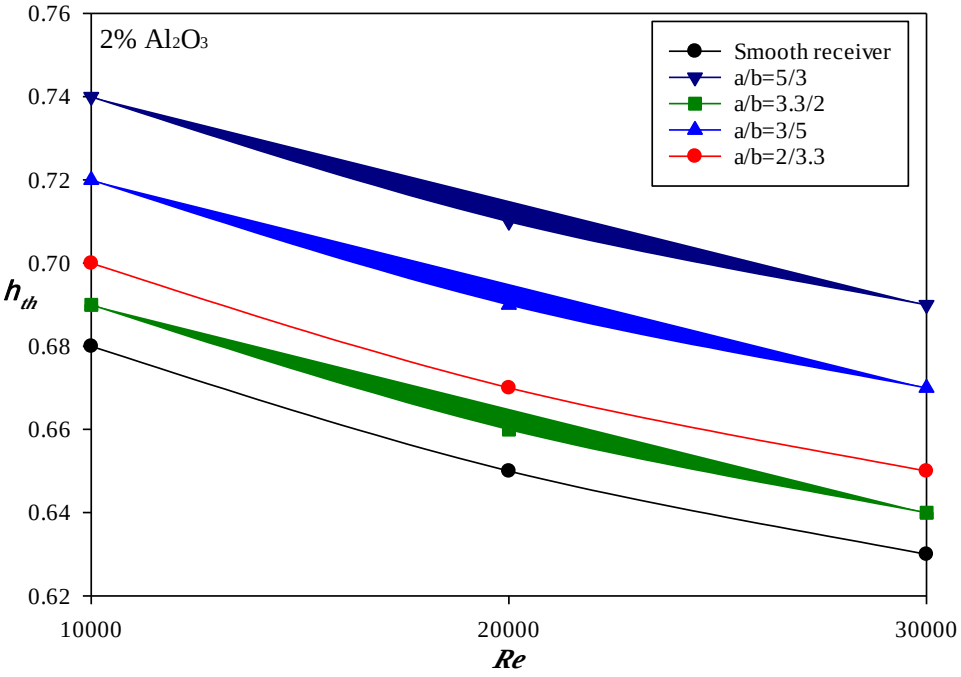
2% Al2O3
Smooth receiver
a/b=5/3
a/b=3.3/2
a/b=3/5
a/b=2/3.3
0.76
0.74
0.72
0.70
0.68
0.66
0.64
0.62
h th
10000
20000
30000
Re

(b)

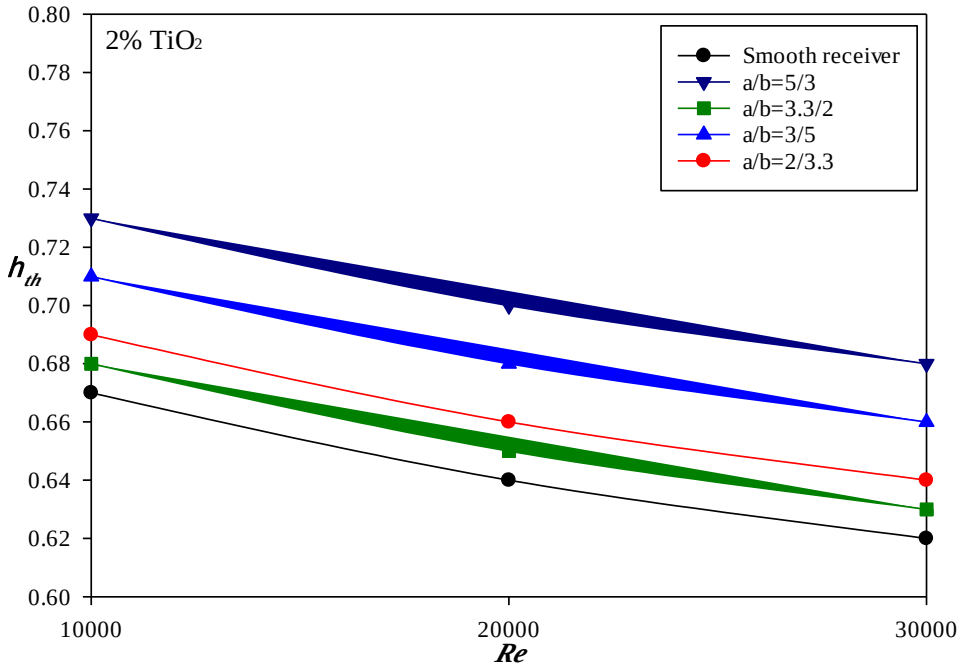
2% TiO2
Smooth receiver
a/b=5/3
a/b=3.3/2
a/b=3/5
a/b=2/3.3
0.80
0.78
0.76
0.74
0.72
0.70
0.68
0.66
0.64
0.62
0.60
h th
10000
20000
30000
Re

(c)

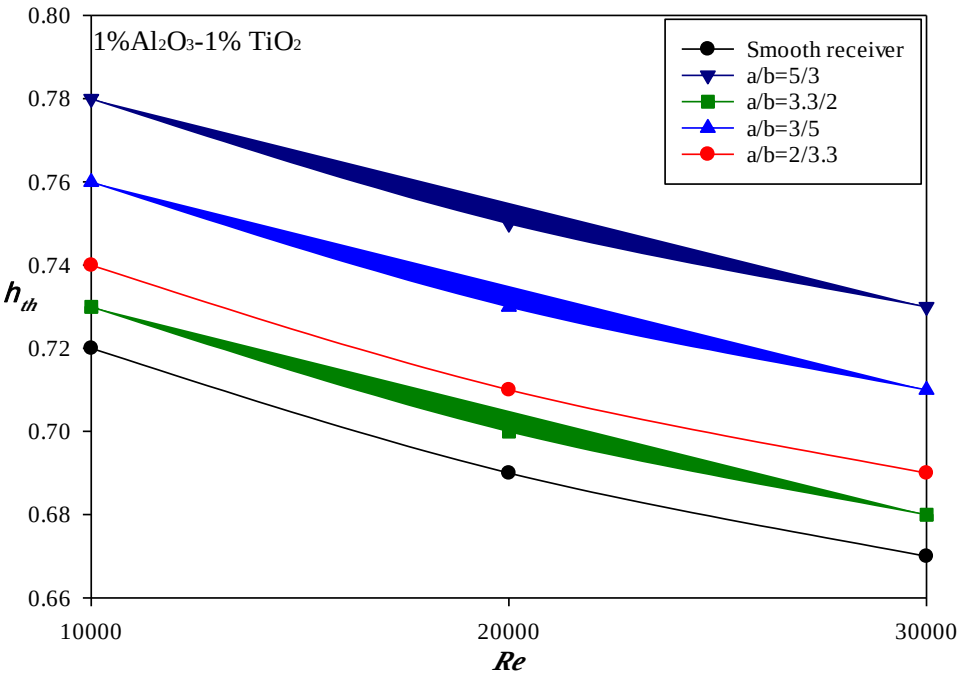
1%Al2O3-1% TiO2
Smooth receiver
a/b=5/3
a/b=3.3/2
a/b=3/5
a/b=2/3.3
0.80
0.78
0.76
0.74
0.72
0.70
0.68
0.66
h th
10000
20000
30000
Re

(d)

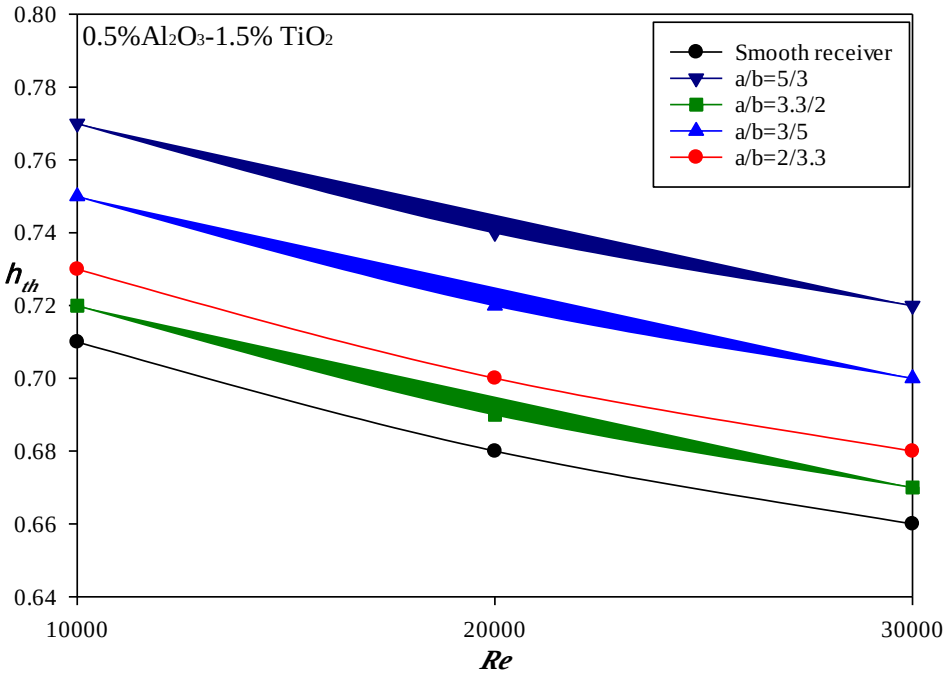
0.5%Al2O3-1.5% TiO2
Smooth receiver
a/b=5/3
a/b=3.3/2
a/b=3/5
a/b=2/3.3
0.80
0.78
0.76
0.74
0.72
0.70
0.68
0.66
0.64
h th
10000
20000
30000
Re

(e)

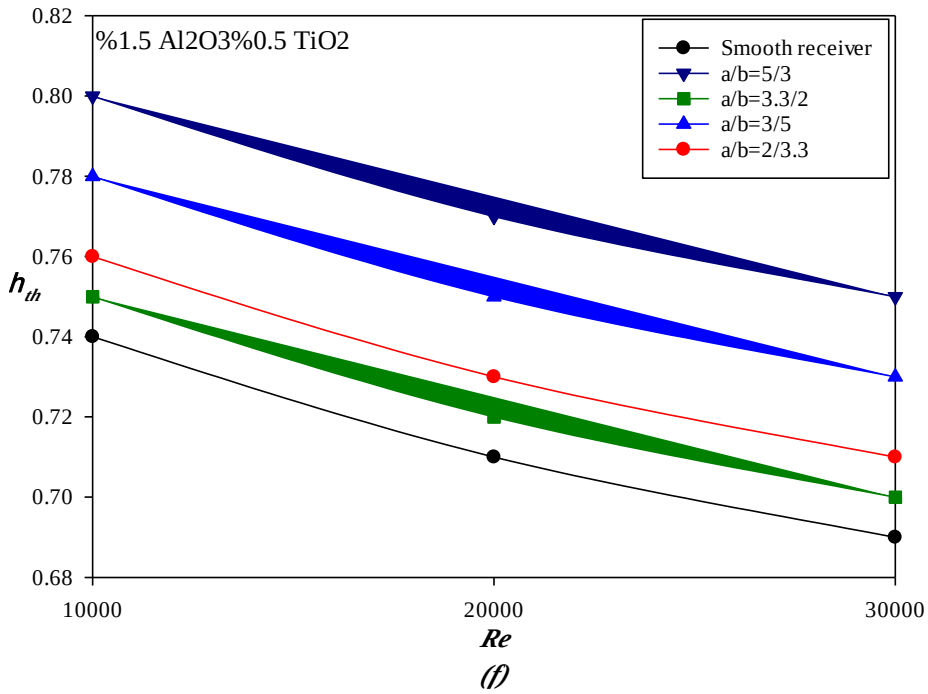

Figure 4.10. Variation of η_{th} with *Re* for elliptical ratios of dimples with working fluids of: (a) *Syltherm800* (b) *2.0% Al_2O_3/Syltherm800* (c) *2%TiO/Syltherm800* (d) *1%Al_2O_3-1%TiO_2/Syltherm800* (e) *0.5%Al_2O_3-1.5%TiO_2/Syltherm800* (f) *1.5%Al_2O_3-0.5%TiO_2/Syltherm800*.

4.6. ENTROPY GENERATION AND THERMODYNAMIC ANALYSIS

4.6.1. Irreversible Heat Transfer and Fluid Friction

The entropy and thermodynamic analysis Irreversible heat transfer and fluid friction

All nanofluids with different volume fractions have been studied and analyzed as shown in Figure 4.11 and Figure 4.13 also, each nanofluid has been examined separately inside the *PTC`s* receiver that containing dimples with different ellipticity ratios as shown in Figure 4. 12. and 4.14 it has been found the generation of entropy due to convective heat transfer in the *PTC`s* receiver consists of two parts: irreversibility of heat transfer and irreversible of fluid friction. These two properties completely contradict each other. So, an irreversible decrease in heat transfer causes an irreversible increase in fluid friction., Increasing the Reynolds number for working fluids, led to increase the property of irreversible of fluid friction, and decrease the property of the heat transfer irreversibility. Whereas in present study it has been found the irreversibility of heat transfer decreases by *53%* when the Reynolds number is

increased from *10000 to 30000*. the Bejan number *(Be)* has been used to know which of the properties is dominant in the working fluids. *Be* is known as the ratio of the irreversibility of heat transfer to the total entropy generation rate. Figure 4.15. and 4.16 indicate to the nanofluids with different volume fractions, and to examine each nanofluid separately inside the receiving tubes containing dimples with different ellipticity ratios. So, if heat transfer irreversibility dominant, the *Be* is close to *1* while if fluid friction is dominant, the *Be* is close to zero.

In the present study, the minimum value of *Be* has been achieved is *0.91* and when increasing the Reynolds number the value of *Be* is increase, but with a very small percentage. For instance, at *Re=30,000* the *Be=0.995* and when the Reynolds number was *10,000* then *Be* is equal to *0.998*. It has been concluded that the number of *Be* was in all cases close to unity, which means that heat transfer irreversibility dominant and all working fluids in present study helps to *H-Tr*.

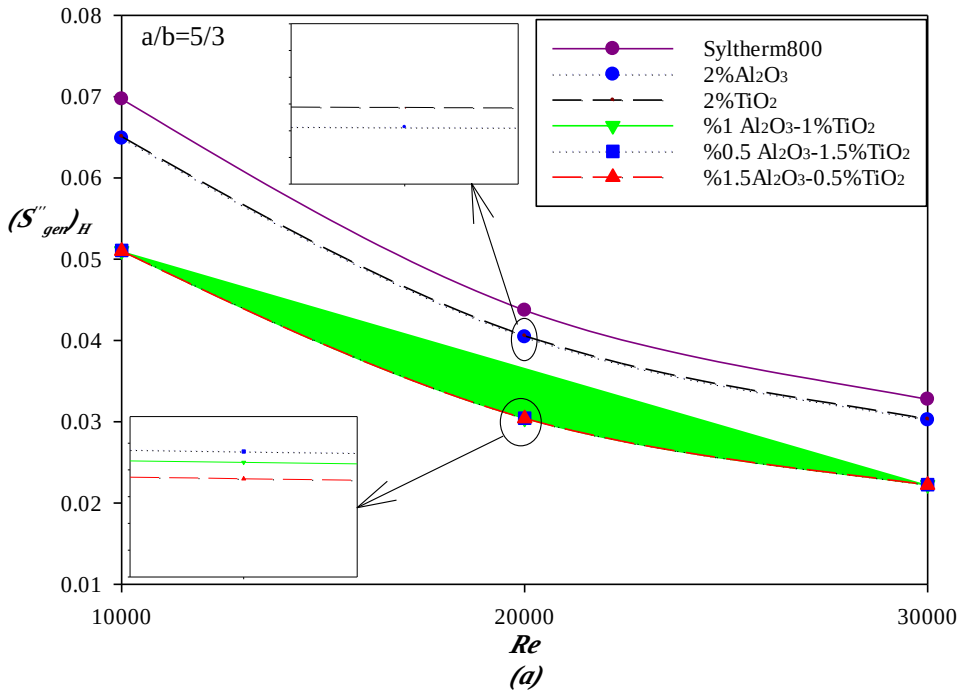

(a)

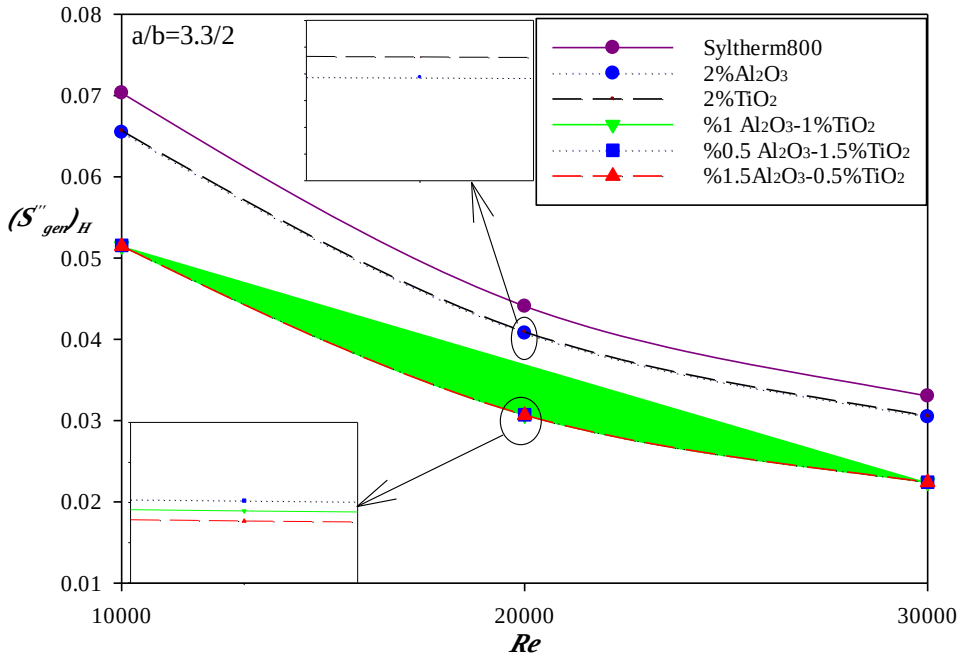
a/b=3.3/2
Syltherm800
2%Al2O3
2%TiO2
%1 Al2O3-1%TiO2
%0.5 Al2O3-1.5%TiO2
%1.5Al2O3-0.5%TiO2
(S''gen)H
0.08
0.07
0.06
0.05
0.04
0.03
0.02
0.01
10000
20000
30000
Re

(b)

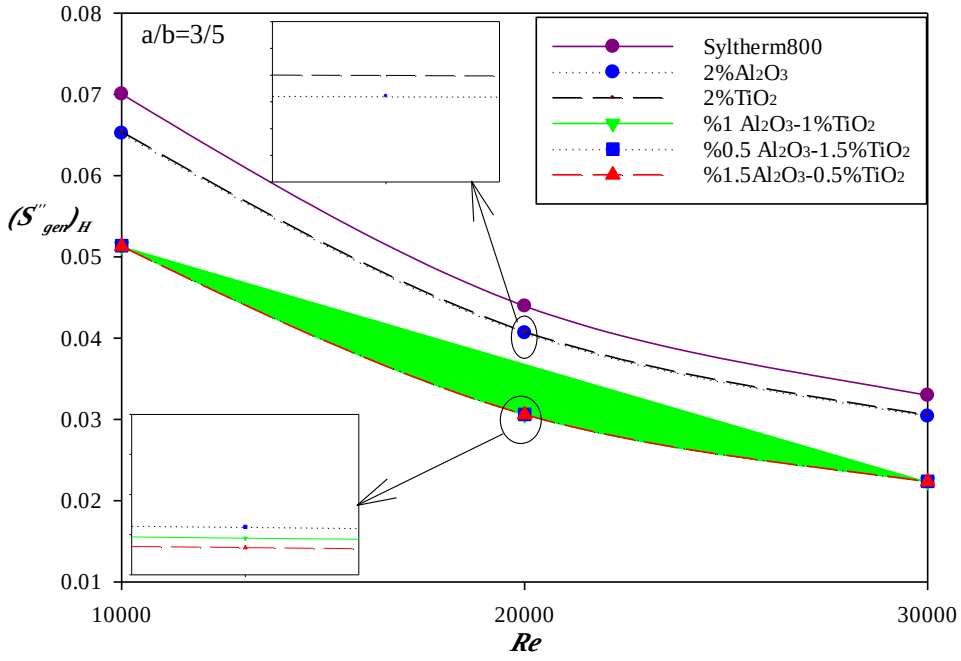
a/b=3/5
Syltherm800
2%Al2O3
2%TiO2
%1 Al2O3-1%TiO2
%0.5 Al2O3-1.5%TiO2
%1.5Al2O3-0.5%TiO2
(S''gen)H
0.08
0.07
0.06
0.05
0.04
0.03
0.02
0.01
10000
20000
30000
Re

(c)

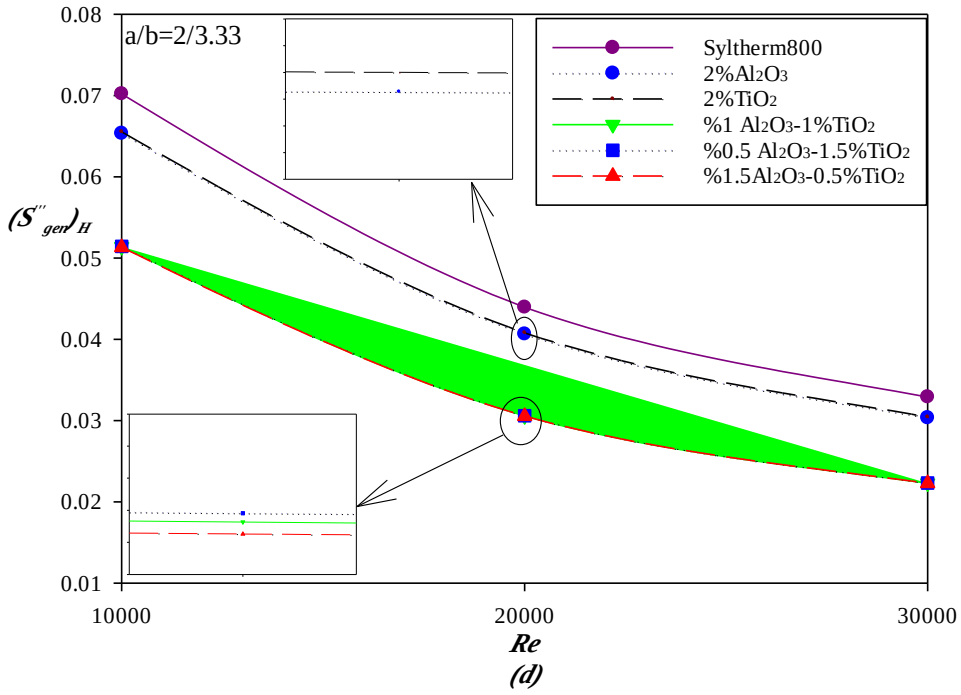

(d)

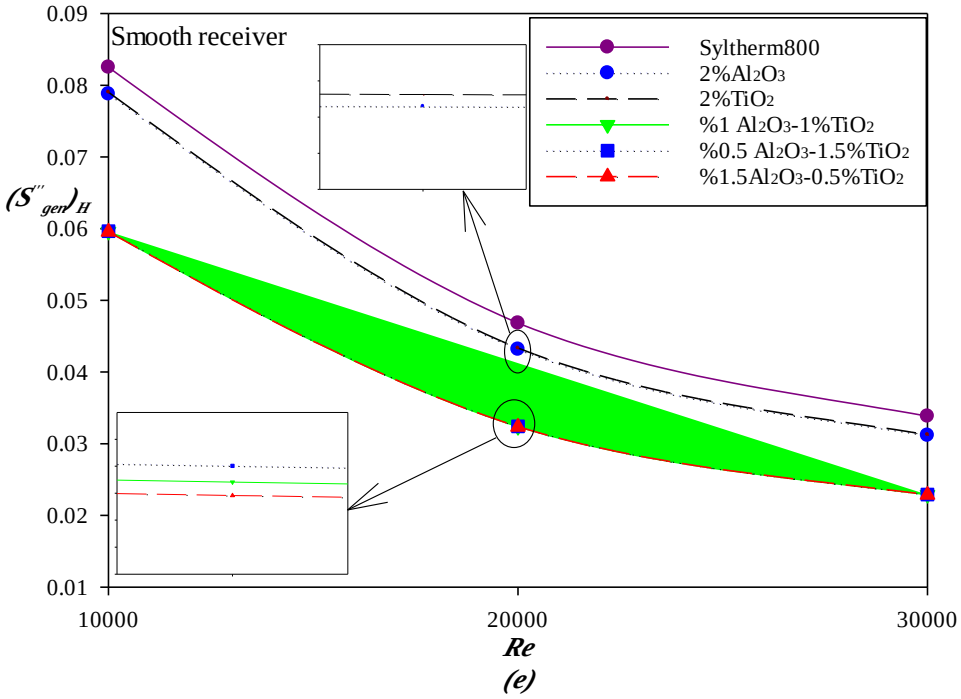

(e)

Figure 4.11. Variation of *Irreversible* heat transfer with different nanofluid types for elliptical ratios of dimples for receiver tube: (a) *ER=5/3* (b) *ER= 3.3/2* (c) *ER=3/5* (d) *ER=2/3.3* (e) *smooth.*

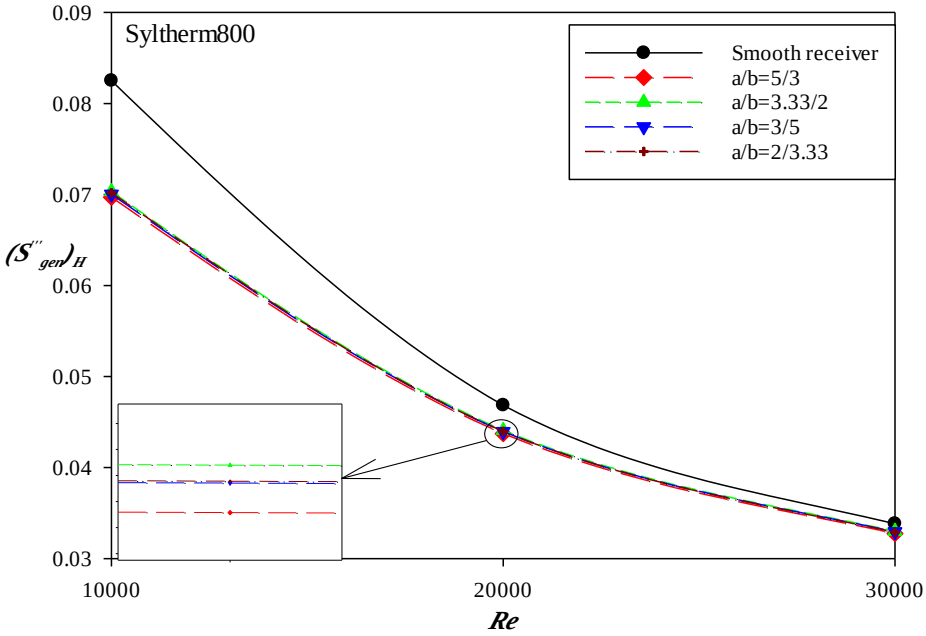
Syltherm800
Smooth receiver
a/b=5/3
a/b=3.33/2
a/b=3/5
a/b=2/3.33
0.09
0.08
0.07
0.06
0.05
0.04
0.03
(S'''gen)H
10000
20000
30000
Re

(a)

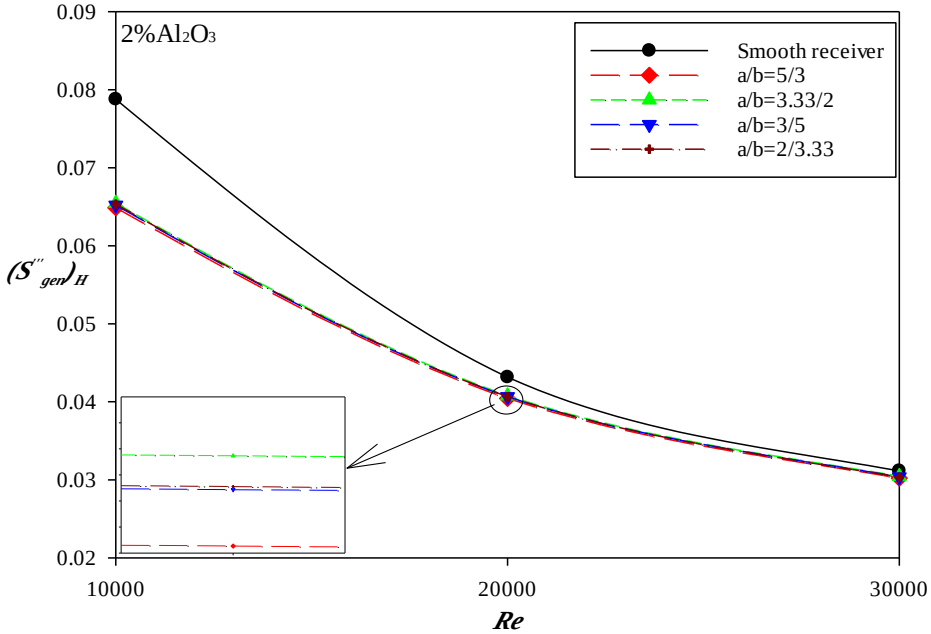
2%Al2O3
Smooth receiver
a/b=5/3
a/b=3.33/2
a/b=3/5
a/b=2/3.33
0.09
0.08
0.07
0.06
0.05
0.04
0.03
0.02
(S'''gen)H
10000
20000
30000
Re

(b)

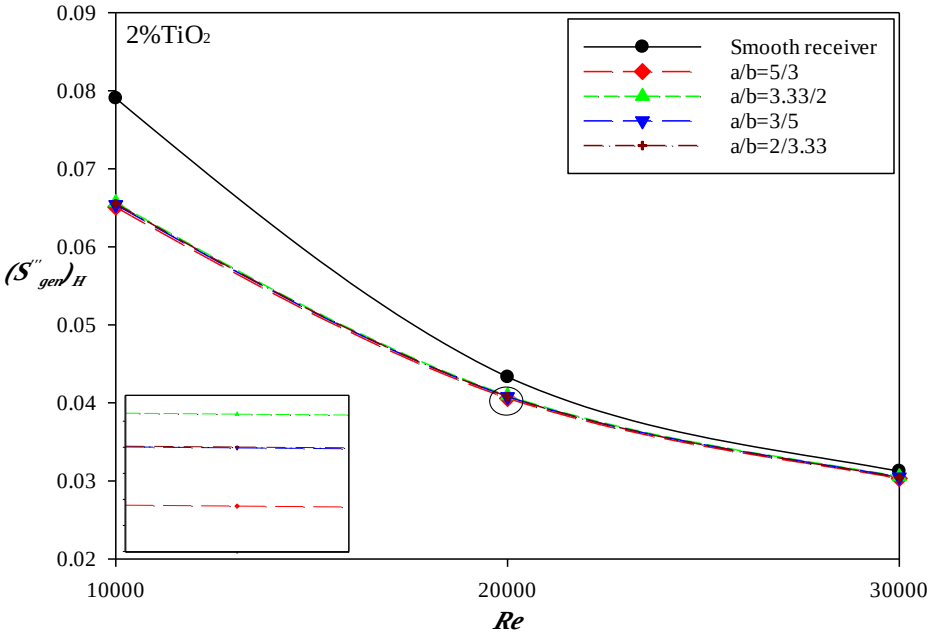
2%TiO2
Smooth receiver
a/b=5/3
a/b=3.33/2
a/b=3/5
a/b=2/3.33
0.09
0.08
0.07
0.06
0.05
0.04
0.03
0.02
(S'''gen)H
10000
20000
30000
Re

(c)

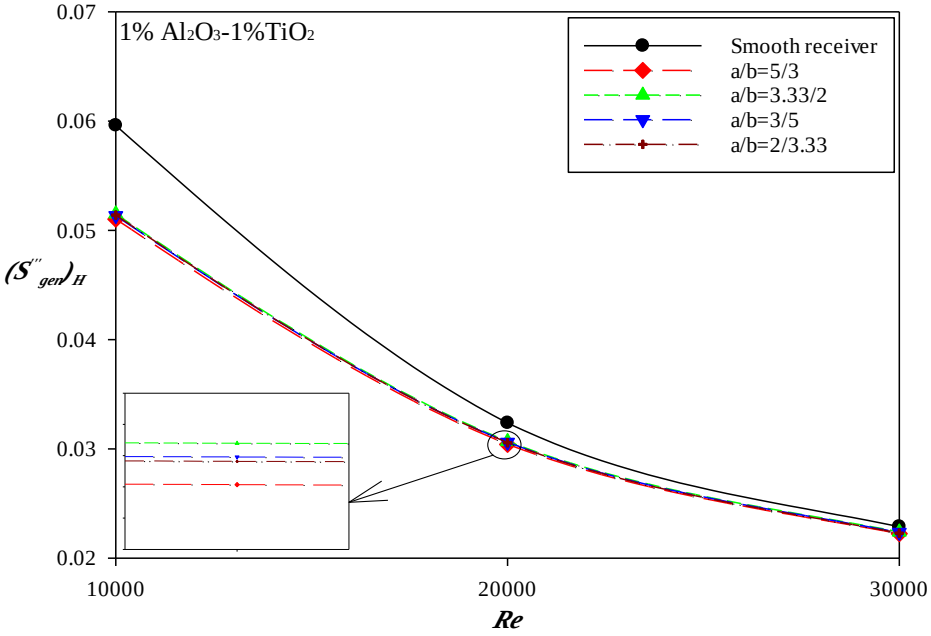
1% Al2O3-1%TiO2
Smooth receiver
a/b=5/3
a/b=3.33/2
a/b=3/5
a/b=2/3.33
0.07
0.06
0.05
0.04
0.03
0.02
(S'''gen)H
10000
20000
30000
Re

(d)

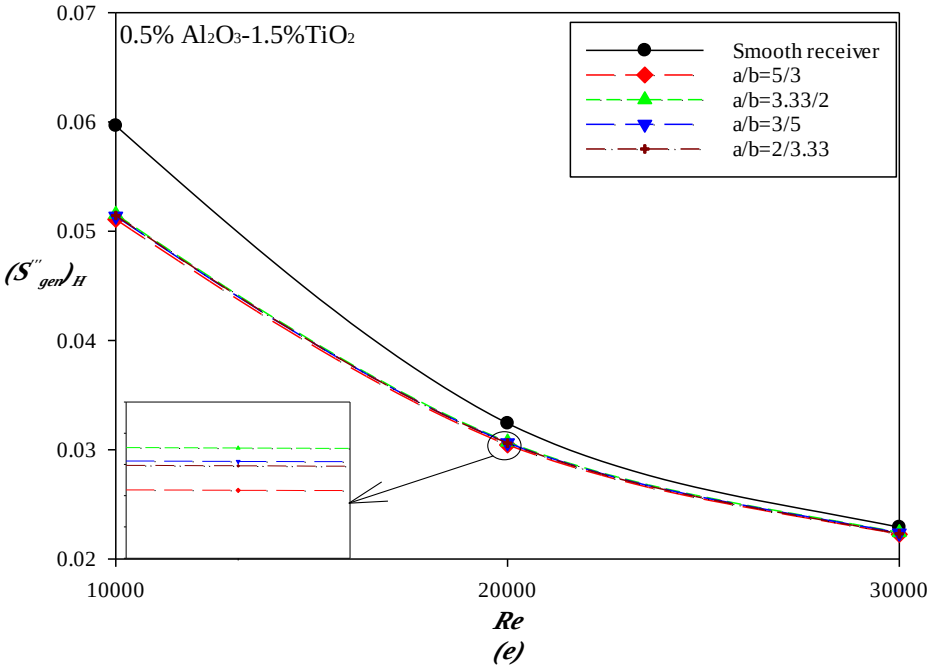

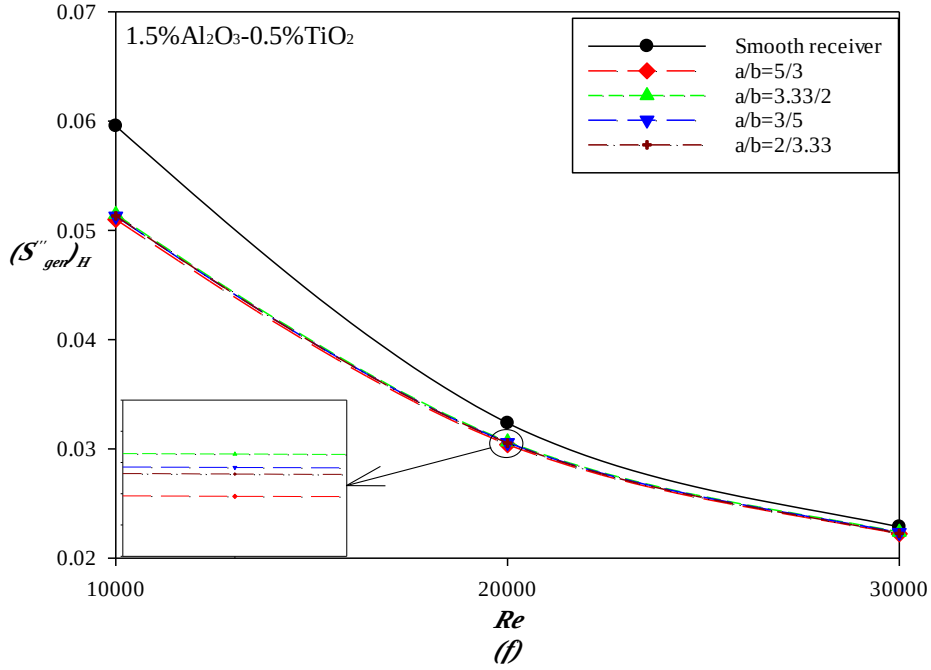

Figure 4.12. Variation of *Irreversible* heat transfer with *Re* for elliptical ratios of dimples with working fluids of: (a) *Syltherm800* (b) *2.0% Al_2O_3/Syltherm800* (c) *2%TiO/Syltherm800* (d) *1%Al_2O_3-1%TiO_2/Syltherm800* (e) *0.5%Al_2O_3-1.5%TiO_2/Syltherm800* (f) *1.5%Al_2O_3-0.5%TiO_2/Syltherm800*.

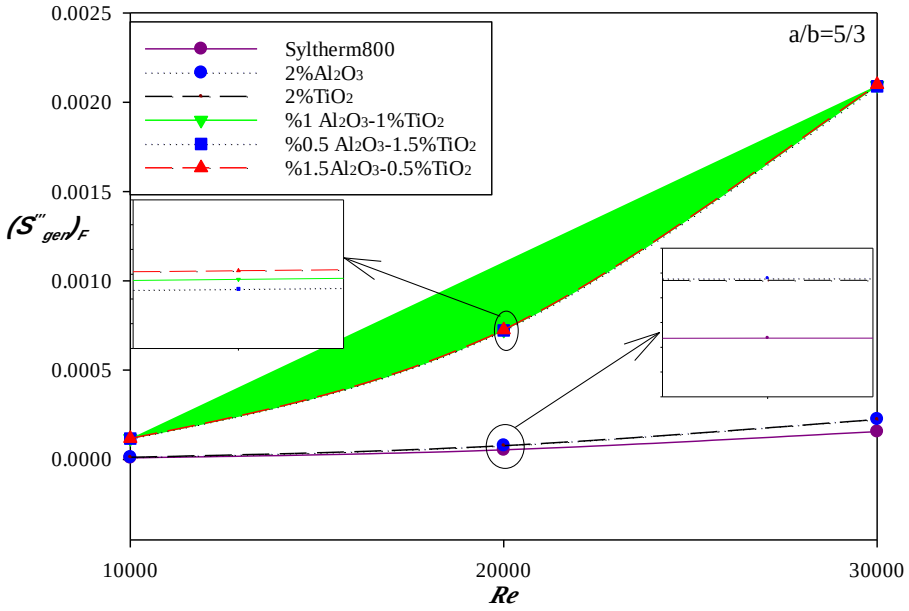
a/b=5/3
Syltherm800
2%Al2O3
2%TiO2
%1 Al2O3-1%TiO2
%0.5 Al2O3-1.5%TiO2
%1.5Al2O3-0.5%TiO2
0.0025
0.0020
0.0015
0.0010
0.0005
0.0000
(S'''gen)F
10000
20000
30000
Re

(a)

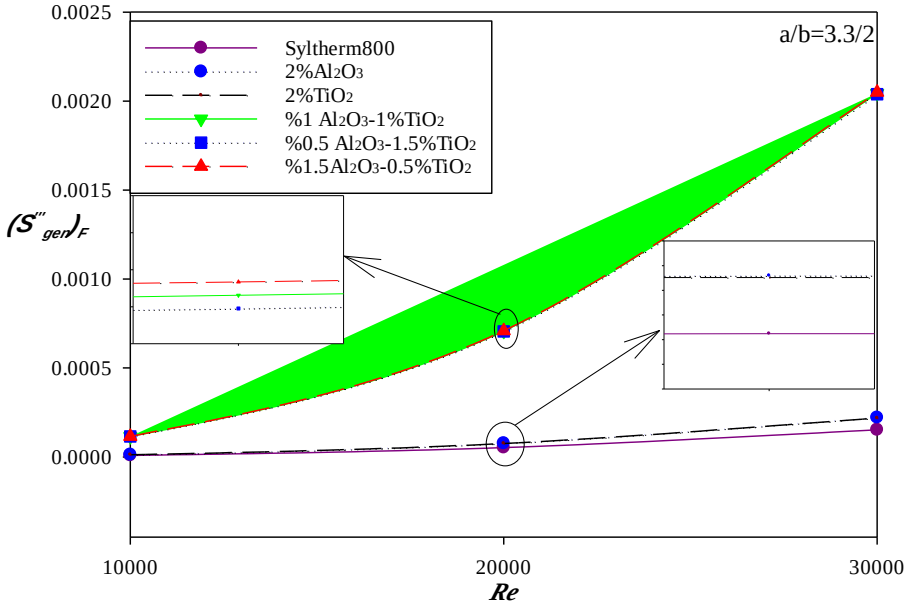
a/b=3.3/2
Syltherm800
2%Al2O3
2%TiO2
%1 Al2O3-1%TiO2
%0.5 Al2O3-1.5%TiO2
%1.5Al2O3-0.5%TiO2
0.0025
0.0020
0.0015
0.0010
0.0005
0.0000
(S'''gen)F
10000
20000
30000
Re

(b)

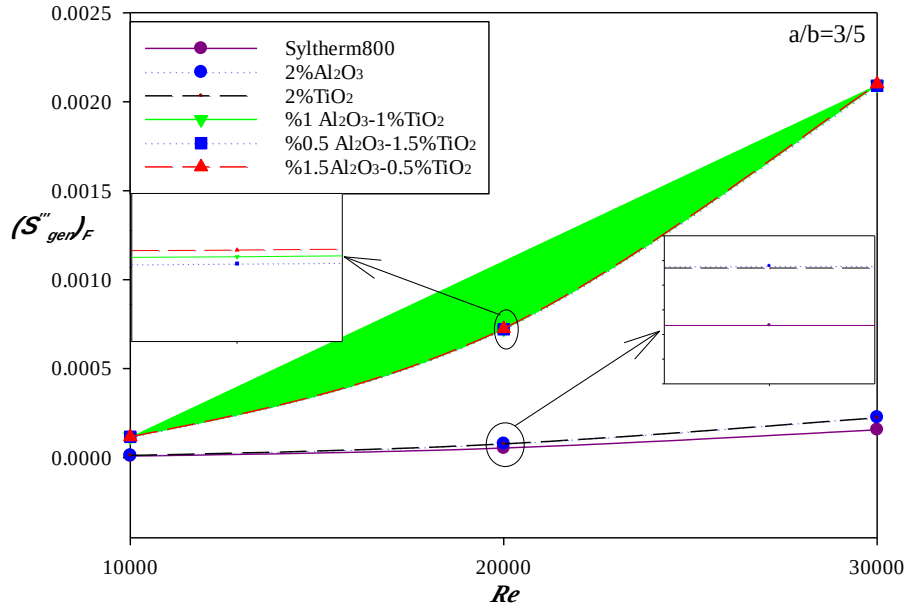
a/b=3/5
Syltherm800
2%Al2O3
2%TiO2
%1 Al2O3-1%TiO2
%0.5 Al2O3-1.5%TiO2
%1.5Al2O3-0.5%TiO2
0.0025
0.0020
0.0015
0.0010
0.0005
0.0000
(S'''gen)F
10000
20000
30000
Re

(c)

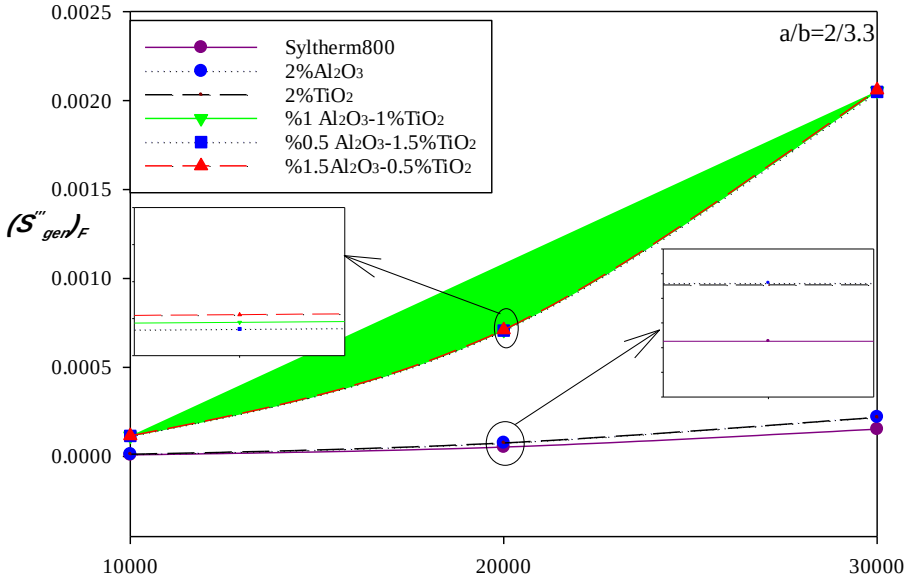
a/b=2/3.3
Syltherm800
2%Al2O3
2%TiO2
%1 Al2O3-1%TiO2
%0.5 Al2O3-1.5%TiO2
%1.5Al2O3-0.5%TiO2
0.0025
0.0020
0.0015
0.0010
0.0005
0.0000
(S'''gen)F
10000
20000
30000
Re

(d)

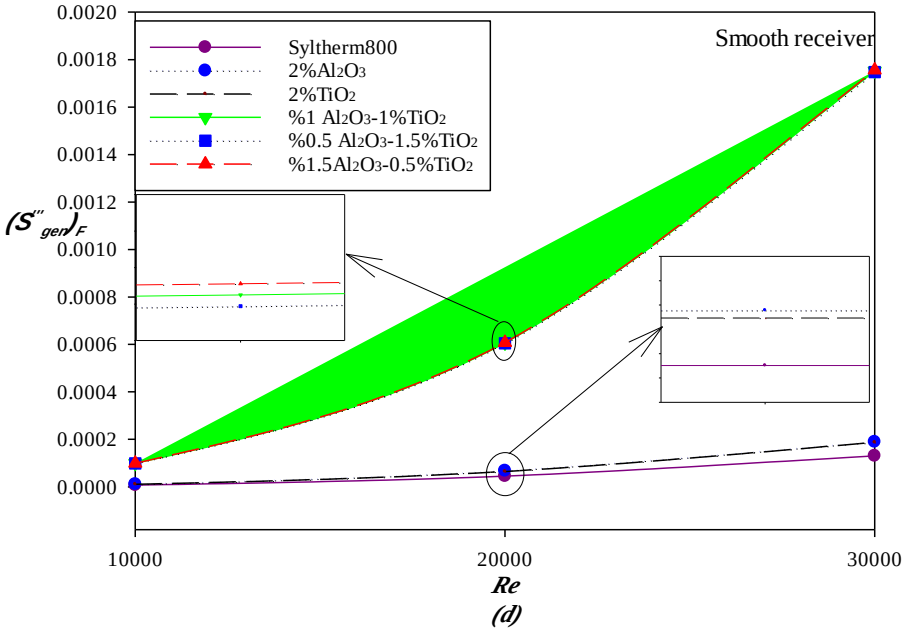

Figure 4.13. Variation of Irreversible fluid friction with *Re* with different nanofluid types for elliptical ratios of dimples for receiver tube: (a) *ER=5/3* (b) *ER= 3.3/2* (c) *ER=3/5* (d) *ER=2/3.3* (e) *smooth*

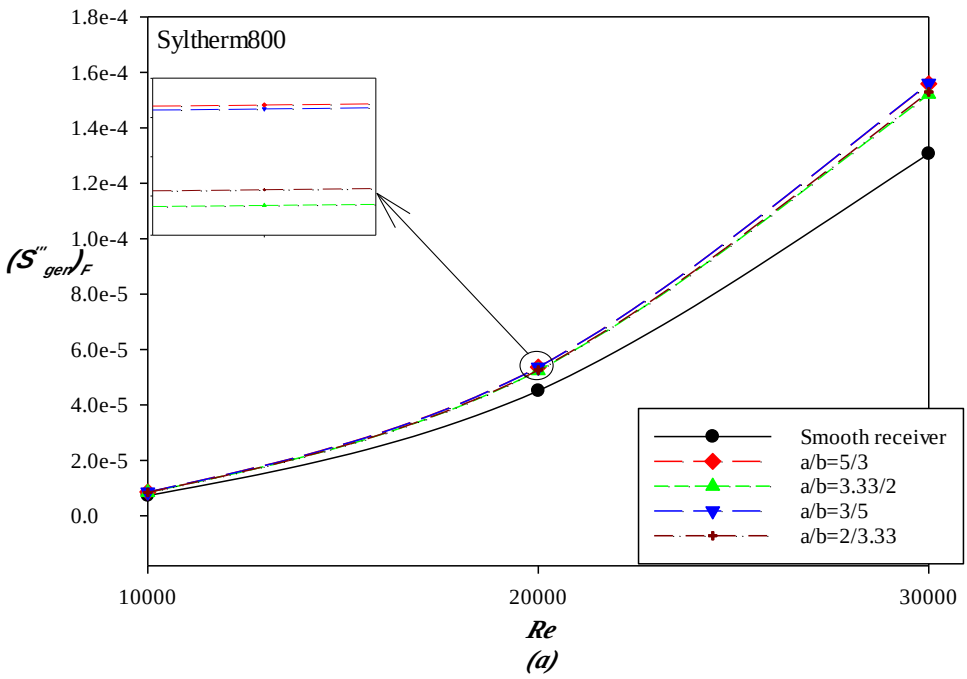

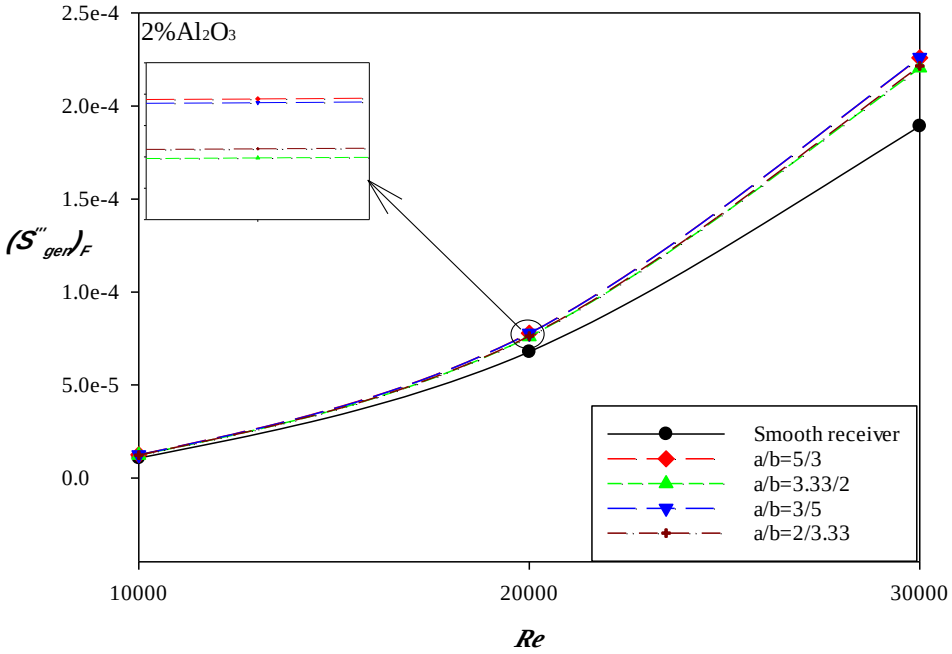
2%Al2O3
2.5e-4
2.0e-4
1.5e-4
1.0e-4
5.0e-5
0.0
(S'''gen)F
10000
20000
30000
Re
Smooth receiver
a/b=5/3
a/b=3.33/2
a/b=3/5
a/b=2/3.33

(b)

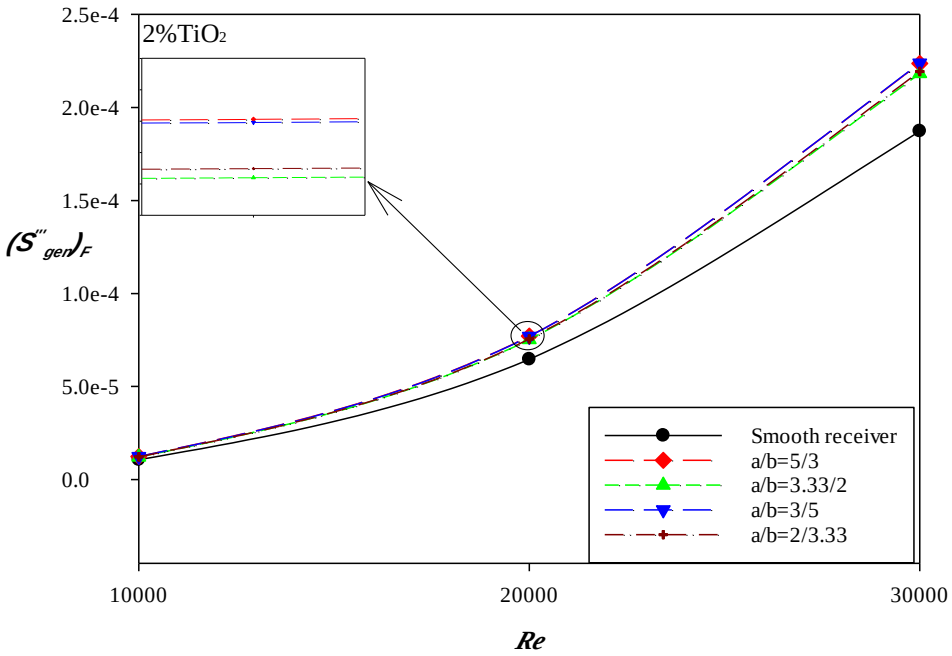
2%TiO2
2.5e-4
2.0e-4
1.5e-4
1.0e-4
5.0e-5
0.0
(S'''gen)F
10000
20000
30000
Re
Smooth receiver
a/b=5/3
a/b=3.33/2
a/b=3/5
a/b=2/3.33

(c)

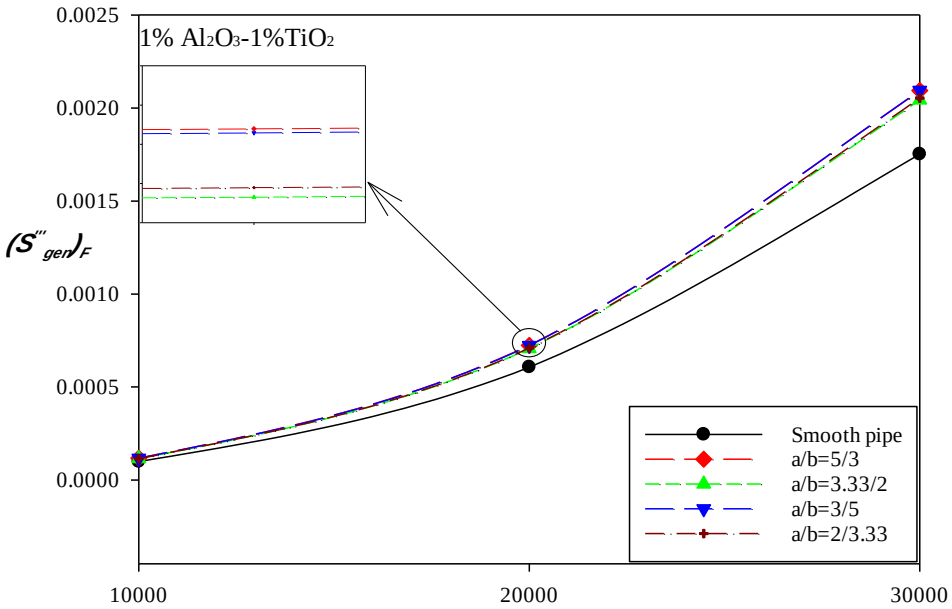
1% Al2O3-1%TiO2
0.0025
0.0020
0.0015
0.0010
0.0005
0.0000
(S'''gen)F
10000
20000
30000
Re
Smooth pipe
a/b=5/3
a/b=3.33/2
a/b=3/5
a/b=2/3.33

(d)

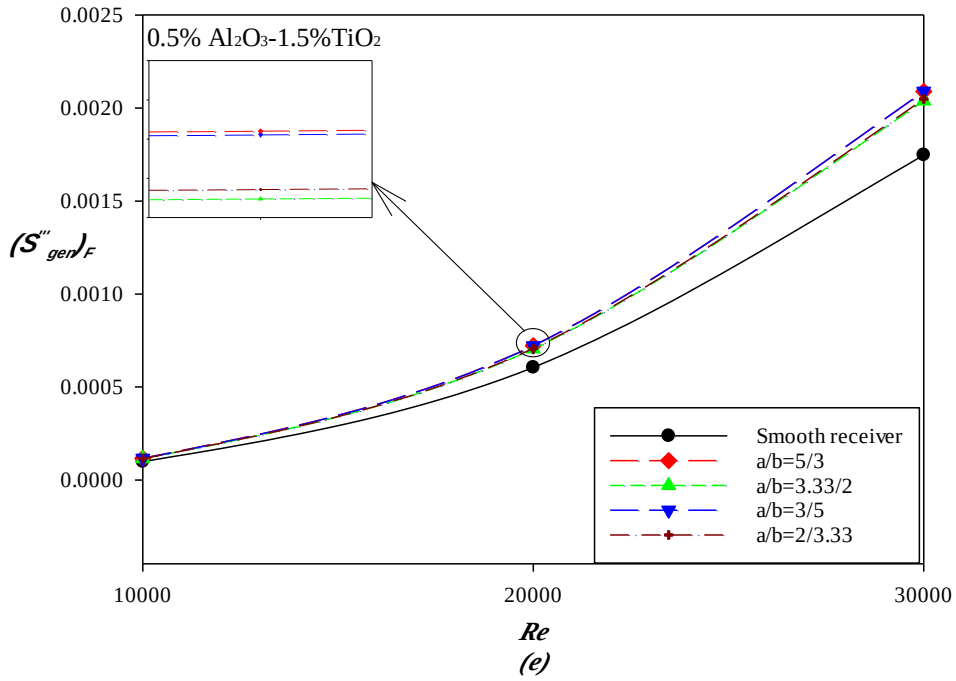

(e)

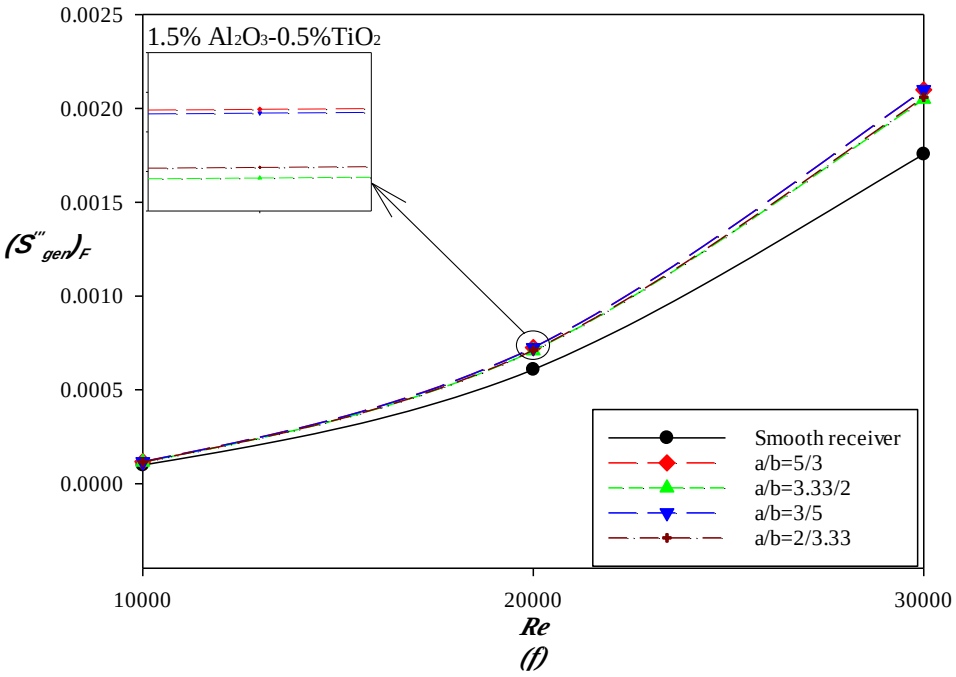

(f)

Figure 4.14. Variation of Irreversible fluid friction with *Re* for elliptical ratios of dimples with working fluids of: (a) *Syltherm800* (b) *2.0% Al_2O_3/Syltherm800* (c) *2%TiO/Syltherm800* (d) *1%Al_2O_3-1%TiO_2/Syltherm800* (e) *0.5%Al_2O_3-1.5%TiO_2/Syltherm800* (f) *1.5%Al_2O_3-0.5%TiO_2/Syltherm800*.

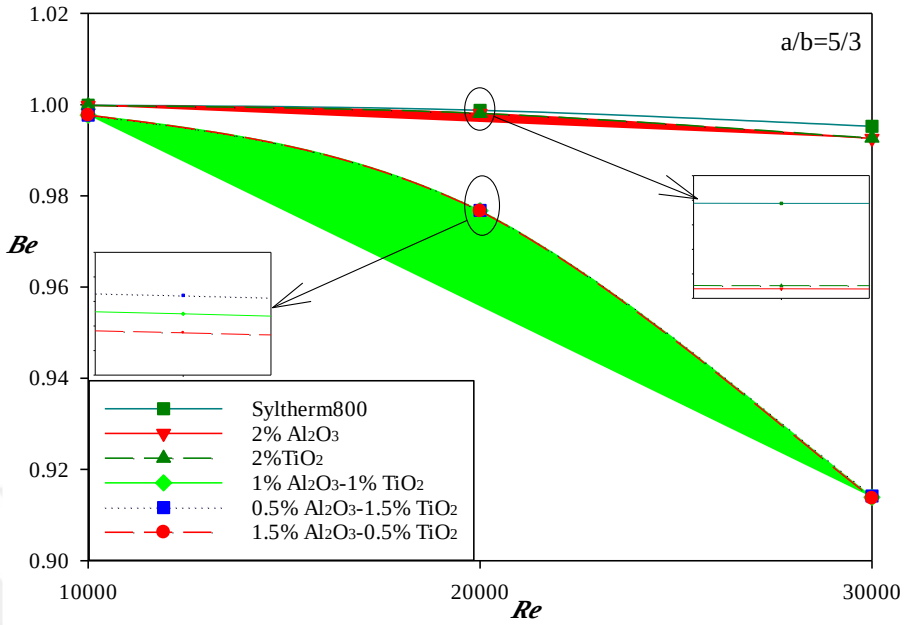
a/b=5/3
1.02
1.00
0.98
0.96
0.94
0.92
0.90
Be
10000
20000
30000
Re
Syltherm800
2% Al2O3
2%TiO2
1% Al2O3-1% TiO2
0.5% Al2O3-1.5% TiO2
1.5% Al2O3-0.5% TiO2

(a)

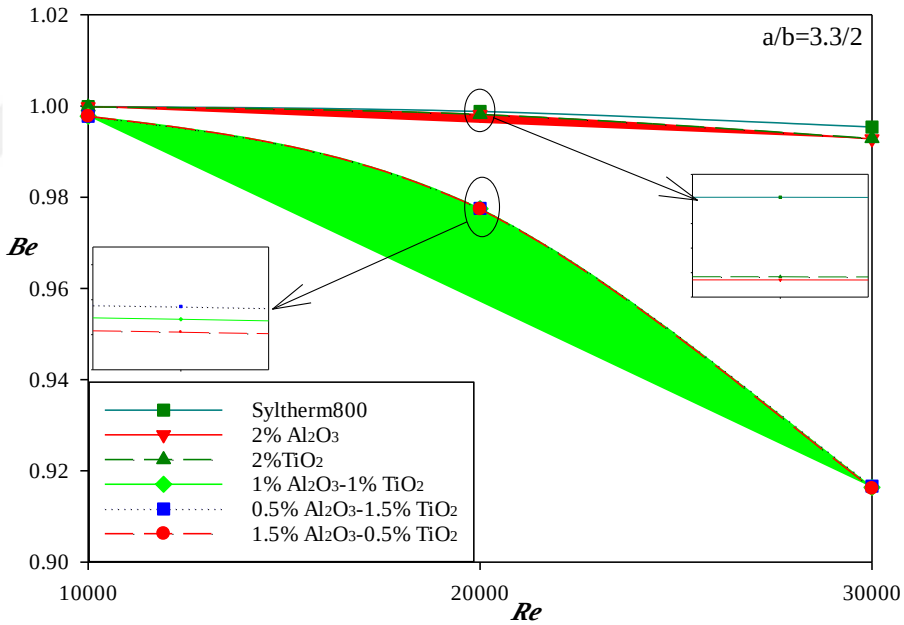
a/b=3.3/2
1.02
1.00
0.98
0.96
0.94
0.92
0.90
Be
10000
20000
30000
Re
Syltherm800
2% Al2O3
2%TiO2
1% Al2O3-1% TiO2
0.5% Al2O3-1.5% TiO2
1.5% Al2O3-0.5% TiO2

(b)

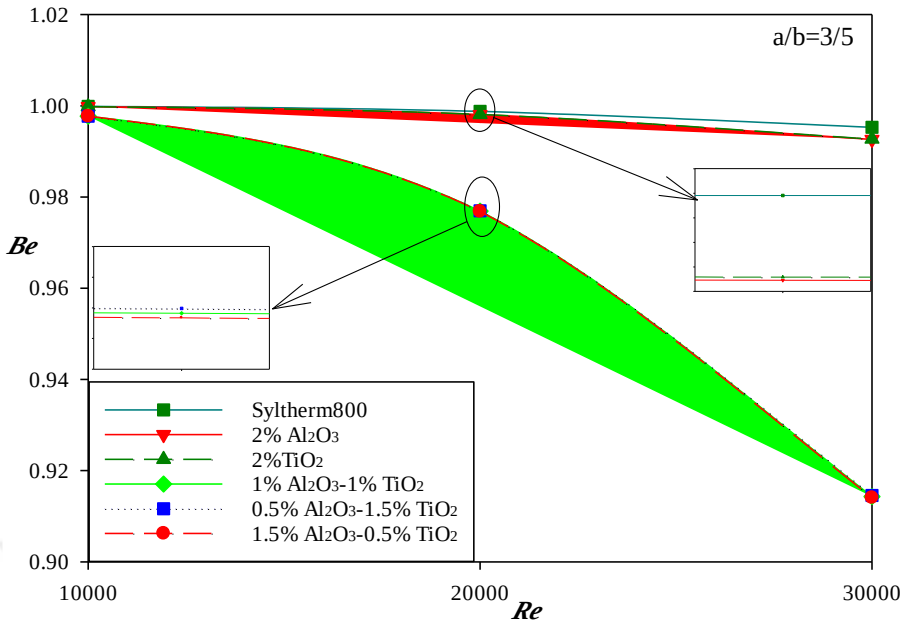
a/b=3/5
1.02
1.00
0.98
0.96
0.94
0.92
0.90
Be
10000
20000
30000
Re
Syltherm800
2% Al2O3
2%TiO2
1% Al2O3-1% TiO2
0.5% Al2O3-1.5% TiO2
1.5% Al2O3-0.5% TiO2

(c)

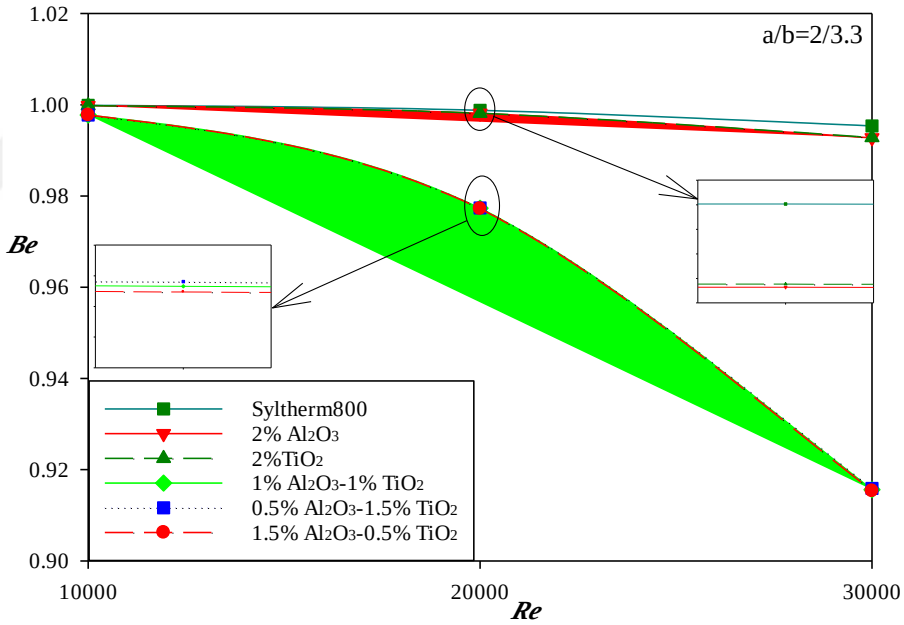
a/b=2/3.3
1.02
1.00
0.98
0.96
0.94
0.92
0.90
Be
10000
20000
30000
Re
Syltherm800
2% Al2O3
2%TiO2
1% Al2O3-1% TiO2
0.5% Al2O3-1.5% TiO2
1.5% Al2O3-0.5% TiO2

(d)

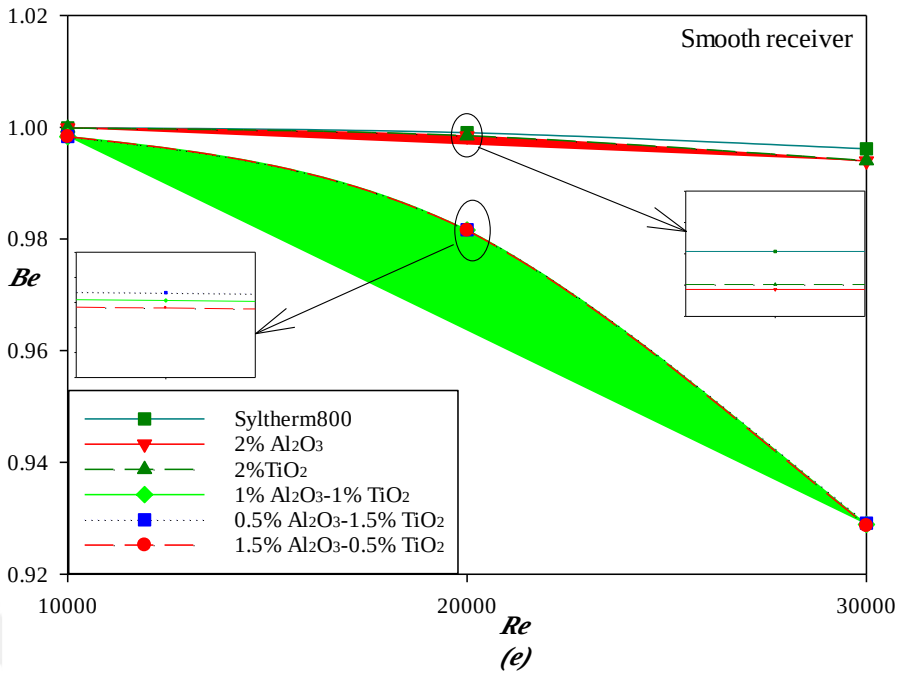

Figure 4. 15. Variation of *Be* with *Re* with different nanofluid types for elliptical ratios of dimples for receiver tube: (a) *ER=5/3* (b) *ER= 3.3/2* (c) *ER=3/5* (d) *ER=2/3.3* (e) *smooth*

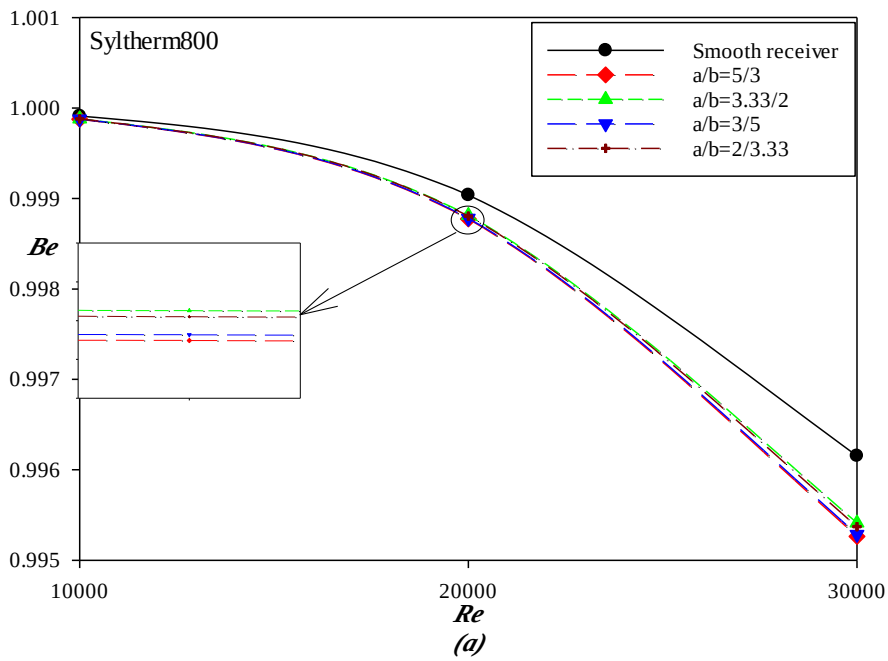

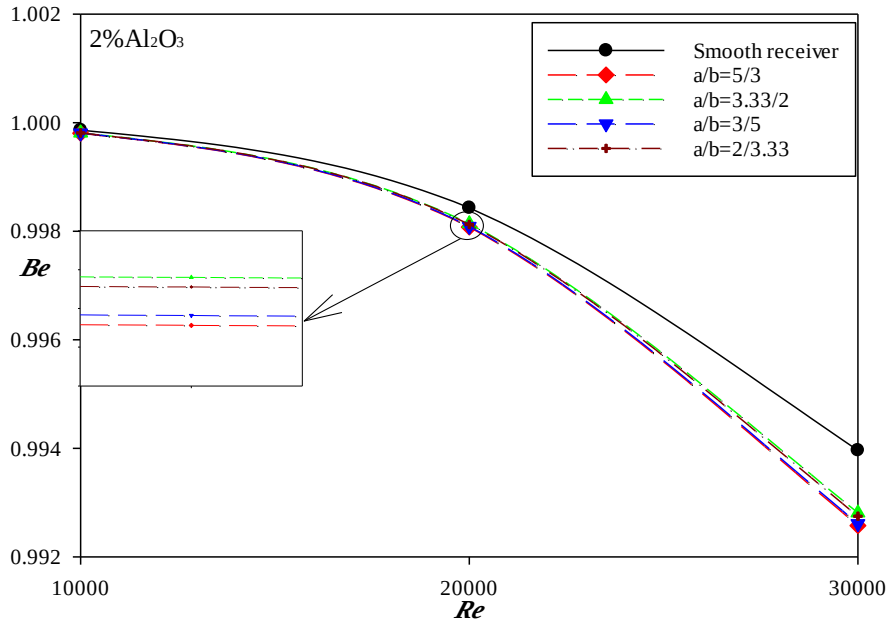
2%Al2O3
Smooth receiver
a/b=5/3
a/b=3.33/2
a/b=3/5
a/b=2/3.33
1.002
1.000
0.998
0.996
0.994
0.992
Be
10000
20000
30000
Re

(b)

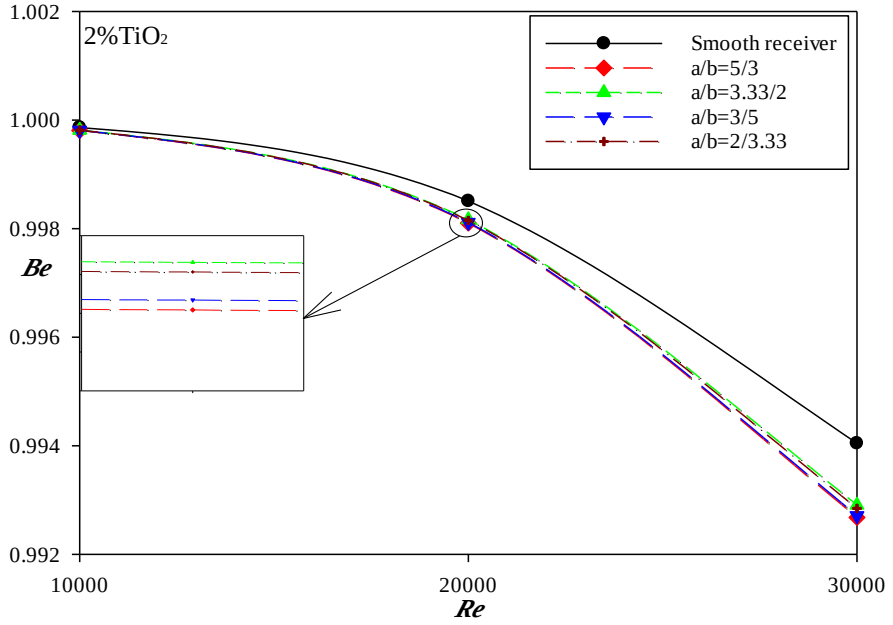
2%TiO2
Smooth receiver
a/b=5/3
a/b=3.33/2
a/b=3/5
a/b=2/3.33
1.002
1.000
0.998
0.996
0.994
0.992
Be
10000
20000
30000
Re

(c)

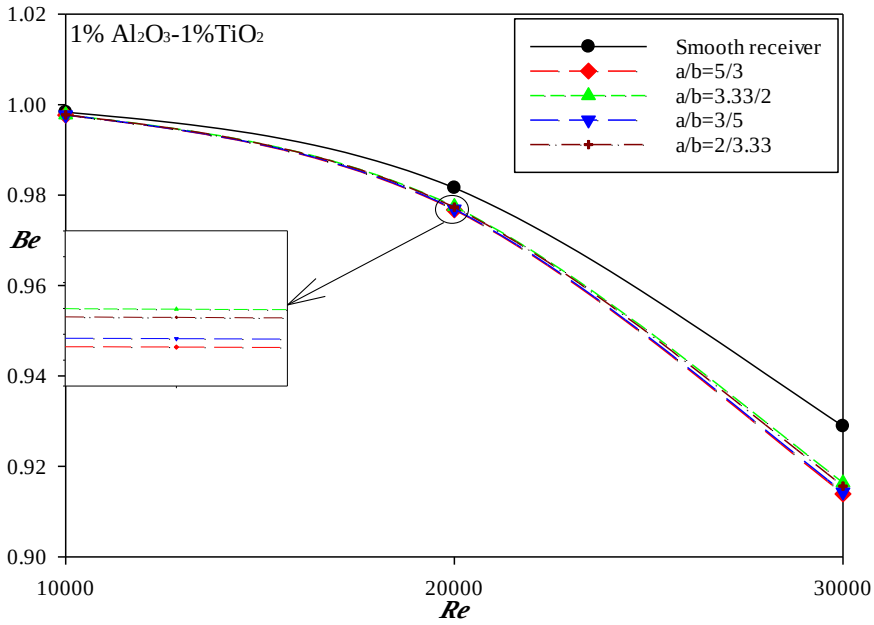
1% Al2O3-1%TiO2
Smooth receiver
a/b=5/3
a/b=3.33/2
a/b=3/5
a/b=2/3.33
1.02
1.00
0.98
Be
0.96
0.94
0.92
0.90
10000
20000
30000
Re

(d)

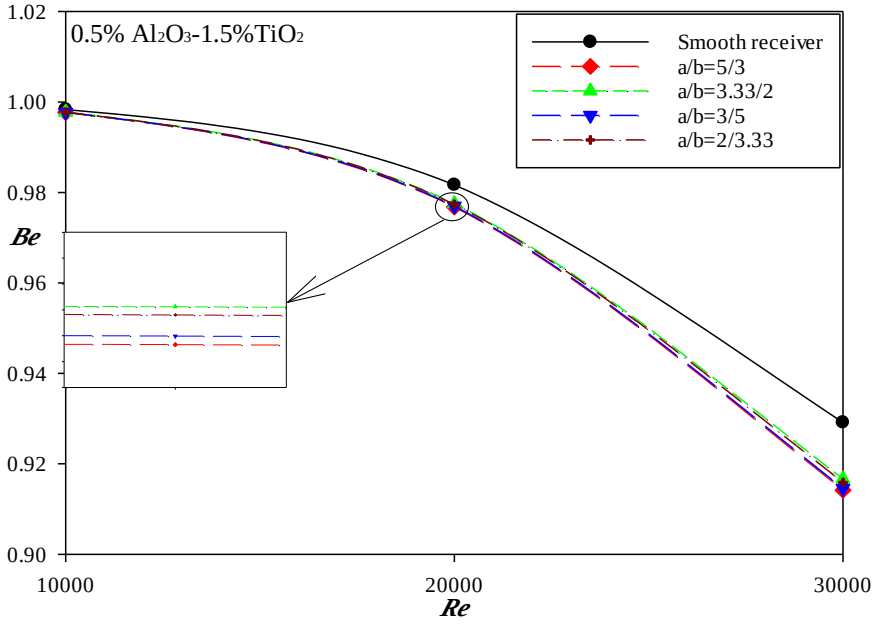
0.5% Al2O3-1.5%TiO2
Smooth receiver
a/b=5/3
a/b=3.33/2
a/b=3/5
a/b=2/3.33
1.02
1.00
0.98
Be
0.96
0.94
0.92
0.90
10000
20000
30000
Re

(e)

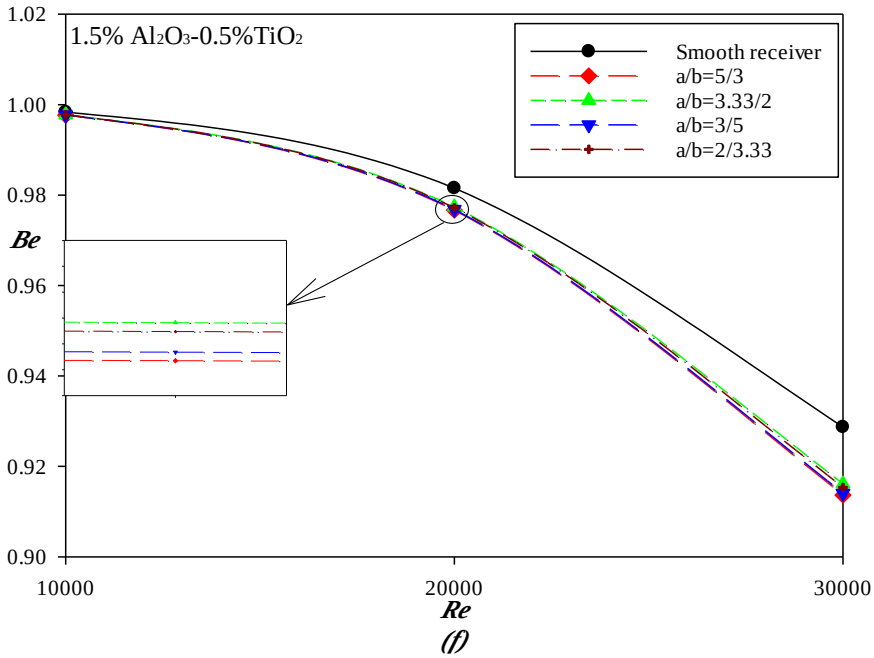

Figure 4.16. Variation of *Be* with *Re* for elliptical ratios of dimples with working fluids of: (a) *Syltherm800* (b) *2.0% Al_2O_3/Syltherm800* (c) *2%TiO/Syltherm800* (d) *1%Al_2O_3- 1%TiO_2/Syltherm800* (e) *0.5%Al_2O_3-1.5%TiO_2/Syltherm800* (f) *1.5%Al_2O_3-0.5%TiO_2/Syltherm800*.

4.6.2. Thermodynamic Performance with Nanofluids

To demonstrate the thermodynamic performance and potential for performance improvement for *PTC`s* receiver, the total rate of generating entropy for different *NPVF* for each receiver tube have been calculated separately. , and each nanofluid has been analyzed individually within the receiver tubes containing dimples of different dimensions as shown in Figure 4.17 and 4.18 the total rate of entropy generation is basically a combination of heat transfer and fluid friction irreversibility., It has been found the Reynolds number decrease causes the decrease in the total rate of generation of entropy too. So, when the Reynolds number is increased from *10,000* to *30,000*, the entropy decreases by an average of *52%*. After that, noted the mono nanofluids and the basic fluid used led to increase the percentage of the generated entropy, and the use of a hybrid nanofluid in *PTC`s* receiver reduces the percentage of the generated entropy by *26%*. The highest value of the entropy has been obtained when using a smooth receiver.

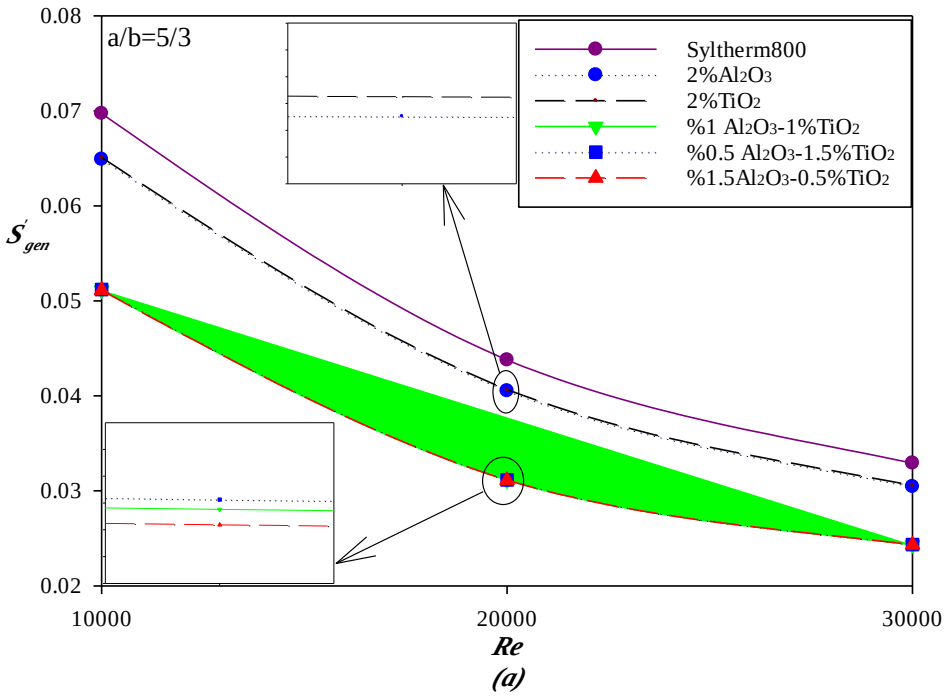

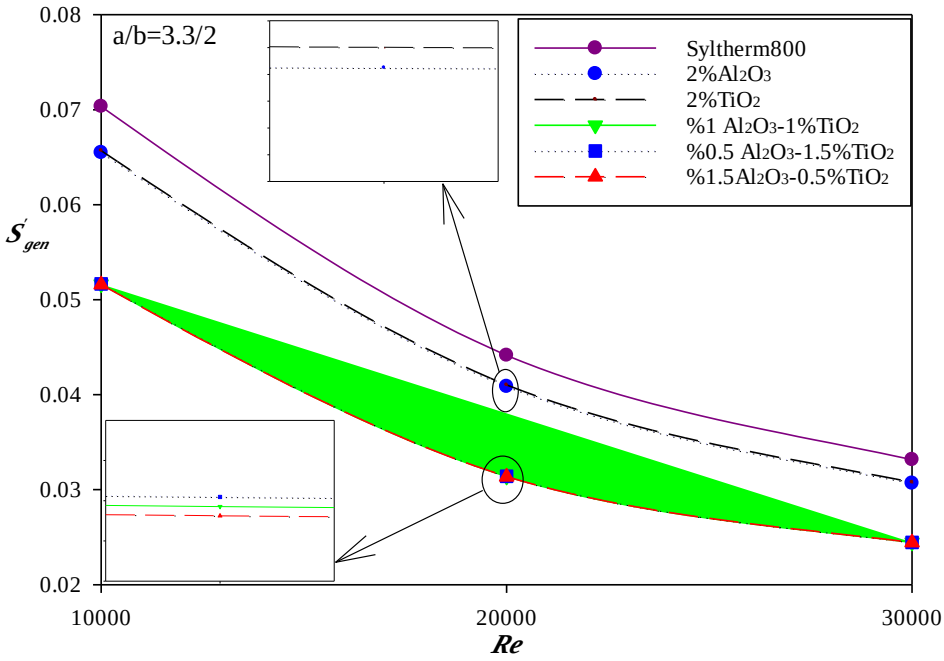
a/b=3.3/2
Syltherm800
2%Al2O3
2%TiO2
%1 Al2O3-1%TiO2
%0.5 Al2O3-1.5%TiO2
%1.5Al2O3-0.5%TiO2
0.08
0.07
0.06
0.05
0.04
0.03
0.02
S'gen
10000
20000
30000
Re

(b)

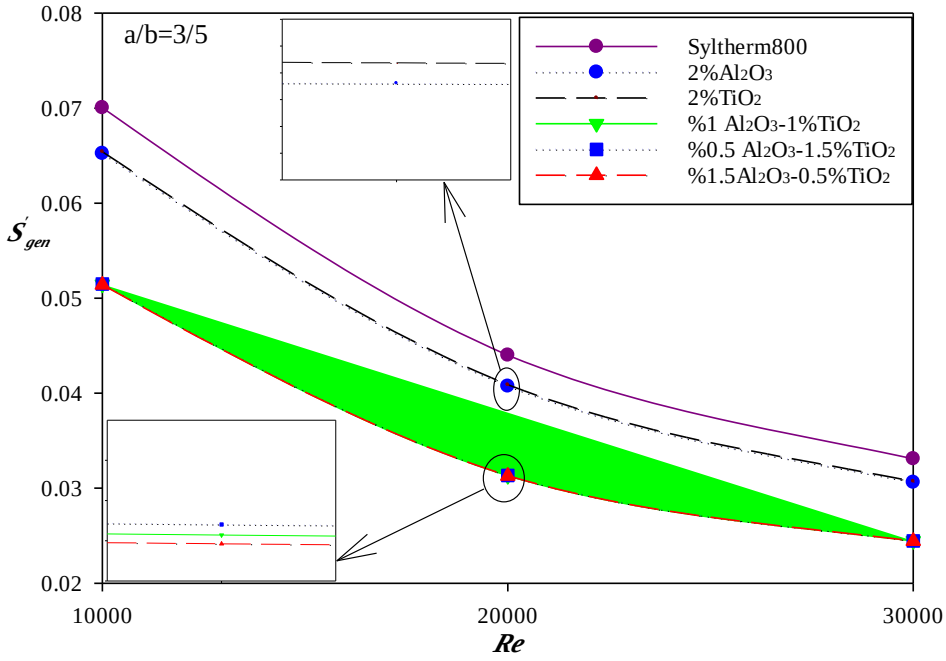
a/b=3/5
Syltherm800
2%Al2O3
2%TiO2
%1 Al2O3-1%TiO2
%0.5 Al2O3-1.5%TiO2
%1.5Al2O3-0.5%TiO2
0.08
0.07
0.06
0.05
0.04
0.03
0.02
S'gen
10000
20000
30000
Re

(c)

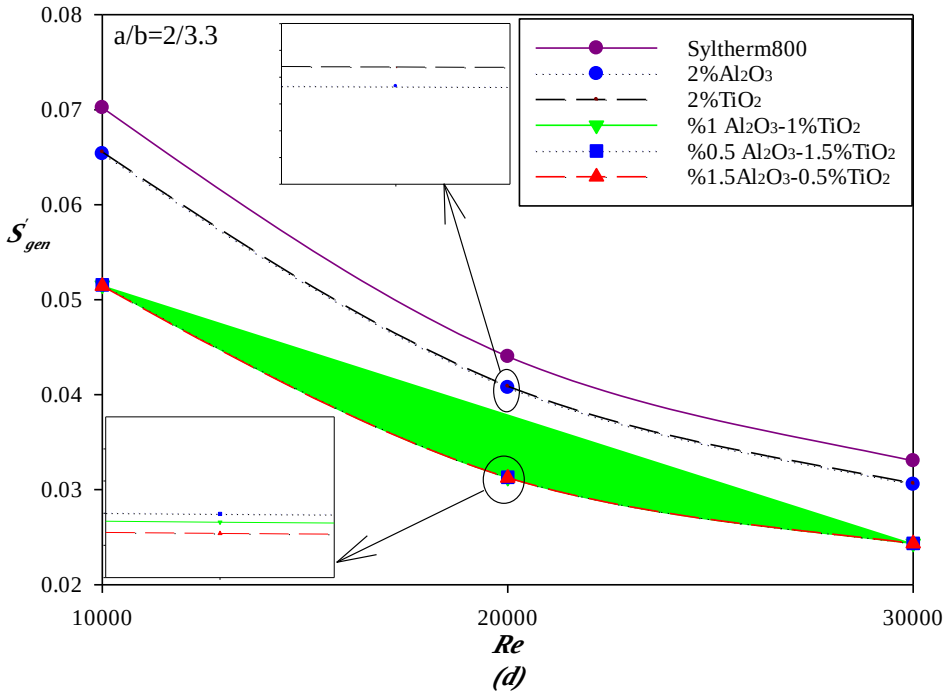

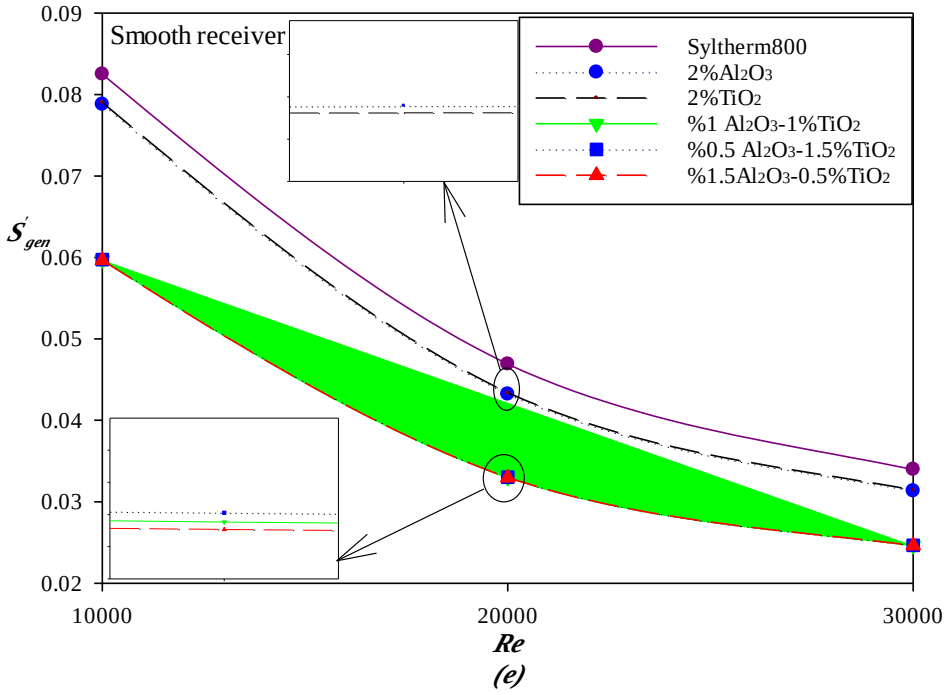

Figure 4.17. Variation of total entropy generation with *Re* with different nanofluid types for elliptical ratios of dimples for receiver tube: (a) *ER=5/3* (b) *ER= 3.3/2* (c) *ER=3/5* (d) *ER=2/3.3* (e) *smooth.*

.

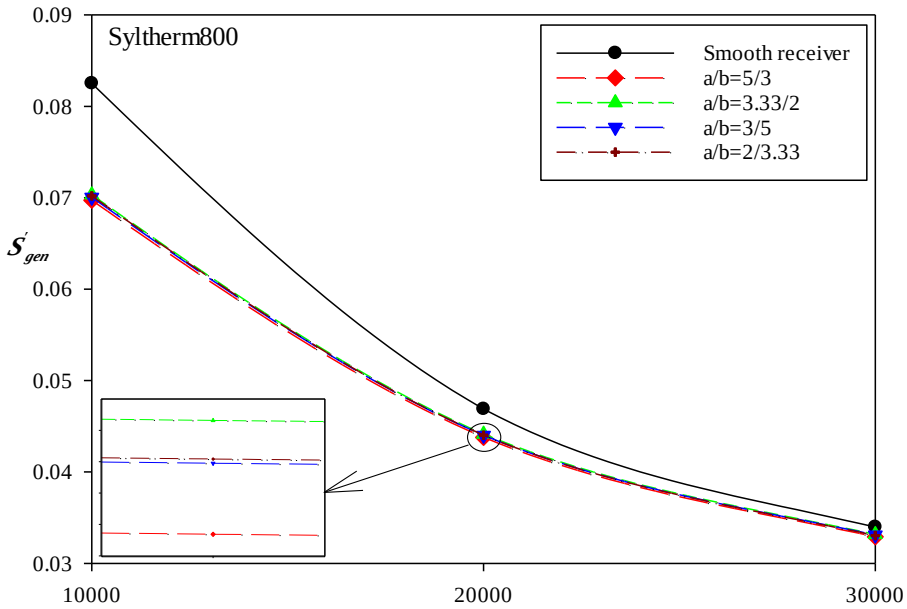
Syltherm800
Smooth receiver
a/b=5/3
a/b=3.33/2
a/b=3/5
a/b=2/3.33
0.09
0.08
0.07
0.06
0.05
0.04
0.03
S'gen
10000
20000
30000
Re

(a)

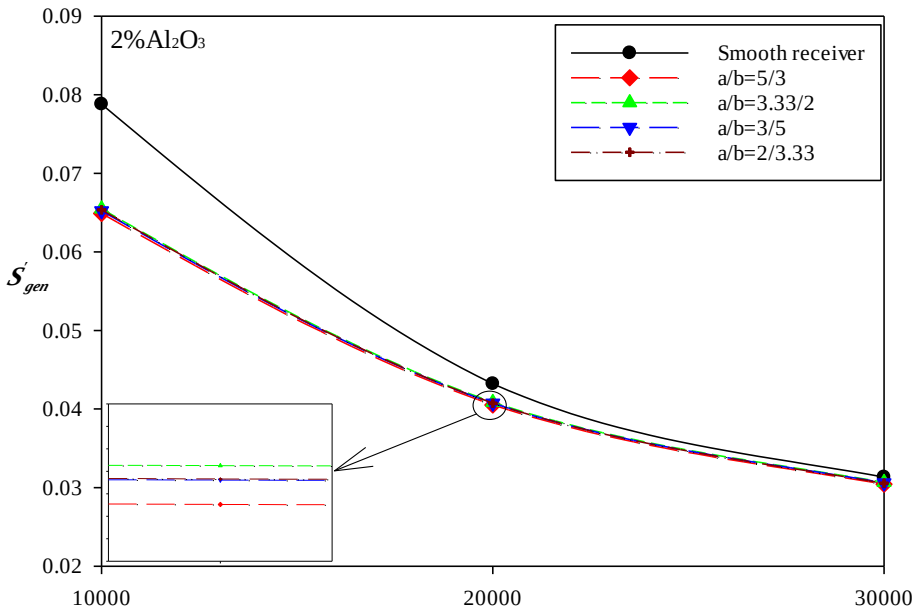
2%Al2O3
Smooth receiver
a/b=5/3
a/b=3.33/2
a/b=3/5
a/b=2/3.33
0.09
0.08
0.07
0.06
0.05
0.04
0.03
0.02
S'gen
10000
20000
30000
Re

(b)

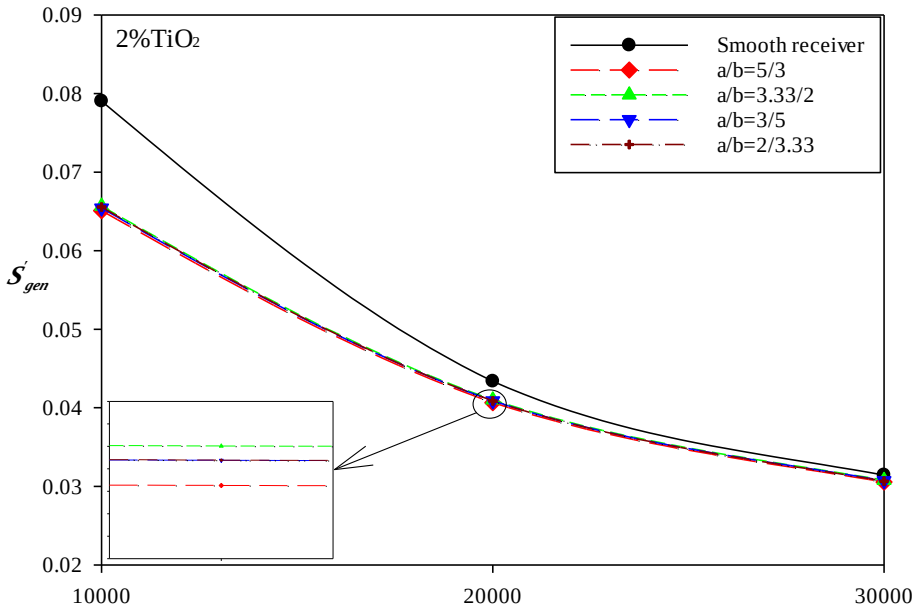
2%TiO2
Smooth receiver
a/b=5/3
a/b=3.33/2
a/b=3/5
a/b=2/3.33
0.09
0.08
0.07
0.06
0.05
0.04
0.03
0.02
S'gen
10000
20000
30000
Re

(c)

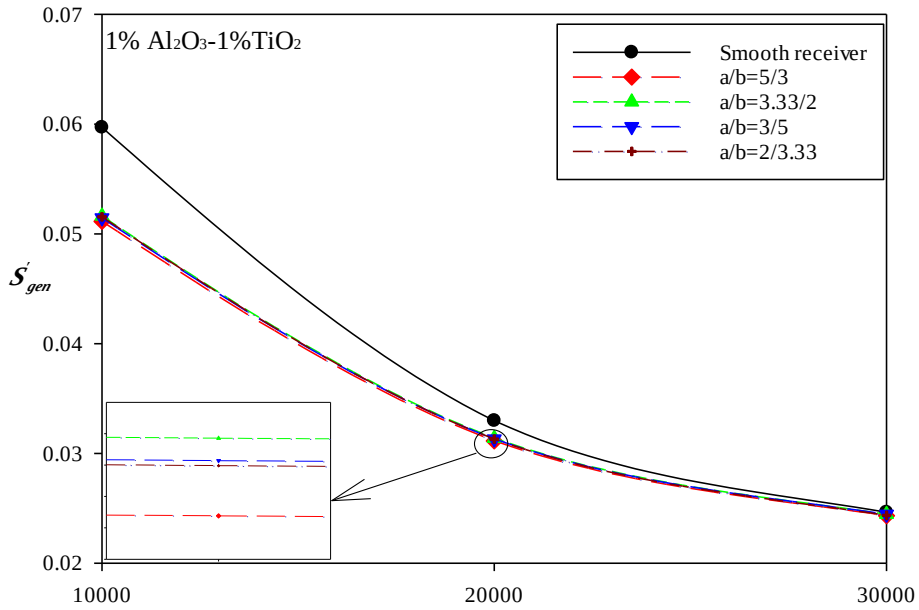
1% Al2O3-1%TiO2
Smooth receiver
a/b=5/3
a/b=3.33/2
a/b=3/5
a/b=2/3.33
0.07
0.06
0.05
0.04
0.03
0.02
S'gen
10000
20000
30000
Re

(d)

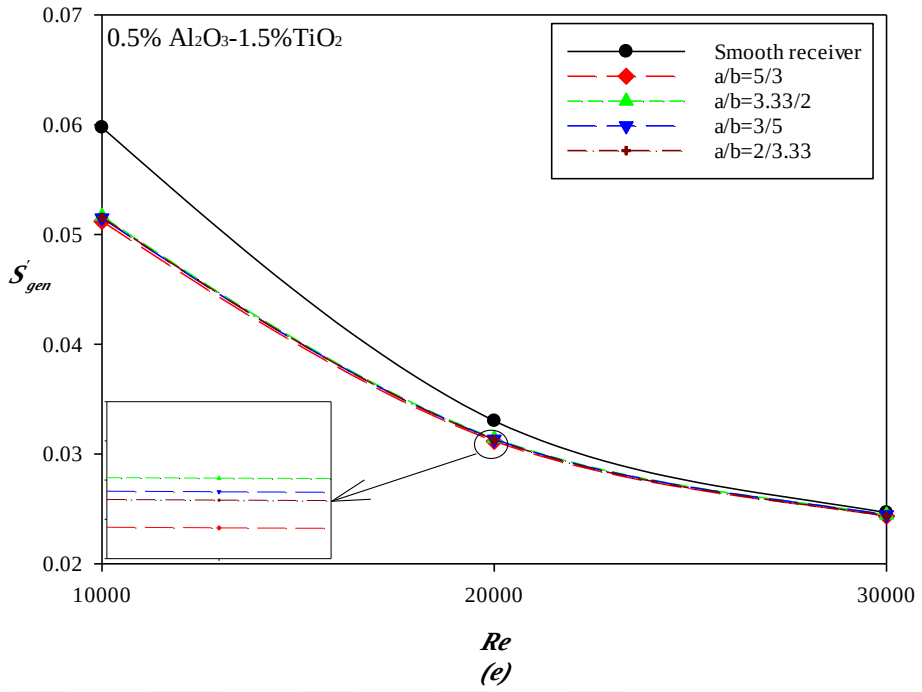

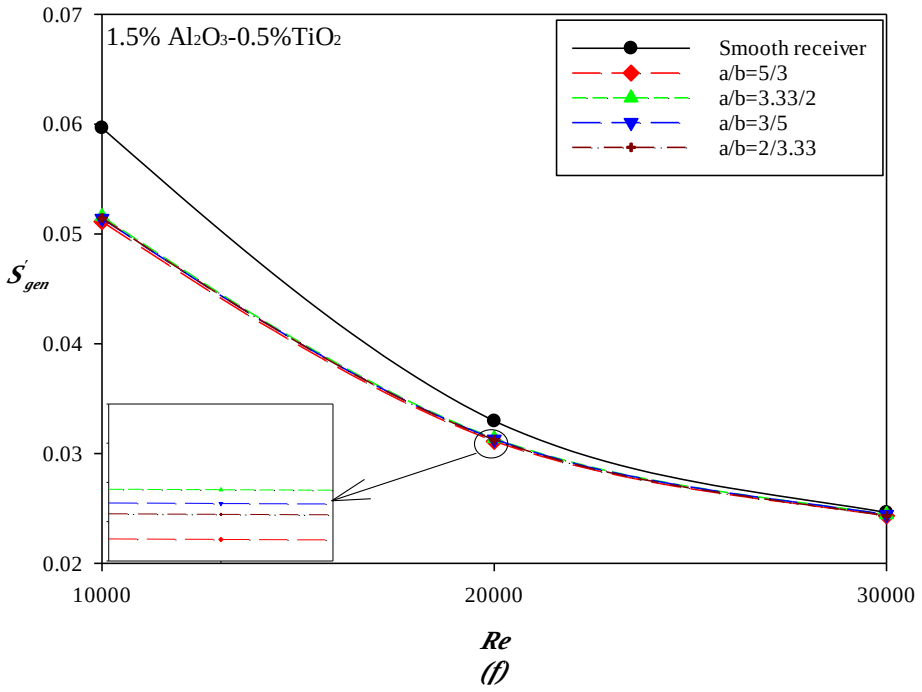

Figure 4.18. Variation of total entropy generation with *Re* for elliptical ratios of dimples with working fluids of: (a) *Syltherm800* (b) *2.0% Al_2O_3/Syltherm800* (c) *2%TiO/Syltherm800* (d) *1%Al_2O_3-1%TiO_2/Syltherm800* (e) *0.5%Al_2O_3-1.5%TiO_2/Syltherm800* (f) *1.5%Al_2O_3-0.5%TiO_2/Syltherm800*.

.

4.7. THE TEMPERATURE DISTRIBUTION OF DIFFERENT PLACES FOR DIFFERENT RECEIVER

The hybrid nanofluid has been selected with hybrid nanofluid of *1.5 %*Al_2O_3*-0.5%*TiO_2*/Syltherm800*.At *Re=30000* to achieve the highest results in thermal efficiency and *PEC* to study the thermal distribution of outlet section in each receiving tube. Figure 4.19 shows the effectiveness of the Reynolds number in the heat distribution inside the receiving tube. The higher the value of the Reynolds number, the more uniform heat distribution in the fluid and the wall of the receiving tube. The temperature of the fluid decreases as the Reynolds number increases.

The heat distribution has been studied for three different regions of *(1.5%*Al_3O_2*-0.5%*TiO_2*/Syltherm800)* at *Re = 30000* along the receiving tube, which include the beginning, middle, and the end regions as shown in Figure 4.20 it was found that the dimples help in the heat transfer process between the receiving tube and the nanofluid. It is also noted that the heat on the smooth tube wall is higher than the heat in the tube containing the dimples, which means that the dimples contribute to the heat transfer process. From the results obtained, the presence of dimples increased the heat transfer coefficient by *27%* compared to a smooth tube.

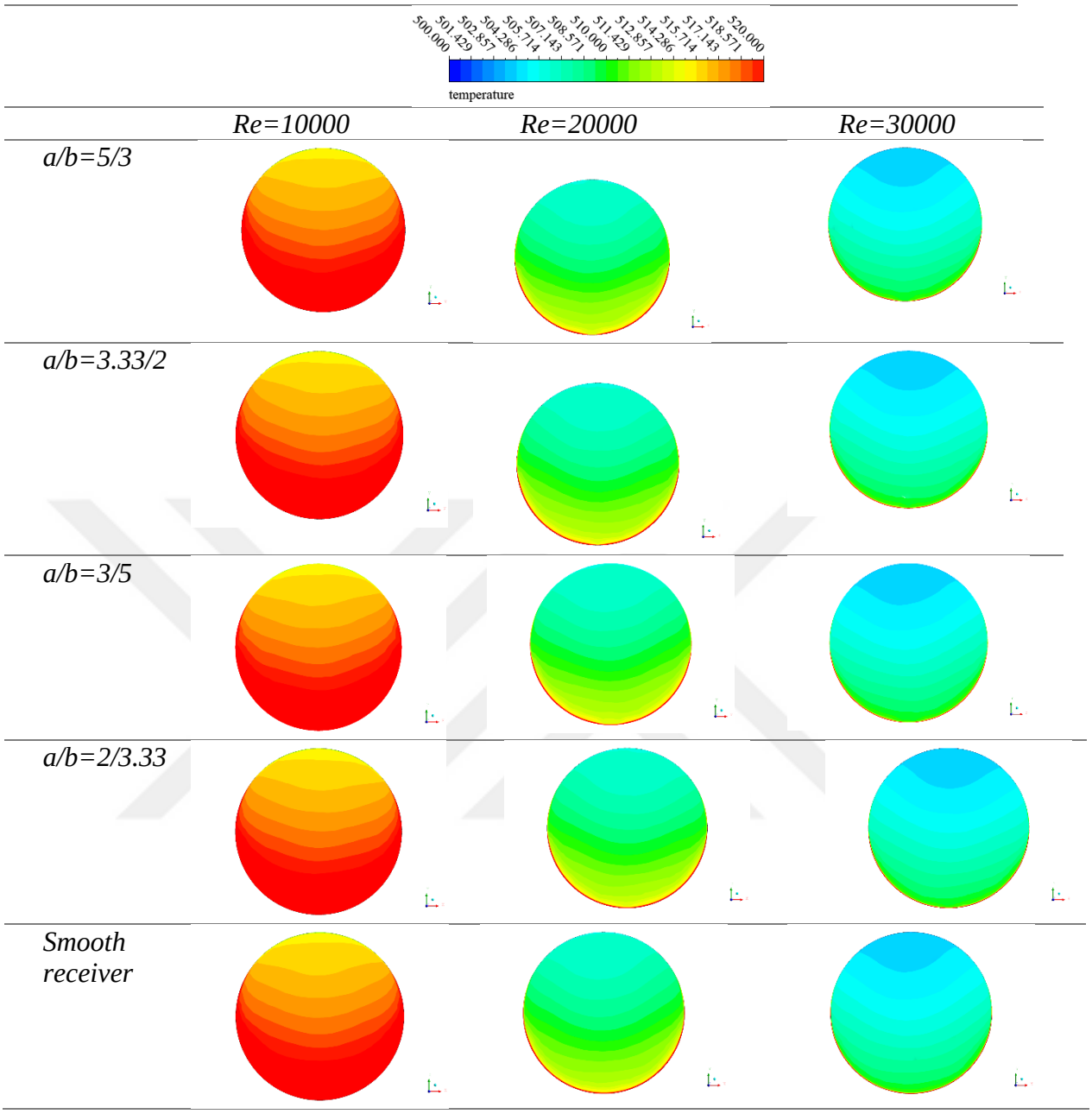

Figure 4.19. Temperature distribution at the outlet section of the receiver tube for different *Re* and elliptical ratios.

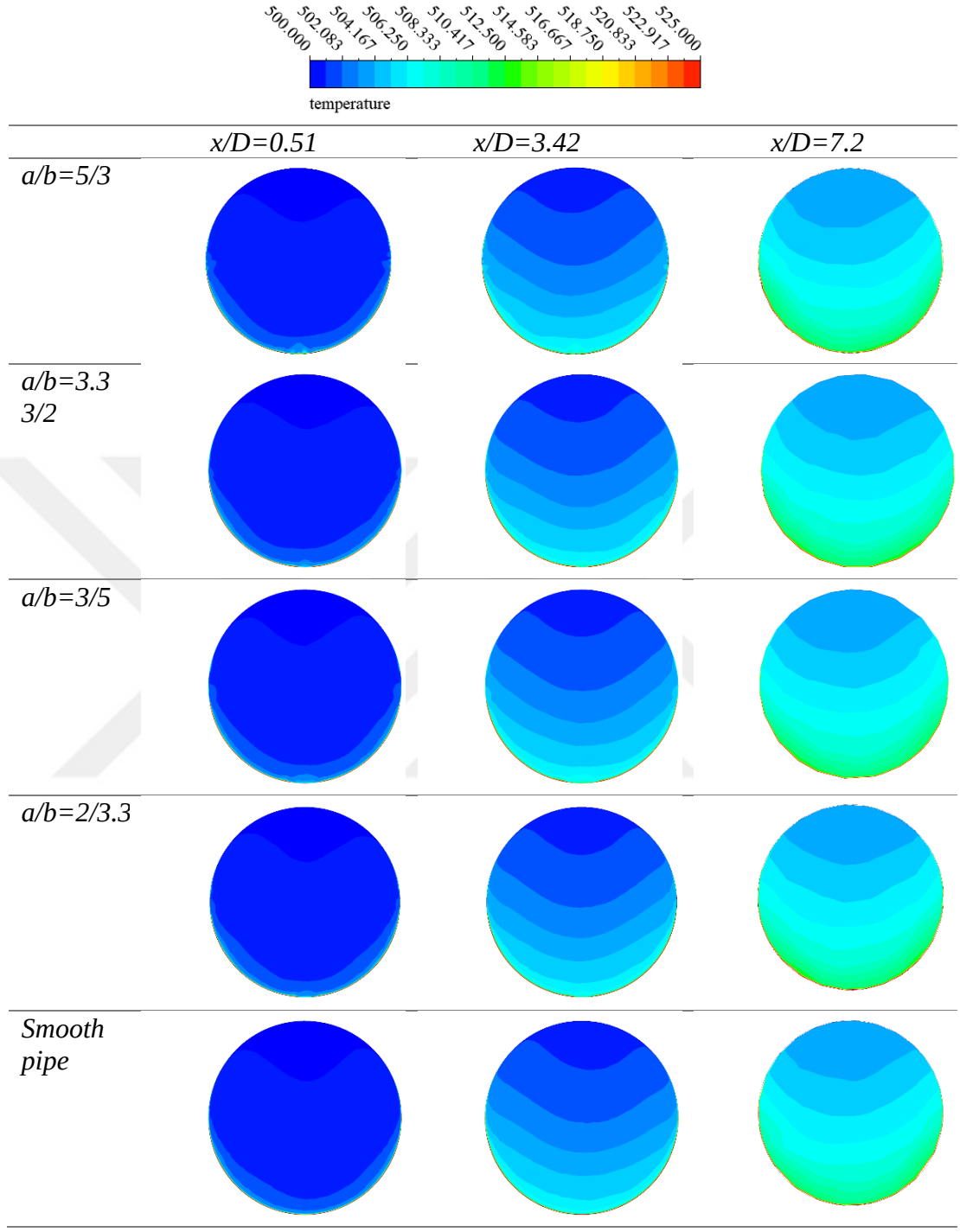

Figure 4.20. Temperature distribution at different sections along the receiver tube for different elliptical ratios.

4.8. THE VELOCITY DISTRIBUTION IN OF DIFFERENT PLACES OF THE RECEIVER OF THE RECEIVER

The velocity distribution at the outlet section of the receiver tube has been studied using *(1.5%Al_3O_2-0.5%TiO_2/Syltherm800)*. It has been observed that the amount of velocity in the dimples area decreased with the increase of the elliptical ratio. The higher the oval ratio, the lower the velocity due to the occurrence of vortices and the vortex produced leads to higher heat transfer. Due to the non-slip condition through the walls, there is a zero value near the wall and a maximum velocity at the center of the collector. And the low speed helps the fluid to transfer heat as shown in Figure 4.21.

The velocity distribution for different places of the receiver length is illustrated in Figure 4.22 for different *ER* by hybrid nanofluid of *0.5%TiO_2-1.5 %Al_2O_3/Syltherm800*. It has three sections with different distances from the inlet tube At *Re = 30000* and studied the velocity distribution in each section. As shown in the figure, the velocity in the areas near the dimples approaches equals zero, and this means that the dimples contributed to a decrease in velocity, which contributes to an increase in the fluid's ability to gain heat. The greater the distance, the more uniform the velocity distribution.

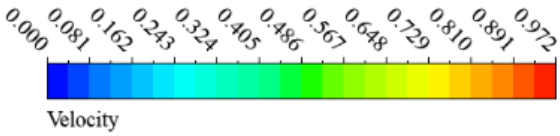

.

	Re=10000	*Re=20000*	*Re=30000*
a/b=5/3	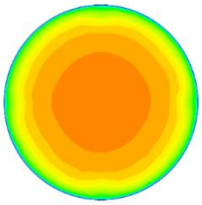	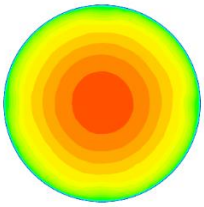	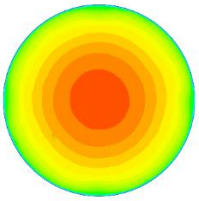
a/b=3.33/2	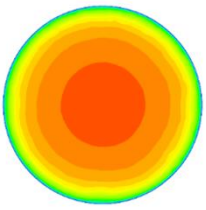	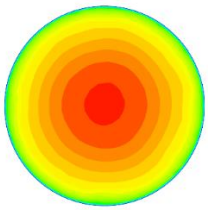	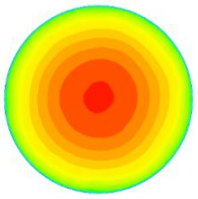
a/b=3/5	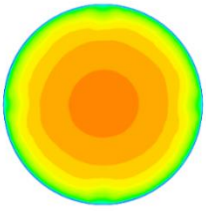	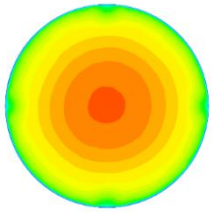	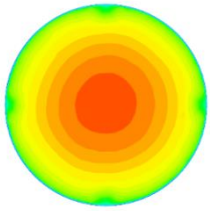
a/b=3/5	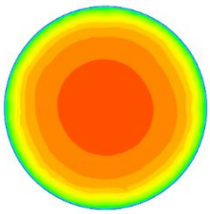	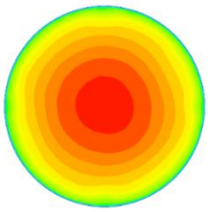	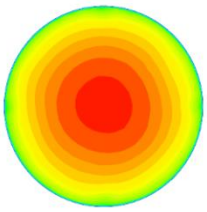
Smooth pipe	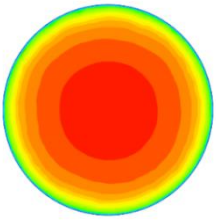	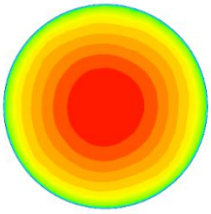	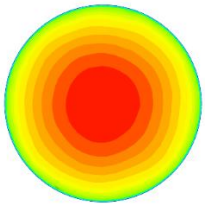

Figure 4.21. Velocity distribution at the outlet section of the receiver tube for different *Re* and elliptical ratios.

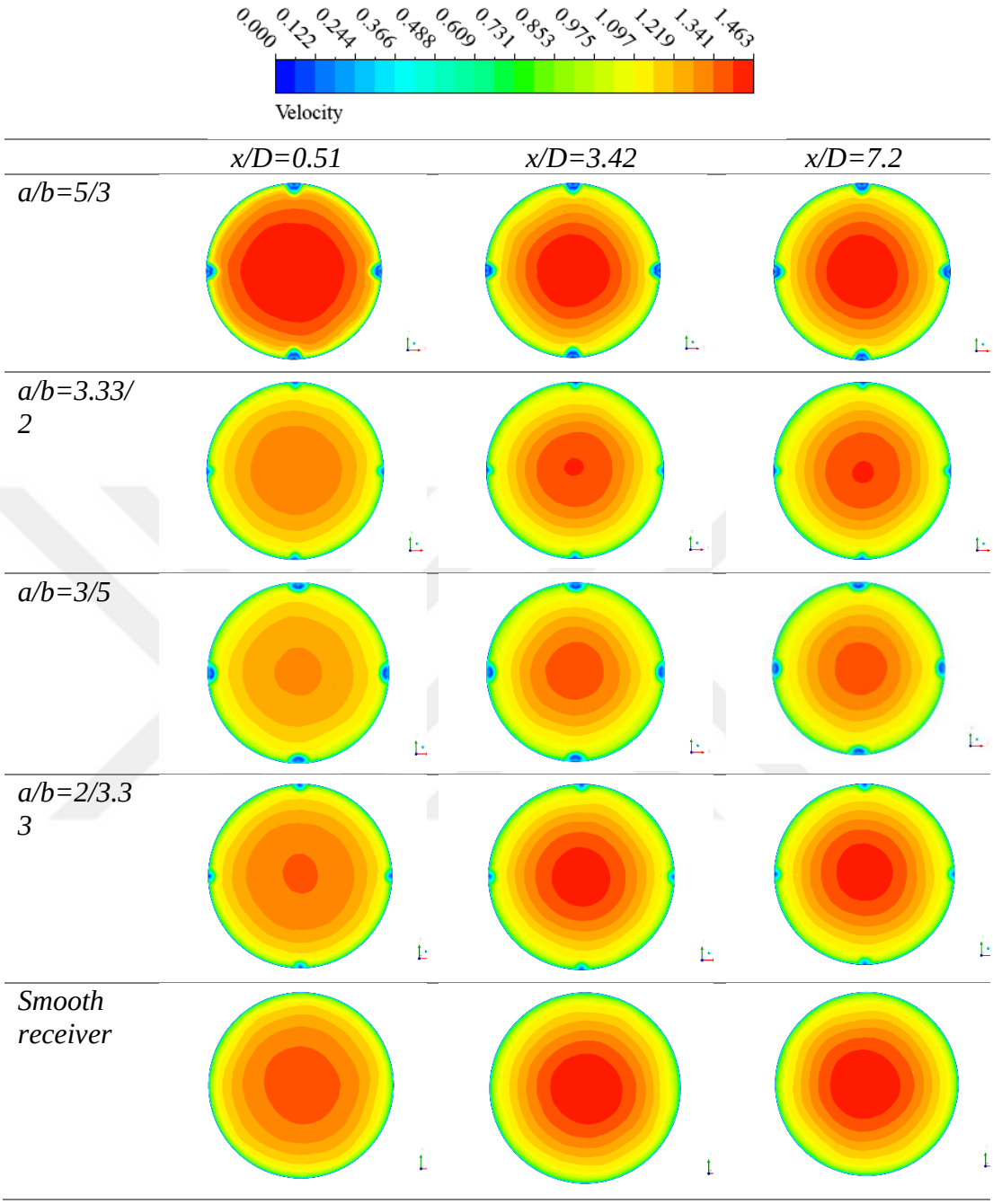

Figure 4.22. Velocity distribution at different sections along the receiver tube for different elliptical ratios.

PART 5

CONCLUSIONS

In this part of the study, the conclusion made and the improvements that occurred in the heat transfer and fluid properties of the *PTC* receiver tube with dimples positioned, which are mentioned and discussed in the fourth section of the paper, are addressed**.**

- Hybrid and mono type nanofluids have been investigated for different nanoparticle volume fractions and it is determined that the highest thermal efficiency is obtained from for using hybrid nanofluids. Hybrid nanofluids have the ability of transfer of the heat faster because they consist of more than one higher heat transfer capacity nanoparticles.
- The heat transfer coefficient increases with increasing Reynolds number, so the ratio of heat transfer coefficient is 57% when the Reynolds number is increased from *10000-30000*. Also, it was found that using the hybrid nanofluid with hybrid nanofluid of *1.5 %*Al_2O_3*-0.5%*TiO_2*/Syltherm800.* It has been achieved that the highest heat transfer in the receiving tube that containing dimples at *ER*=5/3. It has been reached that the presence of dimples inside the receiver tube helped to increase the ratio heat transfer coefficient by 27% when compared with the smooth receiver.
- The velocity of the nanofluid has been reduced when using receiver tubes that contains dimples that mean using dimples inside the receiver tube contributes to the *H-Tr* process, because each dimple generates turbulence around it, which reduces the velocity of the nanofluid, and that helps to increases the *H-Tr* process.
- the *Nu* increases with the increase in *Re*. It has been noted that *27%* increment in *Nu* is observed when using a receiver containing dimples with elliptical ratio of *ER=5/3* when compared with the smooth tube when using nanofluid. With a hybrid nanofluid of *1.5 %*Al_2O_3*-0.5%*TiO_2*/Syltherm800.*

- The *ff* decreases as the *Re* increases, and it has been found that the greater the elliptical ratio inside the receiver tube increases the *ff*. Also, the smooth tube shows the lowest *ff* This is because the presence of grooves in the way of the nanofluid as it passes through the receiver tube will delay its passage and thus increase its *ff*.
- When using nanofluid as working fluid in *PTC`s* receiver gives the higher thermal performance (*PEC*>1). Whereas an increase of *27%* has been obtained when using a hybrid nanofluid inside the receiver tube containing a dimple with elliptical ratio of *ER=5/3* at *Re*=10000 when using the hybrid nanofluid of *1.5 %*Al_2O_3*-0.5%*TiO_2*/Syltherm800.*
- Increasing the value of Reynolds number led to increase the thermal efficiency, so the ratio of thermal efficiency is *6.25%*, when the Reynolds number is increased from *10000-30000*. Also, it has been found that using the hybrid nanofluid with a hybrid nanofluid of *1.5 %*Al_2O_3*-0.5%*TiO_2*/Syltherm800*. The presence of dimples inside the receiver tube helps to increase the ratio of thermal efficiency to *27%* when compared with the smooth receiver.
- It has been studied the entropy generation in the concept of this work. It has been noticed that increasing the Re reduces the entropy generation. The lowest entropy rate was obtained for the case of hybrid nanofluid flowing inside a receiver tube containing dimples with elliptical ratio of *ER=5/3.* Also, it has been increasing *Re* from *10000* to *30000* reduces the entropy generation rate by *52%*.
- It has been observed that the lowest total entropy value could be obtained at hybrid nanofluid of *1.5 %*Al_2O_3*-0.5%*TiO_2*/Syltherm800*. and when the *ER= 5/3*, especially at the *Re= 30,000.* And the thermal efficiency is the largest possible among the cases. It was concluded that the decrease in the total entropy of the fluid increases the heat transfer coefficient and its thermal efficiency.
- It has been concluded that the optimum case obtained for this study is the case of hybrid nanofluid flowing inside a receiver tube containing dimples with elliptical ratio of *ER=5/3* at *Re=10000*.

REFRENCES

[1] W. Jamshed, C. Şirin, F. Selimefendigil, M.D. Shamshuddin, Y. Altowairqi, M.R. Eid, Thermal Characterization Of Coolant Maxwell Type Nanofluid Flowing In Parabolic Trough Solar Collector (Ptsc) Used Inside Solar Powered Ship Application, Coatings. 11 (2021). Https://Doi.Org/10.3390/Coatings11121552.

[2] Global Primary Energy Consumption By Region In 2010 Throug… | Flickr, (N.D.). Https://Www.Flickr.Com/Photos/Eiagov/48821414017 (Accessed April 24, 2022).

[3] D.H.M. Junior, Modelling, Transient Simulations And Parametric Studies Of Parabolic Trough Collectors With Thermal Energy Storage, Territ. E Caracter. Da Popul. Adscrita Da Equipe Saúde Da Família 905. 3 (2014) 1–46. Http://Journal.Stainkudus.Ac.Id/Index.Php/Equilibrium/Article/View/1268/1127.

[4] R. Loni, A.B. Kasaeian, E. Askari Asli-Ardeh, B. Ghobadian, W.G. Le Roux, Performance Study Of A Solar-Assisted Organic Rankine Cycle Using A Dish-Mounted Rectangular-Cavity Tubular Solar Receiver, Appl. Therm. Eng. 108 (2016) 1298–1309. Https://Doi.Org/10.1016/J.Applthermaleng.2016.08.014.

[5] M. Lešina, Position Of Croatia In The New World Division Of Labour Mario Lešina Faculty Of Economics Osijek, Osijek, Croatia, (2015) 2015.

[6] R. York, Do Alternative Energy Sources Displace Fossil Fuels?, Nat. Clim. Chang. 2012 26. 2 (2012) 441–443. Https://Doi.Org/10.1038/Nclimate1451.

[7] Short-Term Energy Outlook - U.S. Energy Information Administration (Eia), (N.D.). Https://Www.Eia.Gov/Outlooks/Steo/Index.Php (Accessed April 18, 2022).

[8] Renewable Energy - Our World In Data, (N.D.). Https://Ourworldindata.Org/Renewable-Energy (Accessed April 18, 2022).

[9] G. Raam Dheep, A. Sreekumar, Influence Of Nanomaterials On Properties Of Latent Heat Solar Thermal Energy Storage Materials - A Review, Energy Convers. Manag. 83 (2014) 133–148. Https://Doi.Org/10.1016/J.Enconman.2014.03.058.

[10] N. Akram, E. Montazer, S.N. Kazi, M.E.M. Soudagar, W. Ahmed, M.N.M. Zubir, A. Afzal, M.R. Muhammad, H.M. Ali, F.P.G. Márquez, W.S. Sarsam, Experimental Investigations Of The Performance Of A Flat-Plate Solar Collector Using Carbon And Metal Oxides Based Nanofluids, Energy. 227

(2021). Https://Doi.Org/10.1016/J.Energy.2021.120452.

[11] A. Menbari, A.A. Alemrajabi, A. Rezaei, Experimental Investigation Of Thermal Performance For Direct Absorption Solar Parabolic Trough Collector (Dasptc) Based On Binary Nanofluids, Exp. Therm. Fluid Sci. 80 (2017) 218–227. Https://Doi.Org/10.1016/J.Expthermflusci.2016.08.023.

[12] C. Chalkias, A. Faka, K. Kalogeropoulos, Assessment Of The Direct Sun-Light On Rural Road Network Through Solar Radiation Analysis Using Gis, Open J. Appl. Sci. 03 (2013) 224–231. Https://Doi.Org/10.4236/Ojapps.2013.32030.

[13] 3.3 Concentrated Solar Power (Csp): How Does It Work? - Jlanka Technologies, (N.D.). Https://Www.Jlankatech.Com/3-3-Concentrated-Solar-Power-Csp-Work/?Msclkid=B5040642bec411ecaf2a2811ff4649f8 (Accessed April 18, 2022).

[14] M.S. Răboacă, G. Badea, A. Enache, C. Filote, G. Răsoi, M. Rata, A. Lavric, R.-A. Felseghi, Concentrating Solar Power Technologies, Energies. 12 (2019) 1048. Https://Doi.Org/10.3390/En12061048.

[15] H. Kettenmann, A. Faissner, J. Trotter, Comprehensive Human Physiology, Springer Berlin Heidelberg, 1996. Https://Doi.Org/10.1007/978-3-642-60946-6_27.

[16] R. Buck, S. Giuliano, R. Uhlig, Central Tower Systems Using The Brayton Cycle, Adv. Conc. Sol. Therm. Res. Technol. (2017) 353–382. Https://Doi.Org/10.1016/B978-0-08-100516-3.00016-2.

[17] L. Li, J. Coventry, R. Bader, J. Pye, W. Lipiński, Optics Of Solar Central Receiver Systems: A Review, Opt. Express. 24 (2016) A985. Https://Doi.Org/10.1364/Oe.24.00a985.

[18] M. Collares-Pereira, D. Canavarro, L.L. Guerreiro, Linear Fresnel Reflector (Lfr) Plants Using Superheated Steam, Molten Salts, And Other Heat Transfer Fluids, Adv. Conc. Sol. Therm. Res. Technol. (2017) 339–352. Https://Doi.Org/10.1016/B978-0-08-100516-3.00015-0.

[19] V.K. Jebasingh, G.M.J. Herbert, A Review Of Solar Parabolic Trough Collector, Renew. Sustain. Energy Rev. 54 (2016) 1085–1091. Https://Doi.Org/10.1016/J.Rser.2015.10.043.

[20] M.J. Blanco, S. Miller, Introduction To Concentrating Solar Thermal (Cst) Technologies, Adv. Conc. Sol. Therm. Res. Technol. (2017) 3–25. Https://Doi.Org/10.1016/B978-0-08-100516-3.00001-0.

[21] S.R. Pavlović, V.P. Stefanović, Systems With Concentrating Solar Radiation, Handb. Res. Nov. Soft Comput. Intell. Algorithms Theory Pract. Appl. 2–2 (2013) 931–988. Https://Doi.Org/10.4018/978-1-4666-4450-2.Ch031.

[22] H. Noori, M. Mohammed, Thermal And Radiative Energy / Exergy Analyses Of Parabolic Trough Collector Systems Thermal And Radiative Energy /

Exergy Analyses Of Parabolic Trough Collector, (2018).

[23] Solar Energy Collectors - Simple Explanation (Part 2: Concentrating Type Solar Collectors), (N.D.). Https://Sciencebanquet.Blogspot.Com/2019/04/Solar-Collector-Concentrated.Html (Accessed September 20, 2022).

[24] What Is Concentrated Solar Thermal? | By Roberto Baldizon | Luszol | Medium, (N.D.). Https://Medium.Com/Luszol/What-Is-Concentrated-Solar-Thermal-B93542ac1e8b (Accessed April 11, 2022).

[25] M. Farhan, U. Malikussaleh, I. Shahid, A Brief Review On Experimental And Simulation-Based Analysis Of Parabolic Trough Solar Collectors Using Nanofluids, International Conference On Energy, Water And Environment (2021) 4–6.

[26] L.Wald, Renewable Energy Systems And Desalination - Volume Ii - Google Kitaplar, (N.D.). Https://Books.Google.Com.Tr/Books?Id=Nsnvdaaaqbaj&Printsec=Frontcover&Hl=Tr&Source=Gbs_Ge_Summary_R&Cad=0#V=Onepage&Q&F=False (Accessed September 20, 2022).

[27] U. Herrmann, B. Kelly, H. Price, Two-Tank Molten Salt Storage For Parabolic Trough Solar Power Plants, 29 (2004) 883–893. Https://Doi.Org/10.1016/S0360-5442(03)00193-2.

[28] M. Gürdal, H.K. Pazarlıoğlu, M. Tekir, K. Arslan, E. Gedik, Numerical Investigation On Turbulent Flow And Heat Transfer Characteristics Of Ferro-Nanofluid Flowing In Dimpled Tube Under Magnetic Field Effect, Appl. Therm. Eng. (2021) 117655. Https://Doi.Org/10.1016/J.Applthermaleng.2021.117655.

[29] M. Gürdal, H.K. Pazarlıoğlu, M. Tekir, K. Arslan, E. Gedik, E. Taşkesen, Experimental Investigation On Thermo Hydraulic Performance Of Ferronanofluid Flow In A Dimpled Tube Under Magnetic Field Effect, Exp. Heat Transf. (2022). Https://Doi.Org/10.1080/08916152.2022.2027575.

[30] M. Leena, S. Srinivasan, Synthesis And Ultrasonic Investigations Of Titanium Oxide Nanofluids, J. Mol. Liq. 206 (2015) 103–109. Https://Doi.Org/10.1016/J.Molliq.2015.02.001.

[31] C.J. Ho, J.B. Huang, P.S. Tsai, Y.M. Yang, Preparation And Properties Of Hybrid Water-Based Suspension Of Al2o3 Nanoparticles And Mepcm Particles As Functional Forced Convection Fluid, Int. Commun. Heat Mass Transf. 37 (2010) 490–494. Https://Doi.Org/10.1016/J.Icheatmasstransfer.2009.12.007.

[32] S. Ebrahim Ghasemi, A. Akbar Ranjbar, Numerical Thermal Study On Effect Of Porous Rings On Performance Of Solar Parabolic Trough Collector, Appl. Therm. Eng. 118 (2017) 807–816. Https://Doi.Org/10.1016/J.Applthermaleng.2017.03.021.

[33] S.A. Kalogirou, A Detailed Thermal Model Of A Parabolic Trough Collector

Receiver, Energy. 48 (2012) 298–306. Https://Doi.Org/10.1016/J.Energy.2012.06.023.

[34] C. Chang, C. Xu, Z.Y. Wu, X. Li, Q.Q. Zhang, Z.F. Wang, Heat Transfer Enhancement And Performance Of Solar Thermal Absorber Tubes With Circumferentially Non-Uniform Heat Flux, Energy Procedia. 69 (2015) 320–327. Https://Doi.Org/10.1016/J.Egypro.2015.03.036.

[35] A. Khanjian, C. Habchi, S. Russeil, D. Bougeard, T. Lemenand, Effect Of Rectangular Winglet Pair Roll Angle On The Heat Transfer Enhancement In Laminar Channel Flow, Int. J. Therm. Sci. 114 (2017) 1–14. Https://Doi.Org/10.1016/J.Ijthermalsci.2016.12.010.

[36] R. Ekiciler, Tez Danışmanı, Parabolik Oluk Tipi Güneş Kolektörlerinde Nanoakişkanin Isi Transferine Etkisinin Deneysel Ve Sayisal İncelenmesi, 2021.

[37] R. Ekiciler, K. Arslan, Cuo/Water Nanofluid Flow Over Microscale Backward-Facing Step And Analysis Of Heat Transfer Performance, Heat Transf. Res. 49 (2018) 1489–1505. Https://Doi.Org/10.1615/Heattransres.2018020931.

[38] V. Nageswara Rao, B. Ravi Sankar, Heat Transfer And Friction Factor Investigations Of Cuo Nanofluid Flow In A Double Pipe U-Bend Heat Exchanger, Mater. Today Proc. 18 (2019) 207–218. Https://Doi.Org/10.1016/J.Matpr.2019.06.294.

[39] K.P. Lok, C.K. Ober, Particle Size Control In Dispersion Polymerization Of Polystyrene, Https://Doi.Org/10.1139/V85-033. 63 (2011) 209–216. Https://Doi.Org/10.1139/V85-033.

[40] A.S. Ahuja, Augmentation Of Heat Transport In Laminar Flow Of Polystyrene Suspensions. I. Experiments And Results, J. Appl. Phys. 46 (2008) 3408. Https://Doi.Org/10.1063/1.322107.

[41] S.U.S. Choi, Enhancing Thermal Conductivity Of Fluids With Nanoparticles, Am. Soc. Mech. Eng. Fluids Eng. Div. Fed. 231 (1995) 99–105.

[42] W. He, D. Toghraie, A. Lotfipour, F. Pourfattah, A. Karimipour, M. Afrand, Effect Of Twisted-Tape Inserts And Nanofluid On Flow Field And Heat Transfer Characteristics In A Tube, Int. Commun. Heat Mass Transf. 110 (2020) 104440. Https://Doi.Org/10.1016/J.Icheatmasstransfer.2019.104440.

[43] O. Mahian, L. Kolsi, M. Amani, P. Estellé, G. Ahmadi, C. Kleinstreuer, J.S. Marshall, M. Siavashi, R.A. Taylor, H. Niazmand, S. Wongwises, T. Hayat, A. Kolanjiyil, A. Kasaeian, I. Pop, Recent Advances In Modeling And Simulation Of Nanofluid Flows-Part I: Fundamentals And Theory, Phys. Rep. 790 (2019) 1–48. Https://Doi.Org/10.1016/J.Physrep.2018.11.004.

[44] M. Sheikholeslami, M. Jafaryar, S. Saleem, Z. Li, A. Shafee, Y. Jiang, Nanofluid Heat Transfer Augmentation And Exergy Loss Inside A Pipe Equipped With Innovative Turbulators, Int. J. Heat Mass Transf. 126 (2018)

156–163. Https://Doi.Org/10.1016/J.Ijheatmasstransfer.2018.05.128.

[45] G. Huminic, A. Huminic, Entropy Generation Of Nanofluid And Hybrid Nanofluid Flow In Thermal Systems: A Review, J. Mol. Liq. 302 (2020). Https://Doi.Org/10.1016/J.Molliq.2020.112533.

[46] S.C. Patil, S.S. Chougule, S.K. Sahu, M. Asme, Soft Template Assisted Synthesis Of Zno:Ag Core-Shell Nanoparticles For Highly Efficient Photo-Catalytalysis View Project Thermal Performance Of Automobile Radiator Using Carbon Nanotube-Water Nanofluid-Experimental Study, Artic. J. Therm. Sci. Eng. Appl. (2014). Https://Doi.Org/10.1115/1.4027678.

[47] H.E. Patel, T. Sundararajan, S.K. Das, An Experimental Investigation Into The Thermal Conductivity Enhancement In Oxide And Metallic Nanofluids, J. Nanoparticle Res. 12 (2010) 1015–1031. Https://Doi.Org/10.1007/S11051-009-9658-2/Tables/2.

[48] A.R. Akash, S. Abraham, A. Pattamatta, S.K. Das, Experimental Assessment Of The Thermo-Hydraulic Performance Of Automobile Radiator With Metallic And Nonmetallic Nanofluids, (2019). Https://Doi.Org/10.1080/01457632.2018.1528055.

[49] N. Sandeep, R.P. Sharma, M. Ferdows, Enhanced Heat Transfer In Unsteady Magnetohydrodynamic Nanofluid Flow Embedded With Aluminum Alloy Nanoparticles, J. Mol. Liq. 234 (2017) 437–443. Https://Doi.Org/10.1016/J.Molliq.2017.03.051.

[50] M. Sheikholeslami, M. Gorji-Bandpy, S. Soleimani, Two Phase Simulation Of Nanofluid Flow And Heat Transfer Using Heatline Analysis, Int. Commun. Heat Mass Transf. 47 (2013) 73–81. Https://Doi.Org/10.1016/J.Icheatmasstransfer.2013.07.006.

[51] N.-M.L.; S. Senthilraja, M. Karthikeyan, R. Gangadevi, Nanofluid Applications In Future Automobiles: Comprehensive Review Of Existing Data, Nano-Micro Lett. 2 (2010) 306–310. Https://Doi.Org/10.3786/Nml.V2i4.P306-310.

[52] E. Abu-Nada, A.J. Chamkha, Effect Of Nanofluid Variable Properties On Natural Convection In Enclosures Filled With A Cuo–Eg–Water Nanofluid, Int. J. Therm. Sci. 49 (2010) 2339–2352. Https://Doi.Org/10.1016/J.Ijthermalsci.2010.07.006.

[53] A. Nasiri, M. Shariaty-Niasar, A. Rashidi, A. Amrollahi, R. Khodafarin, Effect Of Dispersion Method On Thermal Conductivity And Stability Of Nanofluid, Exp. Therm. Fluid Sci. 35 (2011) 717–723. Https://Doi.Org/10.1016/J.Expthermflusci.2011.01.006.

[54] S. Rashidi, M. Eskandarian, O. Mahian, S. Poncet, Combination Of Nanofluid And Inserts For Heat Transfer Enhancement: Gaps And Challenges, J. Therm. Anal. Calorim. 135 (2019) 437–460. Https://Doi.Org/10.1007/S10973-018-7070-9/Figures/3.

[55] G. Sheikhzadeh, A. Aghaei, H. Ehteram, M. Abbaszadeh, Analytical Study Of Parameters Affecting Entropy Generation Of Nanofluid Turbulent Flow In Channel And Micro-Channel, Therm. Sci. 20 (2016) 2037–2050. Https://Doi.Org/10.2298/Tsci151112070s.

[56] B. Farajollahi, S.G. Etemad, M. Hojjat, Heat Transfer Of Nanofluids In A Shell And Tube Heat Exchanger, Int. J. Heat Mass Transf. 53 (2010) 12–17. Https://Doi.Org/10.1016/J.Ijheatmasstransfer.2009.10.019.

[57] M.H. Fard, M.R. Talaie, S. Nasr, Numerical And Experimental Investigation Of Heat Transfer Of Zno/Water Nanofluid In The Concentric Tube And Plate Heat Exchangers, Therm. Sci. 15 (2011) 183–194. Https://Doi.Org/10.2298/Tsci091103048h.

[58] M. Akhtari, M. Haghshenasfard, M.R. Talaie, Numerical And Experimental Investigation Of Heat Transfer Of A-Al 2o3/Water Nanofluid In Double Pipe And Shell And Tube Heat Exchangers, Numer. Heat Transf. Part A Appl. 63 (2013) 941–958. Https://Doi.Org/10.1080/10407782.2013.772855.

[59] R. Ranjbarzadeh, A. Karimipour, M. Afrand, A.H.M. Isfahani, A. Shirneshan, Empirical Analysis Of Heat Transfer And Friction Factor Of Water/Graphene Oxide Nanofluid Flow In Turbulent Regime Through An Isothermal Pipe, Appl. Therm. Eng. 126 (2017) 538–547. Https://Doi.Org/10.1016/J.Applthermaleng.2017.07.189.

[60] Y. Khetib, K. Sedraoui, A.A. Melaibari, R. Alsulami, The Numerical Investigation Of Spherical Grooves On Thermal–Hydraulic Behavior And Exergy Efficiency Of Two-Phase Hybrid Mwcnt-Al2o3/Water Nanofluid In A Parabolic Solar Collector, Sustain. Energy Technol. Assessments. 47 (2021) 101530. Https://Doi.Org/10.1016/J.Seta.2021.101530.

[61] M. Parsaiemehr, F. Pourfattah, O.A. Akbari, D. Toghraie, G. Sheikhzadeh, Turbulent Flow And Heat Transfer Of Water/Al2o3 Nanofluid Inside A Rectangular Ribbed Channel, Phys. E Low-Dimensional Syst. Nanostructures. 96 (2018) 73–84. Https://Doi.Org/10.1016/J.Physe.2017.10.012.

[62] M. Malekan, A. Khosravi, S. Syri, Heat Transfer Modeling Of A Parabolic Trough Solar Collector With Working Fluid Of Fe3o4 And Cuo/Therminol 66 Nanofluids Under Magnetic Field, Appl. Therm. Eng. 163 (2019). Https://Doi.Org/10.1016/J.Applthermaleng.2019.114435.

[63] B. Amina, A. Miloud, L. Samir, B. Abdelylah, J.P. Solano, Heat Transfer Enhancement In A Parabolic Trough Solar Receiver Using Longitudinal Fins And Nanofluids, J. Therm. Sci. 25 (2016) 410–417. Https://Doi.Org/10.1007/S11630-016-0878-3.

[64] M.S. Bretado De Los Rios, C.I. Rivera-Solorio, A.J. García-Cuéllar, Thermal Performance Of A Parabolic Trough Linear Collector Using Al2o3/H2o Nanofluids, Renew. Energy. 122 (2018) 665–673. Https://Doi.Org/10.1016/J.Renene.2018.01.094.

[65] A. Mwesigye, Z. Huan, J.P. Meyer, Thermodynamic Optimisation Of The Performance Of A Parabolic Trough Receiver Using Synthetic Oil-Al2o3 Nanofluid, Appl. Energy. 156 (2015) 398–412. Https://Doi.Org/10.1016/J.Apenergy.2015.07.035.

[66] E. Bellos, C. Tzivanidis, K.A. Antonopoulos, A Detailed Working Fluid Investigation For Solar Parabolic Trough Collectors, Appl. Therm. Eng. 114 (2017) 374–386. Https://Doi.Org/10.1016/J.Applthermaleng.2016.11.201.

[67] A.A. Minea, W.M. El-Maghlany, Influence Of Hybrid Nanofluids On The Performance Of Parabolic Trough Collectors In Solar Thermal Systems: Recent Findings And Numerical Comparison, Renew. Energy. 120 (2018) 350–364. Https://Doi.Org/10.1016/J.Renene.2017.12.093.

[68] R. Ekiciler, K. Arslan, O. Turgut, B. Kurşun, Effect Of Hybrid Nanofluid On Heat Transfer Performance Of Parabolic Trough Solar Collector Receiver, J. Therm. Anal. Calorim. 143 (2021) 1637–1654. Https://Doi.Org/10.1007/S10973-020-09717-5.

[69] E. Bellos, D. Korres, C. Tzivanidis, K.A. Antonopoulos, Design, Simulation And Optimization Of A Compound Parabolic Collector, Sustain. Energy Technol. Assessments. 16 (2016) 53–63. Https://Doi.Org/10.1016/J.Seta.2016.04.005.

[70] F. Vahidinia, H. Khorasanizadeh, A. Aghaei, Comparative Energy, Exergy And Co2 Emission Evaluations Of A Ls-2 Parabolic Trough Solar Collector Using Al2o3/Sio2-Syltherm 800 Hybrid Nanofluid, Energy Convers. Manag. 245 (2021) 114596. Https://Doi.Org/10.1016/J.Enconman.2021.114596.

[71] E. Bellos, C. Tzivanidis, K.A. Antonopoulos, G. Gkinis, Thermal Enhancement Of Solar Parabolic Trough Collectors By Using Nanofluids And Converging-Diverging Absorber Tube, Renew. Energy. 94 (2016) 213–222. Https://Doi.Org/10.1016/J.Renene.2016.03.062.

[72] E. Bellos, C. Tzivanidis, Thermal Analysis Of Parabolic Trough Collector Operating With Mono And Hybrid Nanofluids, Sustain. Energy Technol. Assessments. 26 (2018) 105–115. Https://Doi.Org/10.1016/J.Seta.2017.10.005.

[73] A.A. Alnaqi, J. Alsarraf, A.A.A.A. Al-Rashed, Hydrothermal Effects Of Using Two Twisted Tape Inserts In A Parabolic Trough Solar Collector Filled With Mgo-Mwcnt/Thermal Oil Hybrid Nanofluid, Sustain. Energy Technol. Assessments. 47 (2021) 101331. Https://Doi.Org/10.1016/J.Seta.2021.101331.

[74] E. Bellos, C. Tzivanidis, D. Tsimpoukis, Multi-Criteria Evaluation Of Parabolic Trough Collector With Internally Finned Absorbers, Appl. Energy. 205 (2017) 540–561. Https://Doi.Org/10.1016/J.Apenergy.2017.07.141.

[75] A.A.A.A. Al-Rashed, A.A. Alnaqi, J. Alsarraf, Thermo-Hydraulic And Economic Performance Of A Parabolic Trough Solar Collector Equipped With Finned Rod Turbulator And Filled With Oil-Based Hybrid Nanofluid, J. Taiwan Inst. Chem. Eng. 124 (2021) 192–204.

Https://Doi.Org/10.1016/J.Jtice.2021.04.026.

[76] S. Samiezadeh, R. Khodaverdian, M.H. Doranehgard, H. Chehrmonavari, Q. Xiong, Cfd Simulation Of Thermal Performance Of Hybrid Oil-Cu-Al2o3 Nanofluid Flowing Through The Porous Receiver Tube Inside A Finned Parabolic Trough Solar Collector, Sustain. Energy Technol. Assessments. 50 (2022) 101888. Https://Doi.Org/10.1016/J.Seta.2021.101888.

[77] A. Fernández-García, E. Zarza, L. Valenzuela, M. Pérez, Parabolic-Trough Solar Collectors And Their Applications, Renew. Sustain. Energy Rev. 14 (2010) 1695–1721. Https://Doi.Org/10.1016/J.Rser.2010.03.012.

[78] A. Mwesigye, T. Bello-Ochende, J.P. Meyer, Heat Transfer And Thermodynamic Performance Of A Parabolic Trough Receiver With Centrally Placed Perforated Plate Inserts, Appl. Energy. 136 (2014) 989–1003. Https://Doi.Org/10.1016/J.Apenergy.2014.03.037.

[79] E. Bellos, C. Tzivanidis, D. Tsimpoukis, Thermal Enhancement Of Parabolic Trough Collector With Internally Finned Absorbers, Sol. Energy. 157 (2017) 514–531. Https://Doi.Org/10.1016/J.Solener.2017.08.067.

[80] R. Forristall, Heat Transfer Analysis And Modeling Of A Parabolic Trough Solar Receiver Implemented In Engineering Equation Solver, (2003) 164. Https://Doi.Org/Nrel/Tp-550-34169.

[81] B. Kurşun, Thermal Performance Assessment Of Internal Longitudinal Fins With Sinusoidal Lateral Surfaces In Parabolic Trough Receiver Tubes, Renew. Energy. 140 (2019) 816–827. Https://Doi.Org/10.1016/J.Renene.2019.03.106.

[82] J.E. Matsson, An Introduction To Ansys Fluent 2021, Sdc Publications, 2021.

[83] T.R. Taha, An Introduction To Parallel Computational Fluid Dynamics, 2005. Https://Doi.Org/10.1109/Mcc.1998.736434.

[84] M. Gürdal, H. Kadir Pazarlıoğlu, M. Tekir, K. Arslan, E. Gedik, Numerical Investigation On Turbulent Flow And Heat Transfer Characteristics Of Ferro-Nanofluid Flowing In Dimpled Tube Under Magnetic Field Effect, Appl. Therm. Eng. 200 (2021) 117655. Https://Doi.Org/10.1016/J.Applthermaleng.2021.117655.

[85] Soltrace | Concentrating Solar Power | Nrel, (N.D.). Https://Www.Nrel.Gov/Csp/Soltrace.Html (Accessed April 20, 2022).

[86] A. Mwesigye, J.P. Meyer, Optimal Thermal And Thermodynamic Performance Of A Solar Parabolic Trough Receiver With Different Nanofluids And At Different Concentration Ratios, Appl. Energy. 193 (2017) 393–413. Https://Doi.Org/10.1016/J.Apenergy.2017.02.064.

[87] Z. Huang, Z.Y. Li, G.L. Yu, W.Q. Tao, Numerical Investigations On Fully-Developed Mixed Turbulent Convection In Dimpled Parabolic Trough Receiver Tubes, Undefined. 114 (2017) 1287–1299.

Https://Doi.Org/10.1016/J.Applthermaleng.2016.10.012.

[88] M.A. Taher, Y.W. Lee, H.D. Kim, Heat Transfer Enhancement Of Cu-H≪Sub≫2≪/Sub≫O Nanofluid With Internal Heat Generation Using Lbm, Open J. Fluid Dyn. 03 (2013) 92–99. Https://Doi.Org/10.4236/Ojfd.2013.32a015.

[89] Z. Huang, Z.Y. Li, G.L. Yu, W.Q. Tao, Numerical Investigations On Fully-Developed Mixed Turbulent Convection In Dimpled Parabolic Trough Receiver Tubes, Appl. Therm. Eng. 114 (2017) 1287–1299. Https://Doi.Org/10.1016/J.Applthermaleng.2016.10.012.

[90] P. Wang, D.Y. Liu, C. Xu, Numerical Study Of Heat Transfer Enhancement In The Receiver Tube Of Direct Steam Generation With Parabolic Trough By Inserting Metal Foams, Appl. Energy. 102 (2013) 449–460. Https://Doi.Org/10.1016/J.Apenergy.2012.07.026.

[91] V.E. Dudley, G.J. Kolb, R.A. Mahoney, T.R. Mancini, C.W. Matthews, M. Sloan, D. Kearney, Test Results: Segs Ls-2 Solar Collector, Sandia Natl. Lab. 96 (1994) 140. Http://Www.Nrel.Gov/Csp/Troughnet/Pdfs/Segs_Ls2_Solar_Collector.Pdf%5cnhttp://Adsabs.Harvard.Edu/Abs/1994stin...9611437d.

[92] F. Kock, H. Herwig, Local Entropy Production In Turbulent Shear Flows: A High-Reynolds Number Model With Wall Functions, Int. J. Heat Mass Transf. 47 (2004) 2205–2215. Https://Doi.Org/10.1016/J.Ijheatmasstransfer.2003.11.025.

[93] F. Kock, H. Herwig, Entropy Production Calculation For Turbulent Shear Flows And Their Implementation In Cfd Codes, Int. J. Heat Fluid Flow. 26 (2005) 672–680. Https://Doi.Org/10.1016/J.Ijheatfluidflow.2005.03.005.

[94] T. Optimization, F.-T. Processes, Entropy Generation Optimization, Applied Physics Reviews 1996 .

[95] B.C. Pak, Y.I. Cho, Hydrodynamic And Heat Transfer Study Of Dispersed Fluids With Submicron Metallic Oxide Particles, Exp. Heat Transf. 11 (1998) 151–170. Https://Doi.Org/10.1080/08916159808946559.

[96] M. Jayachandra Babu, N. Sandeep, S. Saleem, Free Convective Mhd Cattaneo-Christov Flow Over Three Different Geometries With Thermophoresis And Brownian Motion, Alexandria Eng. J. 56 (2017) 659–669. Https://Doi.Org/10.1016/J.Aej.2017.01.005.

[97] H.C. Brinkman, The Viscosity Of Concentrated Suspensions And Solutions, J. Chem. Phys. 20 (1952) 571.

[98] J.C. Maxwell, A Treatise On Electricity And Magnetism: Pt. Iii. Magnetism. Pt. Iv. Electromagnetism, Clarendon Press, 1881.

[99] B. Choon Pak, Y.I. Cho, Experimental Heat Transfer An International Journal

Hydrodynamic And Heat Transfer Study Of Dispersed Fluids With Submicron Metallic Oxide Particles, (2007). Https://Doi.Org/10.1080/08916159808946559.

[100] T. Tayebi, A.J. Chamkha, Numerical Heat Transfer, Part A: Applications An International Journal Of Computation And Methodology Free Convection Enhancement In An Annulus Between Horizontal Confocal Elliptical Cylinders Using Hybrid Nanofluids Free Convection Enhancement In An Annulus Between Horizontal Confocal Elliptical Cylinders Using Hybrid Nanofluids, 70 (2016) 1141–1156. Https://Doi.Org/10.1080/10407782.2016.1230423.

[101] H.C. Brinkman, The Viscosity Of Concentrated Suspensions And Solutions, J. Chem. Phys. 20 (2004) 571. Https://Doi.Org/10.1063/1.1700493.

[102] A.A. Minea, Hybrid Nanofluids Based On Al2o3, Tio2 And Sio2: Numerical Evaluation Of Different Approaches, Int. J. Heat Mass Transf. 104 (2017) 852–860. Https://Doi.Org/10.1016/J.Ijheatmasstransfer.2016.09.012.

[103] H. Yang, W. Li, C. Luo, J. Zhang, Z. Si, Research On Error Compensation Property Of Strapdown Inertial Navigation System Using Dynamic Model Of Shearer, Ieee Access. 4 (2016) 2045–2055. Https://Doi.Org/10.1109/Access.2016.2565638.

[104] F.W. Dittus, L.M.K. Boelter, Heat Transfer In Automobile Radiators Of The Tubular Type, Int. Commun. Heat Mass Transf. 12 (1985) 3–22. Https://Doi.Org/10.1016/0735-1933(85)90003-X.

[105] V. Gnielinski, G1 Heat Transfer In Pipe Flow, In: Vdi Heat Atlas, 2010. Https://Doi.Org/10.1007/978-3-540-77877-6_34.

[106] B.S. Petukhov, Heat Transfer And Friction In Turbulent Pipe Flow With Variable Physical Properties, Adv. Heat Transf. 6 (1970) 503–564. Https://Doi.Org/10.1016/S0065-2717(08)70153-9.

[107] K.T. Trinh, On The Blasius Correlation For Friction Factors, (2010). Http://Arxiv.Org/Abs/1007.2466.

RESUME

My name is Noor Adil Mohammed , I am from Iraq , and I studied a master's degree in mechanical engineering at Karabük University .